

## Neutral and charged polymers at interfaces

Roland R. Netz<sup>a,b</sup>, David Andelman<sup>c,\*</sup>

<sup>a</sup>Max-Planck Institute for Colloids and Interfaces, D-14424 Potsdam, Germany

<sup>b</sup>Sektion Physik, Ludwig-Maximilians-Universität, Theresienstr. 37, 80333 München, Germany

<sup>c</sup>School of Physics and Astronomy, Raymond and Beverly Sackler, Faculty of Exact Sciences Tel Aviv University, Ramat Aviv, Tel Aviv 69978, Israel

Accepted 27 February 2003

editor: E. Sackmann

### Abstract

Chain-like macromolecules (polymers) show characteristic adsorption properties due to their flexibility and internal degrees of freedom, when attracted to surfaces and interfaces. In this review we discuss concepts and features that are relevant to the adsorption of neutral and charged polymers at equilibrium, including the type of polymer/surface interaction, the solvent quality, the characteristics of the surface, and the polymer structure. We pay special attention to the case of charged polymers (polyelectrolytes) that have a special importance due to their water solubility. We present a summary of recent progress in this rapidly evolving field. Because many experimental studies are performed with rather stiff biopolymers, we discuss in detail the case of semi-flexible polymers in addition to flexible ones. We first review the behavior of neutral and charged chains in solution. Then, the adsorption of a single polymer chain is considered. Next, the adsorption and depletion processes in the many-chain case are reviewed. Profiles, changes in the surface tension and polymer surface excess are presented. Mean-field and corrections due to fluctuations and lateral correlations are discussed. The force of interaction between two adsorbed layers, which is important in understanding colloidal stability, is characterized. The behavior of grafted polymers is also reviewed, both for neutral and charged polymer brushes. © 2003 Elsevier Science B.V. All rights reserved.

PACS: 61.25.Hq

### Contents

1. Introduction	4
1.1. Types of polymers	5
2. Neutral polymer chains	7
2.1. Flexible chains	7
2.2. Chain swelling and chain collapse: Flory theory and blob formation	11
2.3. Semi-flexible chains	12

\* Corresponding author.

E-mail address: [andelman@post.tau.ac.il](mailto:andelman@post.tau.ac.il) (D. Andelman).

2.4. Dilute, semi-dilute and concentrated solutions	14
3. Charged polymer chains	15
3.1. Interactions between charged objects	15
3.2. Isolated polyelectrolyte chains	17
3.3. Manning condensation	23
3.4. Self-avoidance and polyelectrolyte chain conformations	24
3.5. Dilute polyelectrolyte solutions	25
3.6. Semi-dilute polyelectrolyte solutions	25
4. General considerations on adsorption	29
4.1. Adsorption and depletion	29
4.2. Surface characteristics	30
4.3. Surface–polymer interactions	32
5. Adsorption of a single neutral chain	33
5.1. Mean-field regime	35
5.2. Fluctuation dominated regime	37
6. Adsorption of a single polyelectrolyte chain	40
7. Neutral polymer adsorption from solution	44
7.1. The mean-field approach: ground state dominance	44
7.1.1. The adsorption case	47
7.1.2. The depletion case	49
7.2. Beyond mean-field theory: scaling arguments for good solvents	50
7.2.1. Scaling for polymer adsorption	50
7.2.2. Scaling for polymer depletion	51
7.3. Proximal region corrections	52
7.4. Loops and tails	53
8. Adsorption of polyelectrolytes—mean field	54
8.1. Mean-field theory and its profile equations	55
8.2. Constant $U_s$ : the low-salt limit	57
8.2.1. Numerical solutions of mean-field equations	57
8.2.2. Scaling arguments	57
8.3. Adsorption behavior in the presence of finite salt	60
8.4. Adsorption–depletion crossover in high-salt conditions	61
8.5. Adsorption of PEs for constant surface charge and its overcompensation	63
8.5.1. Low-salt limit: $D \ll \kappa^{-1}$	63
8.5.2. High-salt limit: $D \geq \kappa^{-1}$ and depletion	64
9. Lateral correlation effects in polyelectrolyte adsorption	65
10. Interaction between two adsorbed layers	70
10.1. Non-adsorbing polymers	70
10.2. Adsorbing neutral polymers	71
10.3. Adsorbing charged polymers	72
11. Polymer adsorption on heterogeneous surfaces	73
12. Polymer adsorption on curved and fluctuating interfaces	74
12.1. Neutral polymers	74
12.2. Charged polymers	74
13. Grafted polymer chains	76
13.1. Neutral grafted polymers	77
13.2. Solvent and substrate effects on polymer grafting	81
13.3. Charged grafted polymers	82
14. Concluding remarks	86
Acknowledgements	87
References	87

**Nomenclature**

$a$	Kuhn length or effective monomer size
$b$	monomer size
$c_m$	monomer concentration (per unit volume)
$c_m(x)$	monomer density profile at distance $x$ from the surface
$c_m^b$	bulk monomer concentration in semi-dilute solutions.
$c_m^*$	overlap concentration of bulk polymer solution
$c_{\text{salt}}$	salt concentration in the solution
$c^{\pm}(x)$	profiles of $\pm$ ions
$d$	polymer diameter (or cross-section)
$D$	adsorption layer thickness, height of brush
$e$	electronic unit charge
$f$	fractional charge of the chain $0 < f < 1$
$\hat{f}$	force rescaled by $k_B T$
$F$	intensive free energy in units of $k_B T$ (per unit area or unit volume)
$\mathcal{F}$	extensive free energy in units of $k_B T$
$g$	number of monomers per blob
$h(x)$	dimensionless PE adsorption profile
$H$	height of counterion cloud (PE brush case)
$k_B T$	thermal energy
$L$	contour length of a chain
$L_{\text{el}}$	chain length inside one electrostatic blob
$L_{\text{sw}}$	chain length inside one swollen blob
$\ell_B$	Bjerrum length ( $=e^2/\epsilon k_B T$ )
$\ell_0$	bare (mechanical) persistence length
$\ell_{\text{OSF}}$	electrostatic contribution to persistence length (Odijk, Skolnick, and Fixman length)
$\ell_{\text{eff}}$	effective persistence length
$N$	polymerization index
$R$	end-to-end polymer chain radius
$R_{\text{el}}$	radius of one electrostatic blob
$S(q)$	structure factor (or scattering function) of a PE solution
$S_0(q)$	form factor of a single chain
$U(x)$	electrostatic potential at point $x$ from the surface
$U_s$	surface potential at $x = 0$
$u(x)$	dimensionless potential profile ( $=eU(x)/k_B T$ )
$u_s = u(0)$	rescaled surface potential
$v_2$	2nd virial coefficient of monomers in solution. $v_2 > 0$ for good solvents
$\tilde{v}_2$	dimensionless 2nd virial coefficient of monomers in solution ( $=v_2/a^3$ )
$v(r)$	Coulomb interaction between two ions in units of $k_B T$ ( $=e^2/k_B T \epsilon r$ )
$v_{\text{DH}}(r)$	Debye–Hückel interaction ( $=v(r) \exp(-\kappa r)$ )
$z$	valency of the ions ( $=\pm 1, \pm 2, \dots$ )

$\Gamma$	polymer surface excess per unit area
$\epsilon$	dielectric constant of the medium. $\epsilon = 80$ for water
$\kappa^{-1}$	Debye–Hückel screening length
$\kappa_{\text{salt}}$	salt contribution to $\kappa$
$\mu^{\pm}$	chemical potential of $\pm$ ions
$\mu_p$	chemical potential of polymer
$\nu$	Flory exponent for the polymer size
$\xi_b, \xi_s$	correlation length (mesh size) of semi-dilute polymer solution in bulk and at surface
$\Pi$	osmotic pressure in units of $k_B T$
$\rho$	grafting density of a polymer brush
$\sigma$	surface charge density (in units of $e$ ) at $x = 0$
$\Delta\sigma$	overcharging parameter ( $=f\Gamma - \sigma$ )
$\tau$	linear charge density on the chain ( $=f/b$ )
$\phi(x)$	monomer volume fraction (dimensionless) at distance $x$ from the surface ( $=a^3 c_m(x)$ )
$\phi_b$	bulk value of $\phi$ ( $=a^3 c_m^b$ )
$\phi_s$	surface value of $\phi$
$\psi(x)$	polymer order parameter ( $=\sqrt{\phi(x)}$ )
$\psi_b$	bulk value of polymer order parameter

**1. Introduction**

Polymers are long chain molecules which play important roles in industrial applications and in biological processes. On a more fundamental level, polymers exhibit interesting behavior which can be derived from the knowledge of their statistical mechanics properties. We review the basic mechanisms underlying the equilibrium properties of these macromolecules in solution and, in particular, their behavior at surfaces and interfaces. The understanding of polymer systems progressed tremendously from the late 1960s because of innovation in experimental techniques such as X-ray and neutron diffraction and light scattering. Some techniques like ellipsometry, second harmonics generation (SHG), Brewster angle microscopy, surface force apparatus, atomic force microscopy (AFM) and X-ray or neutron reflectivity are especially appropriate to study polymers at interfaces. Of equal merit was the advancement in theoretical methods ranging from field theoretical methods and scaling arguments to numerical simulations.

The major progress in the field of polymer adsorption at liquid interfaces and solid surfaces is even more recent. Even though several excellent books [1,2] and review articles [3–6] exist, we feel that the present review is timely because we address recent progress in the field of chains at interfaces, paying particular attention to charged chains. Charged polymers are interesting from the application point of view, since they allow for a number of water-based formulations which are advantageous for economical and ecological reasons. Recent years have seen a tremendous research activity on charged polymers in bulk and at interfaces. Likewise, adsorption of biopolymers such as DNA at planar or spherical substrates is an intermediate step in the fabrication of gene-technology related structures, and therefore of great current interest. In addition to being charged, DNA is rather

stiff on the nanoscopic length scale. On intermediate length scales, it can be well described as a semi-flexible polymer, in contrast to most synthetic polymers, which are well represented by flexible polymer models. Accordingly, we discuss the complexity of charged and semi-flexible chains in addition to neutral and flexible ones. We also contrast the situation of physical adsorption of chains with that of terminally attached chains (neutral or charged) to surfaces.

This review is focused on physical aspects of polymer adsorption at thermodynamical equilibrium and summarizes the main theoretical and recent progress. We only outline theoretical calculations and do not explain in detail theoretical and experimental techniques. Whenever possible we try to explain principal concepts in simple terms. Experimental results are mentioned when they are of direct relevance but this review should not be considered as an exhaustive review of various experimental techniques and data.

The review starts by explaining well known facts about conformations of a single ideal chain as well as self-avoiding chain and their behavior in solution (Section 2). We then examine the effect of charges on the statistics of an isolated chain and of multi-chains in solution (Section 3). The rest of the paper deals with adsorption in several distinct situations: a general introduction to adsorption processes (Section 4), adsorption of a single neutral chain (Section 5) and of a single polyelectrolyte chain (Section 6), mean field theories for adsorption of neutral (Section 7) and charged (Section 8) chains. Corrections to mean-field theories are considered in Sections 7 and 9. In Section 10 the interaction between two adsorption layers is presented, while adsorption on more complicated substrates such as heterogeneous and curved interfaces are briefly discussed in Sections 11 and 12. Finally, chains that are terminally anchored to the surface are mentioned in Section 13. These polymer brushes are discussed both for neutral and charged chains.

Although this review is written as one coherent manuscript, expert readers can skip the first three sections and concentrate on adsorption of neutral chains (Sections 4, 5, 7, 10, 12), adsorption of charged chains (Sections 6, 8–12) and grafted polymer layers (brushes) (Section 13).

### 1.1. Types of polymers

The polymers considered here are taken as linear and long chains, as is schematically depicted in Fig. 1a. We briefly mention other, more complex, chain architectures. For example, branched chains [7], Fig. 1b, appear in many applications. One special type of branched structures, Fig. 1f, is a chain having a backbone (main chain) with repeated side branches. The chemical nature of the side and main chain can be different. This demonstrates the difference between homopolymers, formed from a single repeat unit (monomer) and heteropolymers, formed from several chemical different monomers. The heteropolymer can be statistical, e.g. DNA, where the different units repeat in a non-periodic or random fashion, Fig. 1d. Another case is that of block copolymers built from several blocks each being a homopolymer by itself. For example, an A–B–A–C block copolymer is a chain composed of an A, a B, an A and a C block linked serially to form a quater-block chain, Fig. 1e.

Synthetic polymers such as polystyrene and polyethylene are composed of flexible chains which can be solubilized in a variety of organic solvents like toluene, cyclohexane, etc. These polymers are highly insoluble in water. Another class of polymers are water soluble ones. They either have strong dipolar groups which are compatible with the strong polarizability of the aqueous media (e.g., polyethylene oxide) or they carry charged groups.

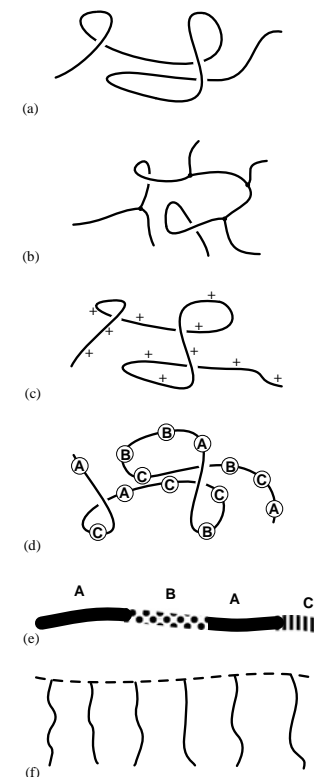


Fig. 1. Schematic view of different polymer types: (a) linear homopolymers that are the main subject of this review; (b) branched polymers; (c) charged polymers or polyelectrolytes (PEs), with a certain fraction of charged monomers; (d) a disordered (hetero) copolymer with no specific order of the different monomers: A, B, C, etc.; (e) a block copolymer. For example, a quater-block A–B–A–C is drawn, where each of the blocks is a homopolymer by itself; (f) a copolymer composed of a backbone (dashed line) and side chains (solid line) of different chemical nature. The backbone could for example be hydrophilic and make the polymer water-soluble as a whole, while the side chain might be hydrophobic and attract other hydrophobic solutes in the solution.

Charged polymers, also known as polyelectrolytes (PE), are shown schematically in Fig. 1c. They are extensively studied not only because of their numerous industrial applications, but also from a pure scientific interest [8–11]. One of the most important properties of PEs is their water solubility

giving rise to a wide range of non-toxic, environmentally friendly and cheap formulations. On the theoretical side, the physics of PEs combines the field of statistical mechanics of charged systems with the field of polymer science and offers quite a number of surprises and challenges.

Two other concepts associated with PEs and water soluble polymers are *associating polymers* (not discussed in this review) and the flexibility of the polymer chain. In cases when the copolymers have both hydrophobic and hydrophilic groups (similarly to short-chain amphiphiles), they will self-assemble in solution to form meso-structures such as lamellae, cylinders and spheres dispersed in solution. The inside of these structures is where the hydrophobic chain sections are packed, away from the water environment. In other cases, association of hydrophobic groups may lead to inter-chain networking and drastically modify the visco-elasticity of the solution. Another concept discussed at large in this review is the chain flexibility. The chains considered here are either flexible or semi-flexible. Flexible chains are chains where it does not cost energy to bend them, while the stiffness of *semi-flexible* chains is an important property. For PEs the charge groups contribute substantially to the chain stiffness, and the chain conformational degrees of freedom are coupled with the electrostatic ones.

## 2. Neutral polymer chains

### 2.1. Flexible chains

The statistical thermodynamics of flexible chains is well developed and the theoretical concepts can be applied with a considerable degree of confidence [7,12–15]. In contrast to other molecules or particles, polymer chains contain not only translational and rotational degrees of freedom, but also a vast number of conformational degrees of freedom. This fact plays a crucial role in determining their behavior in solution and at surfaces. When flexible chains adsorb on surfaces they form *diffusive* adsorption layers extending away from the surface into the solution. This is in contrast to semi-flexible or rigid chains, which can form dense and compact adsorption layers.

From the experimental point of view, the main parameters used to describe a polymer chain are the polymerization index  $N$ , which counts the number of repeat units or monomers along the chain, and the monomer size  $b$ , being the size of one monomer or the distance between two neighboring monomers. The monomer size ranges from a few Angstroms for synthetic polymers to a few nanometers for biopolymers [12].

The simplest theoretical description of flexible chain conformations is achieved with the so-called freely jointed chain (FJC) model, where a polymer consisting of  $N + 1$  monomers is represented by  $N$  bonds defined by bond vectors  $\mathbf{r}_j$  with  $j = 1, \dots, N$ . Each bond vector has a fixed length  $|\mathbf{r}_j| = a$  corresponding to the Kuhn length, but otherwise is allowed to rotate freely, as is schematically shown in Fig. 2a. This model of course only gives a coarse-grained description of real polymer chains, but we will later see that by a careful adjustment of the Kuhn length  $a$  (which is related but not identical to the monomer size  $b$ ), an accurate description of the large-scale properties of real polymer chains is possible. The main advantage is that due to the simplicity of the FJC model, all interesting observables (such as chain size or distribution functions) can be calculated with relative ease. Fixing one of the chain ends at the origin, the position of the  $(k + 1)$ th monomer is given by

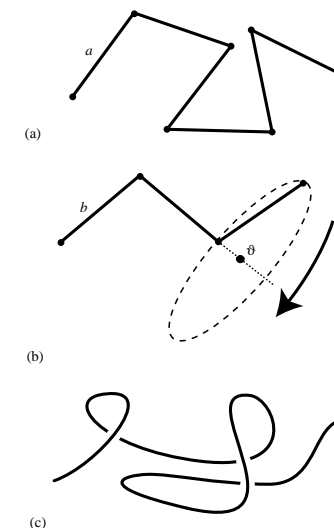


Fig. 2. (a) Freely jointed chain (FJC) model, where  $N$  bonds of length  $a$  are connected to form a flexible chain. (b) Freely rotating chain (FRC) model, which describes a polymer chain with a saturated carbon backbone. It consists of a chain of  $N$  bonds of length  $b$ , with fixed bond angles  $\vartheta$ , reflecting the chemical bond structure, but with freely rotating torsional angles. (c) The simplified model, appropriate for more advanced theoretical calculations, consists of a structureless line, governed by some bending rigidity or line tension. This continuous model can be used when the relevant length scales are much larger than the monomer size.

the vectorial sum

$$\mathbf{R}_k = \sum_{j=1}^k \mathbf{r}_j. \quad (2.1)$$

Because two arbitrary bond vectors are uncorrelated in this simple model, the thermal average over the scalar product of two different bond vectors vanishes,  $\langle \mathbf{r}_j \cdot \mathbf{r}_k \rangle = 0$  for  $j \neq k$ , while the mean squared bond vector length is simply given by  $\langle \mathbf{r}_j^2 \rangle = a^2$ . It follows that the mean squared end-to-end radius  $R^2$  is proportional to the number of monomers,

$$R^2 \equiv \langle \mathbf{R}_N^2 \rangle = Na^2 = La, \quad (2.2)$$

where the contour length of the chain is given by  $L = Na$ . The same result is obtained for the mean quadratic displacement of a freely diffusing particle and alludes to the same underlying physical principle, namely the statistics of Markov processes.



Fig. 3. Snapshot of a Monte-Carlo simulation of a neutral freely jointed chain (FJC) consisting of  $N = 100$  monomers with a diameter corresponding to the Kuhn length  $a$ . The theoretical end-to-end radius,  $R = 10a$ , is indicated by the upper horizontal bar.

In Fig. 3 we show a snapshot of a Monte-Carlo simulation of a freely jointed chain consisting of 100 non-interacting monomers, each being represented by a sphere of diameter  $a$ . The horizontal bar has a length of  $10a$ , which according to Eq. (2.2) is the average distance between the chain ends. As can be seen in the figure, the end-to-end radius gives a good idea of the typical chain size.

In the so-called *freely rotating chain* (FRC) model, different chain conformations are produced by torsional rotations of the polymer backbone bonds of length  $b$  at fixed bond angle  $\vartheta$ , as shown schematically in Fig. 2b. This model is closer to real synthetic polymers than the FJC model, but is also more complicated to calculate. In contrast to the FJC model, the correlation between two neighboring bond vectors does not vanish and is given by  $\langle \mathbf{r}_j \cdot \mathbf{r}_{j+1} \rangle = b^2 \cos \vartheta$ . Correlations between further-nearest neighbors are transmitted through the backbone and one thus obtains for the bond-vector correlation function [7]

$$\langle \mathbf{r}_j \cdot \mathbf{r}_k \rangle = b^2 (\cos \vartheta)^{|j-k|}. \quad (2.3)$$

The mean-squared end-to-end radius is for this model in the limit of long chains ( $N \rightarrow \infty$ ) given by [7]

$$R^2 \simeq Nb^2 \frac{1 + \cos \vartheta}{1 - \cos \vartheta}. \quad (2.4)$$

We will now demonstrate that the simple result for the FJC model, Eq. (2.2), applies on length scales which are large compared with the microscopic chain details also to the more complicated FRC

model (which takes the detailed microscopic chain structure into account). To make the connection between the two models, we observe that the FRC contour length is  $L = Nb \cos(\vartheta/2)$ . Using the scaling relation  $R^2 = aL$  (which we established for the FJC model) as a definition for the Kuhn length  $a$ , we obtain for the FRC model

$$a = b \frac{1 + \cos \vartheta}{\cos(\vartheta/2)(1 - \cos \vartheta)}, \quad (2.5)$$

where the Kuhn length  $a$  is now interpreted as an effective monomer size. For a typical saturated carbon backbone one finds a bond angle  $\vartheta \approx 70^\circ$  and thus obtains for the relation between the Kuhn length and the monomer size  $a \approx 2.5b$ . With a typical bond length of  $b \approx 0.15$  nm this results in a Kuhn length of  $a \approx 0.38$  nm. Clearly, the Kuhn length  $a$  is always larger than the monomer size  $b$ . We have thus shown that it is possible to use the simple FJC model also for more detailed chain models if one interprets the Kuhn length  $a$  as an effective length which takes correlations between chemical bonds into account. In the remainder of this review, we will in most cases use a flexible chain model characterized by the Kuhn length  $a$ . Only in cases where the microscopic structure of the polymer chains matters will we use more detailed models (and then have to distinguish between the Kuhn length  $a$ , characterizing the large-scale properties of a chain, and the monomer size  $b$ ).

In many theoretical calculations aimed at elucidating large-scale properties, the simplification is carried even a step further and a continuous model is used, as schematically shown in Fig. 2c. In such models the polymer backbone is replaced by a continuous line and all microscopic details are neglected.

The models discussed so far describe ideal Gaussian chains and do not account for interactions between monomers which are not necessarily close neighbors along the backbone. Including these interactions will give a different scaling behavior for long polymer chains. The end-to-end radius,  $R = \sqrt{\langle R_N^2 \rangle}$ , can be written more generally for  $N \gg 1$  as

$$R \simeq aN^\nu. \quad (2.6)$$

For an ideal polymer chain (no interactions between monomers), Eq. (2.2) implies  $\nu = 1/2$ . This holds only for polymers where the attraction between monomers (as compared with the monomer–solvent interaction) cancels the steric repulsion (which is due to the fact that the monomers cannot penetrate each other). This situation can be achieved in the condition of “theta” solvents. More generally, polymers in solution can experience three types of solvent conditions, with theta solvent condition being intermediate between “good” and “bad” solvent conditions. The solvent quality depends mainly on the specific chemistry determining the interaction between the solvent molecules and monomers. It can be changed by varying the temperature.

In good solvents the monomer–solvent interaction is more favorable than the monomer–monomer one. Single polymer chains in good solvents have “swollen” spatial configurations dominated by the steric repulsion, characterized by an exponent  $\nu \simeq 3/5$  [12]. This spatial size of a polymer coil is much smaller than the extended contour length  $L = aN$  but larger than the size of an ideal chain  $aN^{1/2}$ . The reason for this peculiar behavior is entropy combined with the favorable interaction between monomers and solvent molecules in good solvents, as we will see in the following section. Similarly, for adsorption of polymer chains on solid substrates, the conformational degrees of freedom of polymer coils lead to salient differences between the adsorption of polymers and small molecules.

In the opposite case of “bad” (sometimes called “poor”) solvent conditions, the effective interaction between monomers is attractive, leading to collapse of the chains and to their precipitation from solution (phase separation between the polymer and the solvent). In this case, the polymer size, like any space filling object embedded in three-dimensional space, scales as  $N \sim R^3$ , yielding  $\nu = 1/3$ .

## 2.2. Chain swelling and chain collapse: Flory theory and blob formation

The standard way of taking into account interactions between monomers is the Flory theory, which treats these interactions on a mean-field level [7,12–15]. Let us first consider the case of repulsive interactions between monomers, which can be described by a positive second-virial coefficient  $v_2$ . This corresponds to the aforementioned good-solvent condition. For pure hard-core interactions and with no additional attractions between monomers, the second virial coefficient (which corresponds to the excluded volume) is of the order of  $a^3$ , the monomer volume. The repulsive interaction between monomers, which tends to swell the chain, is counteracted and balanced by the ideal chain elasticity, which is brought about by the entropy loss associated with stretching the chain. The analogy with an external stretching force is helpful: For a freely jointed chain, the stretching response due to an external force  $\hat{f}$  (rescaled by the thermal energy  $k_B T$ ) is  $R \simeq a^2 N \hat{f} / 3$  for weak forces  $\hat{f} \ll 1/a$  [14]. Hence, a freely jointed chain acts like an ideal spring with a spring constant (rescaled by  $k_B T$ ) of  $3/(2a^2 N)$ . The temperature dependence of the spring constant tells us that the chain elasticity is purely entropic. The origin is that the number of polymer configurations having an end-to-end radius of the order of the unperturbed end-to-end radius is large. These configurations are entropically favored over configurations characterized by a large end-to-end radius, for which the number of possible polymer conformations is drastically reduced. The standard Flory theory [12] for a flexible chain of radius  $R$  is based on writing the free energy  $\mathcal{F}$  (in units of the thermal energy  $k_B T$ ) as a sum of two terms (omitting numerical prefactors)

$$\mathcal{F} \simeq \frac{R^2}{a^2 N} + v_2 R^3 \left( \frac{N}{R^3} \right)^2, \quad (2.7)$$

where the first term is the entropic elastic energy associated with swelling a polymer chain to a radius  $R$ , proportional to the effective spring constant of an ideal chain, and the second term is the second-virial repulsive energy proportional to the coefficient  $v_2$ , and the segment density squared. It is integrated over the volume  $R^3$ . The optimal radius  $R$  is calculated by minimizing this free energy and gives the swollen radius

$$R \sim a(v_2/a^3)^{1/5} N^\nu \quad (2.8)$$

with  $\nu = 3/5$ . For purely steric interactions with  $v_2 \simeq a^3$  we obtain  $R \sim aN^\nu$ . For  $v_2 < a^3$  one finds that the swollen radius Eq. (2.8) is only realized above a minimal monomer number  $N_{sw} \simeq (v_2/a^3)^{-2}$  below which the chain statistics is unperturbed by the interaction and the scaling of the chain radius is Gaussian and given by Eq. (2.2). A different way of looking at this crossover from Gaussian to swollen behavior is to denote a Gaussian coil of monomer number  $N_{sw}$  as a blob with size  $R_{sw} = aN_{sw}^{1/2} \simeq a^4/v_2$ , after which the swollen radius Eq. (2.8) can be rewritten as

$$R \sim R_{sw} (N/N_{sw})^\nu. \quad (2.9)$$

The swollen chain can be viewed as chain of  $N/N_{sw}$  impenetrable blobs, each with a spatial size  $R_{sw}$  [14].

In the opposite limit of negative second virial coefficient, corresponding to the bad or poor solvent regime, the polymer coil will be collapsed due to the attractions between monomers. In this case, the attraction term in the free energy is balanced by the third-virial term in a low-density expansion (where we assume that  $v_3 > 0$ ),

$$\mathcal{F} \simeq v_2 R^3 \left( \frac{N}{R^3} \right)^2 + v_3 R^3 \left( \frac{N}{R^3} \right)^3. \quad (2.10)$$

Minimizing this free energy with respect to the chain radius one obtains

$$R \simeq (v_3/|v_2|)^{1/3} N^\nu. \quad (2.11)$$

with  $\nu = 1/3$ . This indicates the formation of a compact globule, since the monomer density inside the globule,  $c_m \sim N/R^3$ , is independent of the chain length. The minimal chain length to observe a collapse behavior is  $N_{col} \sim (v_3/a^3 v_2)^2$ , and the chain radius Eq. (2.11) can be rewritten as  $R \sim R_{col} (N/N_{col})^{1/3}$ , where the size of a Gaussian blob is  $R_{col} \sim aN_{col}^{1/2}$ . For not too long chains and a second virial coefficient not too much differing from zero, the interaction is irrelevant and one obtains effective Gaussian or ideal behavior. It should be noted, however, that even small deviations from the exact theta conditions (defined by strictly  $v_2 = 0$ ) will lead to chain collapse or swelling for very long chains.

## 2.3. Semi-flexible chains

The freely rotating chain model exhibits orientational correlations between bonds that are not too far from each other, see Eq. (2.3). These correlations give rise to a certain chain stiffness, which plays an important role for the local structure of polymers, and leads to more rigid structures. For synthetic polymers with bond torsional degrees of freedom, this stiffness is due to fixed bond angles and is further enhanced by the hindered rotations around individual back-bone bonds [12], as schematically shown in Fig. 2b. This effect is even more pronounced for polymers with bulky side chains, where, because of steric constraints, the persistence length can be of the order of a few nanometers [12]. This stiffness can be conveniently characterized by the persistence length  $\ell_0$ , defined as the length over which the normalized bond (tangent) vectors at different locations on the chain are correlated. In other words, the persistence length gives an estimate for the typical radius of curvature, while taking into account thermal fluctuations. For the FRC model, the persistence length  $\ell_0$  is defined by

$$\langle \mathbf{r}_j \cdot \mathbf{r}_k \rangle = b^2 e^{-|j-k|b \cos(\vartheta/2)/\ell_0}. \quad (2.12)$$

With the result Eq. (2.3), one obtains for the FRC model the persistence length

$$\ell_0 = \frac{b \cos(\vartheta/2)}{|\ln \cos \vartheta|}. \quad (2.13)$$

For typical saturated carbon backbones with  $\vartheta \approx 70^\circ$  one obtains a persistence length of  $\ell_0 \approx 0.8b$  which is thus of the order of the bond length. Clearly, as the bond angle goes down, the persistence length increases dramatically.

Biopolymers with a more complex structure on the molecular level tend to be stiffer than simple synthetic polymers. Some typical persistence lengths encountered in biological systems are

$\ell_0 \approx 5$  nm for tubulin [16],  $\ell_0 \approx 20$   $\mu$ m for actin [17,18], and  $\ell_0 \approx 50$  nm for double-stranded DNA [19]. Because some of these biopolymer are charged, we will discuss in Section 3.2 at length the dependence of the persistence length on the electrostatic conditions. In some cases the main contribution to the persistence length comes from the repulsion between charged monomers. In these cases, it is important to include the effect of stiffness into the theoretical description, even if the bare or mechanical stiffness is only slightly larger than the monomer size.

To describe the bending rigidity of neutral polymers, it is easier to use a continuum model, where one neglects the discrete nature of monomers, as shown in Fig. 2c. In this approach the bending energy (rescaled by the thermal energy,  $k_B T$ ) of a stiff or semi-flexible polymer of contour length  $L$ , which is parameterized by the space curve  $\mathbf{r}(s)$ , is given by [7]

$$\frac{\ell_0}{2} \int_0^L ds \left( \frac{d^2 \mathbf{r}(s)}{ds^2} \right)^2, \quad (2.14)$$

where  $d^2 \mathbf{r}(s)/ds^2$  is the local curvature of the polymer. We assume here that the polymer segments are non-expendable, i.e. the tangent vectors  $\dot{\mathbf{r}}(s) = d\mathbf{r}(s)/ds$  are always normalized,  $|\dot{\mathbf{r}}(s)| = 1$ . Clearly, this continuum description will only be good if the persistence length is larger than the monomer size  $b$ . For the semi-flexible polymer model, the correlations between tangent vectors exhibit a purely exponential decay,

$$\langle \dot{\mathbf{r}}(s) \cdot \dot{\mathbf{r}}(s') \rangle = e^{-|s-s'|/\ell_0}. \quad (2.15)$$

From this result, the mean-squared end-to-end radius of a semi-flexible chain, described by the bending energy Eq. (2.14), can be calculated and reads [7]

$$R^2 = 2\ell_0 L + 2\ell_0^2 (e^{-L/\ell_0} - 1), \quad (2.16)$$

where the persistence length is  $\ell_0$  and the total contour length of a chain is  $L$ . Two limiting behaviors are obtained for  $R$  from Eq. (2.16): for long chains  $L \gg \ell_0$ , the chain behaves as a flexible one,  $R^2 \simeq 2\ell_0 L$ ; while for rather short chains,  $L \ll \ell_0$ , the chain behaves as a rigid rod,  $R \simeq L$ . Comparison with the scaling of the freely jointed chain model (having no persistence length,  $\ell_0 = 0$ ), Eq. (2.2), shows that a semi-flexible chain can, for  $L \gg \ell_0$ , be described by a freely jointed chain model with an effective Kuhn length of

$$a = 2\ell_0, \quad (2.17)$$

and an effective number of segments

$$N = \frac{L}{2\ell_0}. \quad (2.18)$$

In this case the Kuhn length takes into account the chain stiffness. In Fig. 4 we show snapshots taken from a Monte-Carlo simulation of a semi-flexible chain consisting of 100 polymer beads of diameter  $b$ . The persistence length is varied from  $\ell_0 = 2b$  (Fig. 4a), over  $\ell_0 = 10b$  (Fig. 4b), to  $\ell_0 = 100b$  (Fig. 4c). Comparison with the freely jointed chain model is given in Fig. 3 ( $a = b$ ,  $\ell_0 = 0$ ). It is seen that as the persistence length is increased, the chain structure becomes more expanded. The average end-to-end radius  $R$ , Eq. (2.16), is shown as the bar on the figure and gives a good estimate on typical sizes of semi-flexible polymers.

The main point here is that even though the semi-flexible polymer model describes biopolymers much better than the freely jointed model does, on large length scales both models coincide if the

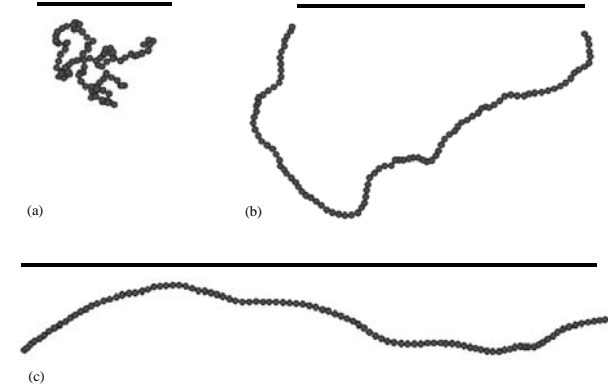


Fig. 4. Snapshots of Monte-Carlo simulations of a neutral and semi-flexible chain consisting of  $N = 100$  monomers with a diameter  $b$ . The theoretical end-to-end radius  $R$  is indicated by a straight bar. The persistence lengths used in the simulations are: (a)  $\ell_0/b = 2$ , leading according to Eq. (2.16) to  $R/b = 19.8$ , (b)  $\ell_0/b = 10$ , leading to  $R/b = 42.4$ , (c)  $\ell_0/b = 100$ , leading to  $R/b = 85.8$ .

Kuhn length  $a$  of the freely jointed chain model is the effective length which is extracted from the scaling of the end-to-end radius in the semi-flexible model, Eq. (2.16). When the small-scale behavior is probed, as for example in the case of polymer adsorption with short-ranged potentials, see Section 6, the difference between the models matters and one has to use the semi-flexible model. On the other hand, it should be kept in mind that the semi-flexible polymer model is an idealization, which neglects the detailed architecture of the polymer at the molecular level. For synthetic polymers, a freely rotating chain model with a bond length  $b$  and a bond angle  $\vartheta$  as shown in Fig. 2b is closer to reality but is more complicated to handle theoretically [7].

#### 2.4. Dilute, semi-dilute and concentrated solutions

It is natural to generalize the discussion of single chain behavior to that of many chains for dilute monomer concentrations. The dilute regime is defined by  $c_m < c_m^*$ , for which  $c_m$  denotes the monomer concentration (per unit volume) and  $c_m^*$  is the concentration where individual chains start to overlap. Clearly, the overlap concentration is reached when the average bulk monomer concentration exceeds the monomer concentration inside a polymer coil. To estimate the overlap concentration  $c_m^*$ , we simply note that the average monomer concentration inside a coil with radius  $R \sim aN^\nu$  is given by

$$c_m^* \simeq \frac{N}{R^3} \sim N^{1-3\nu} a^{-3}. \quad (2.19)$$

For ideal chains with  $\nu = 1/2$  the overlap concentration scales as  $a^3 c_m^* \sim N^{-1/2}$  and thus decreases slowly as the polymerization index  $N$  increases. For swollen chains with  $\nu = 3/5$ , on the other hand,

the overlap concentration scales as  $a^3 c_m^* \sim N^{-4/5}$  and thus decreases more rapidly with increasing chain length. The crossover to the concentrated or melt-like regime occurs when the monomer concentration in the solution reaches the local monomer concentration inside a Gaussian blob, which is for good solvent conditions given by (see the discussion before Eq. (2.9))

$$c_m^{**} \simeq N_{sw}/R_{sw}^3 \simeq v_2/a^6. \quad (2.20)$$

It is seen that the semi-dilute regime, obtained for concentrations  $c_m^* < c_m < c_m^{**}$ , spans for long chains and under good solvent conditions a rather wide range of concentrations and is thus important for typical applications.

For chains characterized by a negative second virial coefficient, attractions between collapsed single-chain globules lead to phase separation between a very dilute solution of single-polymer globules and a dense melt-like phase of entangled polymer coils [14].

### 3. Charged polymer chains

#### 3.1. Interactions between charged objects

A polyelectrolyte (PE) is a polymer where a fraction  $f$  of its monomers are charged. When this fraction is small,  $f \ll 1$ , the PE is weakly charged, whereas when  $f$  is close to unity, the polyelectrolyte is strongly charged. There are two common ways to control  $f$  [11]. One way is to polymerize a heteropolymer using strongly acidic and neutral monomers as building blocks. Upon contact with water, the acidic groups dissociate into positively charged protons ( $H^+$ ) that bind immediately to water molecules, and negatively charged monomers. Although this process effectively charges the polymer molecules, the counterions make the PE solution electro-neutral on larger length scales. The charge distribution along the chain is quenched (“frozen”) during the polymerization stage, and it is characterized by the fraction of charged monomers on the chain,  $f$ . In the second way, the PE is a weak polyacid or polybase. The effective charge of each monomer is controlled by the pH of the solution. Moreover, this annealed fraction depends on the local electric potential. This is in particular important for adsorption processes since the local electric field close to a strongly charged surface can be very different from its value in the bulk solution.

The counterions are attracted to the charged polymers via long-ranged Coulomb interactions, but this physical association typically only leads to a rather loosely bound counterion cloud around the PE chain. Because PEs are present in a background of a polarizable and diffusive counterion cloud, there is a strong influence of the counterion distribution on the PE structure, as will be discussed at length in this section. Counterions contribute significantly towards bulk properties, such as the osmotic pressure, and their translational entropy is responsible for the generally good water solubility of charged polymers. In addition, the statistics of PE chain conformation is governed by intra-chain Coulombic repulsion between charged monomers, resulting in a more extended and swollen conformation of PEs as compared to neutral polymers.

For polyelectrolytes, electrostatic interactions provide the driving force for their salient features and have to be included in any theoretical description. The reduced electrostatic interaction between two point-like charges can be written as  $z_1 z_2 v(r)$  where

$$v(r) = \ell_B/r \quad (3.1)$$

is the Coulomb interaction between two elementary charges in units of  $k_B T$  and  $z_1$  and  $z_2$  are the valencies (or the reduced charges in units of the elementary charge  $e$ ). The Bjerrum length  $\ell_B$  is defined as

$$\ell_B = \frac{e^2}{\epsilon k_B T}, \quad (3.2)$$

where  $\epsilon$  is the medium dielectric constant. It denotes the distance at which the Coulombic interaction between two unit charges in a dielectric medium is equal to thermal energy ( $k_B T$ ). It is a measure of the distance below which the Coulomb energy is strong enough to compete with the thermal fluctuations; in water at room temperatures, one finds  $\ell_B \approx 0.7$  nm.

The electrostatic interaction in a homogeneous medium depends only on the distance  $r$  between the charges. The total electrostatic energy of a given distribution of charges is obtained from adding up all pairwise interactions between charges according to Eq. (3.1). In principle, the equilibrium behavior of an ensemble of charged particles (e.g. a salt solution) follows from the partition function, i.e. the weighted sum over all different microscopic configurations, which—via the Boltzmann factor—depends on the electrostatic energy of each configuration. In practice, however, this route is very complicated for several reasons:

(i) The Coulomb interaction, Eq. (3.1), is long-ranged and couples many charged particles. Electrostatic problems are typically *many-body problems*, even for low densities.

(ii) Charged objects in most cases are dissolved in water. Like any material, water is polarizable and reacts to the presence of a charge with polarization charges. In addition, and this is by far a more important effect, water molecules carry a permanent dipole moment that partially orients in the vicinity of charged objects. Within linearized response theory, these polarization effects can be incorporated by the dielectric constant of water, a procedure which of course neglects non-local and non-linear effects. Note that for water,  $\epsilon \approx 80$ , so that electrostatic interactions and self energies are much weaker in water than in air (where  $\epsilon \approx 1$ ) or some other low-dielectric solvents. Still, the electrostatic interactions are especially important in polar solvents because in these solvents, charges dissociate more easily than in apolar solvents.

(iii) In biological systems and most industrial applications, the aqueous solution contains mobile salt ions. Salt ions of opposite charge are drawn to the charged object and form a loosely bound counterion cloud around it. They effectively reduce or *screen* the charge of the object. The effective (screened) electrostatic interaction between two charges  $z_1 e$  and  $z_2 e$  in the presence of salt ions and a polarizable solvent can be written as  $z_1 z_2 v_{DH}(r)$ , with the Debye–Hückel (DH) potential  $v_{DH}(r)$  given (in units of  $k_B T$ ) by

$$v_{DH}(r) = \frac{\ell_B}{r} e^{-\kappa r}. \quad (3.3)$$

The exponential decay is characterized by the screening length  $\kappa^{-1}$ , which is related to the salt concentration  $c_{\text{salt}}$  by

$$\kappa^2 = 8\pi z^2 \ell_B c_{\text{salt}}, \quad (3.4)$$

where  $z$  denotes the valency of  $z : z$  salt. At physiological conditions the salt concentration is  $c_{\text{salt}} \approx 0.1$  M and for monovalent ions ( $z = 1$ ) this leads to  $\kappa^{-1} \approx 1$  nm. This means that although the Coulombic interactions are long-ranged, in physiological conditions they are highly screened above length scales of a few nanometers, which results from multi-body correlations between ions in a salt solution.

The Debye–Hückel potential in Eq. (3.3) results from a linearized mean-field procedure, and becomes inaccurate when (i) the number of correlated ions is small and (ii) when the typical interaction between ions exceeds the thermal energy. In the following we estimate the validity of the DH approximation using simple scaling arguments: The number of ions which are correlated in a salt solution with concentration  $c_{\text{salt}}$  is of the order of  $n \sim \kappa^{-3} c_{\text{salt}}$ , where one employs the screening length  $\kappa^{-1}$  as the scale over which ions are correlated. Using the definition  $\kappa^2 = 8\pi z^2 \ell_B c_{\text{salt}}$ , one obtains  $n \sim (z^2 \ell_B c_{\text{salt}})^{-3/2}$ . The average distance between ions is roughly  $r_{\text{salt}} \sim c_{\text{salt}}^{-1/3}$ . The typical electrostatic interaction between two ions in the solution, rescaled by the thermal energy, thus is  $W_{\text{el}} \sim z^2 \ell_B / r_{\text{salt}} \sim z^2 \ell_B c_{\text{salt}}^{1/3}$  and we obtain  $W_{\text{el}} \sim n^{-2/3}$ . Using these scaling arguments one obtains that either (i) many ions are weakly coupled together (i.e.  $n \gg 1$  and  $W_{\text{el}} \ll 1$ ), or (ii) a few ions interact strongly with each other ( $n \simeq W_{\text{el}} \simeq 1$ ). In the first case, and in the absence of external fields, the approximations leading to the Debye–Hückel approximation, Eq. (3.3), are valid. In the second case, correlation effects and non-linear effects become important, as will be discussed at various points in this review.

### 3.2. Isolated polyelectrolyte chains

We discuss now the scaling behavior of a single semi-flexible PE in the bulk, including chain stiffness and electrostatic repulsion between monomers. For charged polymers, the effective persistence length is increased due to electrostatic repulsion between monomers. This effect modifies considerably not only the PE behavior in solution but also their adsorption characteristics.

The scaling analysis is a simple extension of previous calculations for flexible (Gaussian) PE's [20–23]. The semi-flexible polymer chain is characterized by a bare persistence length  $\ell_0$  and a linear charge density  $\tau$ . Using the monomer length  $b$  and the fraction of charged monomers  $f$  as parameters, the linear charge density can be expressed as  $\tau = f/b$ . Note that in the limit where the persistence length is small and comparable to a monomer size, only a single length scale remains,  $\ell_0 \simeq a \simeq b$ . Many interesting effects, however, are obtained in the general case treating the persistence length  $\ell_0$  and the monomer size  $b$  as two independent parameters. In the regime where the electrostatic energy is weak, and for long enough contour length  $L$ ,  $L \gg \ell_0$ , a polymer coil will be formed with a radius  $R$  unperturbed by the electrostatic repulsion between monomers. According to Eq. (2.16) we get  $R^2 \simeq 2\ell_0 L$ . To estimate when the electrostatic interaction will be sufficiently strong to swell the polymer coil we recall that the electrostatic energy (rescaled by the thermal energy  $k_B T$ ) of a homogeneously charged sphere of total charge  $Z$  (in units of the elementary charge  $e$ ) and radius  $R$  is

$$W_{\text{el}} = \frac{3\ell_B Z^2}{5R}. \quad (3.5)$$

The exact charge distribution inside the sphere only changes the prefactor of order unity and is not important for the scaling arguments. For a polymer of length  $L$  and line charge density  $\tau$  the total charge is  $Z = \tau L$ . The electrostatic energy of a (roughly spherical) polymer coil is then

$$W_{\text{el}} \simeq \ell_B \tau^2 L^{3/2} \ell_0^{-1/2}. \quad (3.6)$$

The polymer length  $L_{\text{el}}$  at which the electrostatic self energy is of order  $k_B T$ , i.e.  $W_{\text{el}} \simeq 1$ , is then

$$L_{\text{el}} \simeq \ell_0 (\ell_B \ell_0 \tau^2)^{-2/3}, \quad (3.7)$$

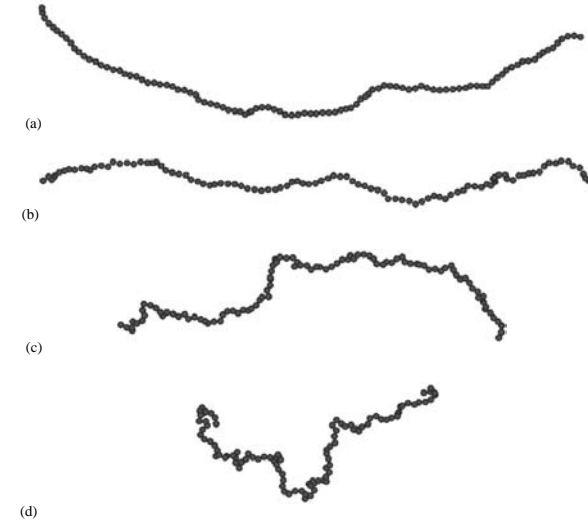


Fig. 5. Snapshots of Monte-Carlo simulations of a PE chain of  $N = 100$  monomers of size  $b$ . In all simulations the bare persistence length is fixed at  $\ell_0/b = 1$ , and the screening length and the charge interactions are tuned such that the electrostatic persistence length is constant and  $\ell_{\text{OSF}}/b = 100$  according to Eq. (3.11). The parameters used are: (a)  $\kappa^{-1}/b = \sqrt{50}$  and  $\tau^2 \ell_B \ell_0 = 8$ , (b)  $\kappa^{-1}/b = \sqrt{200}$  and  $\tau^2 \ell_B \ell_0 = 2$ , (c)  $\kappa^{-1}/b = \sqrt{800}$  and  $\tau^2 \ell_B \ell_0 = 1/2$ , and (d)  $\kappa^{-1}/b = \sqrt{3200}$  and  $\tau^2 \ell_B \ell_0 = 1/8$ . Noticeably, the weakly charged chains crumple at small length scales and show a tendency to form electrostatic blobs.

and defines the electrostatic blob size or electrostatic polymer length. We expect a locally crumpled polymer configuration if  $L_{\text{el}} > \ell_0$ , i.e. if

$$\tau \sqrt{\ell_B \ell_0} < 1, \quad (3.8)$$

because the electrostatic repulsion between two segments of length  $\ell_0$  is smaller than the thermal energy and is not sufficient to align the two segments. This is in accord with more detailed calculations by Joanny and Barrat [22]. A recent general Gaussian variational calculation confirms this scaling result and in addition yields logarithmic corrections [23]. Conversely, for

$$\tau \sqrt{\ell_B \ell_0} > 1, \quad (3.9)$$

electrostatic chain–chain repulsion is already relevant on length scales comparable to the persistence length. The chain is expected to have a conformation characterized by an effective persistence length  $\ell_{\text{eff}}$ , larger than the bare persistence length  $\ell_0$ , i.e. one expects  $\ell_{\text{eff}} > \ell_0$ .

This effect is visualized in Fig. 5, where we show snapshots of Monte-Carlo simulations for charged chains consisting of 100 monomers of size  $b$ . The monomers are interacting solely via

screened DH potentials as defined in Eq. (3.3). In all simulations the bare persistence length equals the monomer size,  $\ell_0 = b$ . The screening length  $\kappa^{-1}$  and the linear charge density  $\tau$  are varied such that the ratio  $\tau/\kappa$  is the same for all four simulations. The number of persistent segments in an electrostatic blob can be written according to Eq. (3.7) as  $L_{\text{el}}/\ell_0 = (\tau^2 \ell_B \ell_0)^{-2/3}$  and yields for Fig. 5a  $L_{\text{el}}/\ell_0 = 0.25$ , for Fig. 5b  $L_{\text{el}}/\ell_0 = 0.63$ , for Fig. 5c  $L_{\text{el}}/\ell_0 = 1.6$ , and for Fig. 5d  $L_{\text{el}}/\ell_0 = 4$ . In other words, in Fig. 5d the electrostatic blobs consist of four persistent segments, and indeed this weakly charged chain crumples at small length scales. On the other hand, in Fig. 5a the persistence length is four times larger than the electrostatic blob length and therefore the chain is straight locally. A typical linear charge density reached with synthetic PEs is one charge per two carbon bonds (or, equivalently, one charge per monomer), and it corresponds to  $\tau \approx 4 \text{ nm}^{-1}$ . Since for these highly flexible synthetic PEs the bare persistence length is of the order of the monomer size,  $\ell_0 \approx b \approx 0.25 \text{ nm}$ , the typical value of  $\tau^2 \ell_B \ell_0$  is roughly  $\tau^2 \ell_B \ell_0 \approx 3$ , and thus intermediate between the values in Fig. 5a and b. Smaller linear charge densities can always be obtained by replacing some of the charged monomers on the polymer backbone with neutral ones. In this case the crumpling observed in Fig. 5d becomes relevant. On the other hand, increasing the bare stiffness  $\ell_0$ , for example by adding bulky side chains to a synthetic PE backbone, increases the value of  $\tau^2 \ell_B \ell_0$  and, therefore, increases the electrostatic stiffening of the backbone. This is an interesting illustration of the fact that electrostatic interactions and chain architecture (embodied via the persistence length) combine to control the polymer configurational behavior.

The question now arises as to what are the typical chain conformations at much larger length scales. Clearly, they will be influenced by the electrostatic repulsions between monomers. Indeed, in the *persistent regime*, obtained for  $\tau\sqrt{\ell_B \ell_0} > 1$ , the polymer remains locally stiff even for contour lengths larger than the bare persistence length  $\ell_0$  and the effective persistence length is given by

$$\ell_{\text{eff}} \simeq \ell_0 + \ell_{\text{OSF}}. \quad (3.10)$$

The electrostatic contribution to the effective persistence length, first derived by Odijk and independently by Skolnick and Fixman, reads [24,25]

$$\ell_{\text{OSF}} = \frac{\ell_B \tau^2}{4\kappa^2}, \quad (3.11)$$

and is calculated from the electrostatic energy of a slightly bent polymer using the linearized Debye–Hückel approximation, Eq. (3.3). It is valid only for polymer conformations which do not deviate too much from the rod-like reference state and for weakly charged polymers (two conditions that are often not simultaneously satisfied in practice and therefore have led to criticism of the OSF result, as will be detailed below). The electrostatic persistence length gives a sizable contribution to the effective persistence length only for  $\ell_{\text{OSF}} > \ell_0$ . This is equivalent to the condition

$$\tau\sqrt{\ell_B \ell_0} > \ell_0 \kappa. \quad (3.12)$$

The *persistent regime* is obtained for parameters satisfying both conditions (3.9) and (3.12) and exhibits chains that do not crumple locally and are stiffened electrostatically. Another regime called the *Gaussian regime* is obtained in the opposite limit of  $\tau\sqrt{\ell_B \ell_0} < \ell_0 \kappa$  and does not exhibit chain stiffening due to electrostatic monomer–monomer repulsions.

The effects of the electrostatic persistence length are visualized in Fig. 6, where we present snapshots of a Monte-Carlo simulation of a charged chain consisting of 100 monomers of size  $b$ . The bare persistence length is fixed at  $\ell_0 = b$ , and the charge-interaction parameter is chosen to be



Fig. 6. Snapshots of Monte-Carlo simulations of a PE chain consisting of  $N = 100$  monomers of size  $b$ . In all simulations, the bare persistence length is fixed at  $\ell_0/b = 1$ , and the charge-interaction parameter is chosen to be  $\tau^2 \ell_B \ell_0 = 2$ . The snapshots correspond to varying screening length of: (a)  $\kappa^{-1}/b = \sqrt{2}$ , leading to an electrostatic contribution to the persistence length of  $\ell_{\text{OSF}}/b = 1$ , (b)  $\kappa^{-1}/b = \sqrt{18}$ , leading to  $\ell_{\text{OSF}}/b = 9$ , and (c)  $\kappa^{-1}/b = \sqrt{200}$ , leading to  $\ell_{\text{OSF}}/b = 100$ . According to the simple scaling principle, Eq. (3.10), the effective persistence length in the snapshots (a)–(c) should be similar to the bare persistence length in Fig. 4(a)–(c).

$\tau^2 \ell_B b = 2$  for all three simulations, close to the typical charge density obtained with fully charged synthetic PEs. In Fig. 6 we show configurations for three different values of the screening length, namely (a)  $\kappa^{-1}/b = \sqrt{2}$ , leading to an electrostatic contribution to the persistence length of  $\ell_{\text{OSF}}/b = 1$ ; (b)  $\kappa^{-1}/b = \sqrt{18}$ , or  $\ell_{\text{OSF}}/b = 9$ ; and (c)  $\kappa^{-1}/b = \sqrt{200}$ , equivalent to an electrostatic persistence length of  $\ell_{\text{OSF}}/b = 100$ . According to the simple scaling principle, Eq. (3.10), the effective persistence length in the snapshots, Fig. 6a–c, should be similar to the bare persistence length in Fig. 4a–c, and indeed, the chain structures in Figs. 6c and 4c are very similar. Figs. 6a and 4a are clearly different, although the effective persistence length is predicted to be quite similar. This deviation is mostly due to self-avoidance effects which are present in charged chains and which will be discussed in detail in Section 3.4.

For the case where the polymer crumples on length scales larger than the bare persistence length, i.e. for  $L_{\text{el}} > \ell_0$  or  $\tau\sqrt{\ell_B \ell_0} < 1$ , the electrostatic repulsion between polymer segments is not strong enough to prevent crumpling on length scales comparable to  $\ell_0$ , but can give rise to a chain stiffening

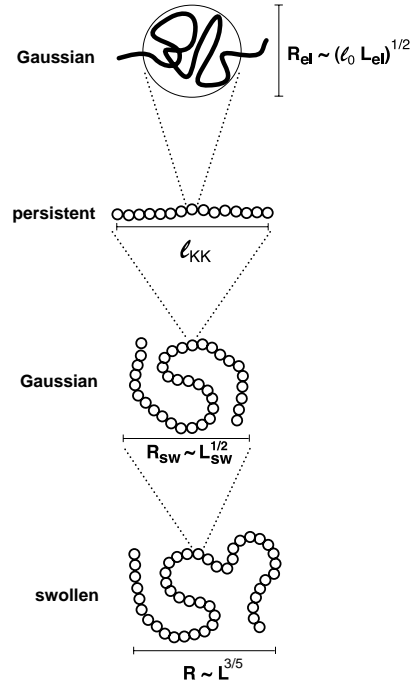


Fig. 7. Schematic view of the four scaling ranges in the Gaussian-persistent regime. On spatial scales smaller than  $R_{el}$  the chain behavior is Gaussian; on length scales larger than  $R_{el}$  but smaller than  $l_{KK}$  the Gaussian blobs are aligned linearly. On larger length scales the chain is isotropically swollen with an exponent  $\nu = 1/2$ , and on even larger length scales self-avoidance effects become important and the exponent changes to  $\nu = 3/5$ .

on larger length scales, as explained by Khokhlov and Khachaturian [21] and confirmed by Gaussian variational methods [23]. Fig. 7 schematically shows the PE structure in this Gaussian-persistent regime, where the chain on small scales consists of Gaussian blobs of size  $R_{el}$ , each containing a chain segment of length  $L_{el}$ . Within these blobs electrostatic interactions are not important. On larger length scales electrostatic repulsion leads to a chain stiffening, so that the PE forms a linear array of electrostatic blobs. To quantify this effect, one defines an effective line charge density  $\tilde{\tau}$  of a linear array of electrostatic blobs with blob size  $R_{el} \simeq \sqrt{l_0 L_{el}}$ ,

$$\tilde{\tau} \simeq \frac{\tau L_{el}}{R_{el}} \simeq \tau \left( \frac{L_{el}}{l_0} \right)^{1/2}. \quad (3.13)$$

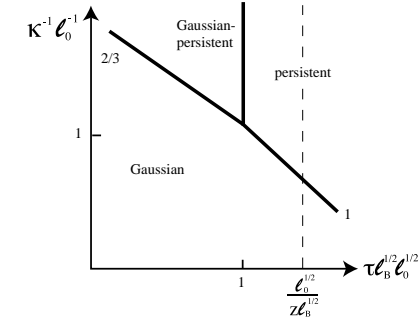


Fig. 8. Behavior diagram of a single semi-flexible PE in bulk solution with bare persistence length  $l_0$  and line charge density  $\tau$ , exhibiting various scaling regimes. High-salt concentration and small  $\tau$  correspond to the Gaussian regime, where the electrostatic interactions are irrelevant. In the persistent regime, the polymer persistence length is increased, and in the Gaussian-persistent regime the polymer forms a persistent chain of Gaussian blobs as indicated in Fig. 7. The broken line indicates the Manning condensation, at which counterions condense on the polymer and reduce the effective polymer line charge density. We use a log–log plot, and the various power-law exponents for the crossover boundaries are denoted by numbers.

Combining Eqs. (3.13) and (3.11) gives the effective electrostatic persistence length for a string of electrostatic blobs,

$$l_{KK} \simeq \frac{l_B^{1/3} \tau^{2/3}}{l_0^{2/3} \kappa^2}. \quad (3.14)$$

This electrostatic stiffening is only relevant for the so-called *Gaussian-persistent regime* valid for  $l_{KK} > R_{el}$ , or equivalently

$$\tau \sqrt{l_B l_0} > (l_0 \kappa)^{3/2}. \quad (3.15)$$

When this inequality is inverted the Gaussian persistence regime crosses over to the Gaussian one.

The crossover boundaries (3.9), (3.12), (3.15) between the various scaling regimes are summarized in Fig. 8. We obtain three distinct regimes. In the persistent regime, for  $\tau \sqrt{l_B l_0} > l_0 \kappa$  and  $\tau \sqrt{l_B l_0} > 1$ , the polymer takes on a rod-like structure with an effective persistence length given by the OSF expression, and larger than the bare persistence length Eq. (3.11). In the Gaussian-persistent regime, for  $\tau \sqrt{l_B l_0} < 1$  and  $\tau \sqrt{l_B l_0} > (l_0 \kappa)^{3/2}$ , the polymer consists of a linear array of Gaussian electrostatic blobs, as shown in Fig. 7, with an effective persistence length  $l_{KK}$  larger than the electrostatic blob size and given by Eq. (3.14). Finally, in the Gaussian regime, for  $\tau \sqrt{l_B l_0} < (l_0 \kappa)^{3/2}$  and  $\tau \sqrt{l_B l_0} < l_0 \kappa$ , the electrostatic repulsion does not lead to stiffening effects at any length scale (though the chain will be non-ideal).

The persistence length  $l_{KK}$  was also obtained from Monte-Carlo simulations with parameters similar to the ones used for the snapshot shown in Fig. 5d, where chain crumpling at small length scales and chain stiffening at large length scales occur simultaneously [26–29]. However, extremely

long chains are needed in order to obtain reliable results for the persistence length, since the stiffening occurs only at intermediate length scales and, therefore, fitting of the tangent–tangent correlation function is non-trivial. Whereas previous simulations for rather short chains point to a different scaling than in Eq. (3.14), with a dependence on the screening length closer to a linear one, in qualitative agreement with experimental results [10], more recent simulations for very long chains exhibit a persistence length in agreement with Eq. (3.14) [30,31]. The situation is complicated by the fact that recent theories for the single PE chain make conflicting predictions, some confirming the simple scaling results described in Eqs. (3.11) and (3.14) [23,32,33], while others confirming Eq. (3.11) but disagreeing with Eq. (3.14) [22,34,35]. This issue is not resolved and still under intense current investigation. For multivalent counterions fluctuation effects can even give rise to a PE collapse purely due to electrostatic interactions [36–41], which is accompanied by a negative contribution to the effective persistence length [42–46]. A related issue is the effective interaction between highly charged parallel rods, which has been shown to become attractive in the presence of multivalent counterions [47–51].

### 3.3. Manning condensation

A peculiar phenomenon occurs for highly charged PEs and is known as the Manning condensation of counterions [52–55]. Strictly speaking, this phenomenon constitutes a true phase transition only in the absence of any added salt ions. For a single rigid PE chain represented by an infinitely long and straight cylinder with a linear charge density larger than

$$\ell_B \tau z = 1, \quad (3.16)$$

where  $z$  is the counterion valency, it was shown that counterions condense on the oppositely charged cylinder in the limit of infinite solvent dilution. Namely, in the limit where the inter-chain distance tends to infinity. This is an effect which is not captured by the linear Debye–Hückel theory used in the last section to calculate the electrostatic persistence length Eq. (3.11). A simple heuristic way to incorporate the non-linear effect of Manning condensation is to replace the bare linear charge density  $\tau$  by the renormalized one  $\tau_{\text{renorm}} = 1/(z/\ell_B)$  whenever  $\ell_B \tau z > 1$  holds. This procedure, however, is not totally satisfactory at high-salt concentrations [56,57]. Also, real polymers have a finite length, and are neither completely straight nor in the infinite dilution limit [58–60]. Still, Manning condensation has an experimental significance for polymer solutions [61–63] because thermodynamic quantities, such as counterion activities [64] and osmotic coefficients [65], show a pronounced signature of Manning condensation. Locally, polymer segments can be considered as straight over length scales comparable to the persistence length. The Manning condition Eq. (3.16) usually denotes a region where the binding of counterions to charged chain sections begins to deplete the solution from free counterions. Within the scaling diagram of Fig. 8, the Manning threshold (denoted by a vertical broken line) is reached typically for charge densities larger than the one needed to straighten out the chain. This holds for monovalent ions provided  $\ell_0 > \ell_B$ , as is almost always the case. The Manning condensation of counterions will therefore not have a profound influence on the local chain structure since the chain is rather straight already due to monomer–monomer repulsion. A more complete description of various scaling regimes related to Manning condensation, chain collapse and chain swelling has recently been given in Ref. [66].

### 3.4. Self-avoidance and polyelectrolyte chain conformations

Let us now consider how the self-avoidance of PE chains comes into play, concentrating on the persistent regime defined by  $\tau\sqrt{\ell_B\ell_0} > 1$ . The end-to-end radius  $R$  of a strongly charged PE chain shows three distinct scaling ranges. For a chain length  $L$  smaller than the effective persistence length  $\ell_{\text{eff}}$ , which according to Eq. (3.10) is the sum of the bare and electrostatic persistence lengths,  $R$  grows linearly with the length,  $R \sim L$ . Self-avoidance plays no role in this case, because the chain is too short to fold back on itself.

For much longer chains,  $L \gg \ell_{\text{eff}}$ , we envision a single polymer coil as a solution of separate polymer pieces of length  $\ell_{\text{eff}}$ , and treat their interactions using a virial expansion. The second virial coefficient  $v_2$  of a rod of length  $\ell_{\text{eff}}$  and diameter  $d$  scales as  $v_2 \sim \ell_{\text{eff}}^2 d$  [67,68]. The chain connectivity is taken into account by adding the entropic chain elasticity as a separate term. The standard Flory theory [12] (see Section 2.2) modified to apply to a semi-flexible chain is based on writing the free energy  $\mathcal{F}$  (in units of  $k_B T$ ) as a sum of two terms

$$\mathcal{F} \simeq \frac{R^2}{\ell_{\text{eff}} L} + v_2 R^3 \left( \frac{L/\ell_{\text{eff}}}{R^3} \right)^2, \quad (3.17)$$

where the first term is the entropic elastic energy associated with swelling a semi-flexible polymer chain to a radius  $R$  and the second term is the second-virial repulsive energy proportional to the coefficient  $v_2$  and the segment density squared. It is integrated over the volume  $R^3$ . The optimal radius  $R$  is calculated by minimizing this free energy and gives the swollen radius

$$R \sim (v_2/\ell_{\text{eff}})^{1/5} L^v, \quad (3.18)$$

with  $v = 3/5$  which is the semi-flexible analogue of Eq. (2.8). This radius is only realized above a minimal chain length  $L > L_{\text{sw}} \simeq \ell_{\text{eff}}^7/v_2^2 \sim \ell_{\text{eff}}^3/d^2$ . For elongated segments with  $\ell_{\text{eff}} \gg d$ , or, equivalently, for a highly charged PE, we obtain an intermediate range of chain lengths  $\ell_{\text{eff}} < L < L_{\text{sw}}$  for which the chain is predicted to be Gaussian and the chain radius scales as

$$R \sim \ell_{\text{eff}}^{1/2} L^{1/2}. \quad (3.19)$$

For charged chains, the effective rod diameter  $d$  is given in low-salt concentrations by the screening length, i.e.  $d \sim \kappa^{-1}$  plus logarithmic corrections [67,68]. The condition to have a Gaussian scaling regime, Eq. (3.19), thus becomes  $\ell_{\text{eff}} \gg \kappa^{-1}$ . For the case  $\tau\sqrt{\ell_B\ell_0} < 1$ , where the chain crumples and locally forms Gaussian blobs, a similar calculation to the one outlined here leads to the condition  $\ell_{\text{KK}} > \kappa^{-1}$  in order to see a Gaussian regime between the persistent and the swollen one. Within the persistent and the Gaussian-persistent scaling regimes depicted in Fig. 8 the effective persistence length is dominated by the electrostatic contribution and given by Eqs. (3.11) and (3.14), respectively, which in turn are always larger than the screening length  $\kappa^{-1}$ . It follows that a Gaussian scaling regime, Eq. (3.19), always exists between the persistent regime where  $R \sim L$  and the asymptotically swollen scaling regime, Eq. (3.18). This situation is depicted in Fig. 7 for the Gaussian-persistent scaling regime, where the chain shows two distinct Gaussian scaling regimes at the small and large length scales. This multi-hierarchical scaling structure is only one of the many problems one faces when trying to understand the behavior of PE chains, be it experimentally, theoretically, or by simulations.

A different situation occurs when the polymer backbone is under bad-solvent conditions, in which case an intricate interplay between electrostatic chain swelling and short-range collapse occurs [69].

Quite recently, this interplay was theoretically shown to lead to a Rayleigh instability in the form of a necklace structure consisting of compact globules connected by stretched chain segments [70–74]. Small-angle X-ray scattering on solvophobic PEs in a series of polar organic solvents of various solvent quality could qualitatively confirm these theoretical predictions [75].

### 3.5. Dilute polyelectrolyte solutions

In accordance with our discussion for neutral chains in Section 2.4, the dilute regime is defined by  $c_m < c_m^*$ , where  $c_m$  denotes the monomer concentration (per unit volume) and  $c_m^*$  is the concentration where individual chains start to overlap. Using Eq. (2.19), for rigid polymers with  $\nu=1$  the overlap concentration scales as  $c_m^* \sim a^{-3}N^{-2}$  and decreases strongly as  $N$  increases. This means that the dilute regime for semi-flexible PE chains corresponds to extremely low monomer concentrations. For example taking a Kuhn length  $a \approx 0.25$  nm (corresponding to the projected length of two carbon bonds) and a polymerization index of  $N = 10^4$ , the overlap concentration becomes  $c_m^* \approx 6 \times 10^{-7} \text{ nm}^{-3} \approx 10^{-3}$  mM, which is a very small concentration.

The osmotic pressure (rescaled by  $k_B T$ ) in the dilute regime in the limit  $c_m \rightarrow 0$  is given by

$$\Pi = \frac{f c_m}{z} + \frac{c_m}{N}, \quad (3.20)$$

and consists of the ideal pressure of non-interacting counterions (first term) and polymer coils (second term). Note that since the second term scales as  $N^{-1}$ , it is quite small for large  $N$  and can be neglected. Hence, the main contribution to the osmotic pressure comes from the counterion entropy. This entropic term explains also why charged polymers can be dissolved in water even when their backbone is quite hydrophobic. Precipitation of the PE chains will also mean that the counterions are confined within the precipitate. The entropy loss associated with this confinement is too large and keeps the polymers dispersed in solution. In contrast, for neutral polymers there are no counterions in solution. Only the second term in the osmotic pressure exists and contributes to the low osmotic pressure of these polymer solutions. In addition, this explains the trend towards precipitation even for very small attractive interactions between neutral polymers: The entropic pressure scale as  $c_m/N$ , while the enthalpic pressure which favors precipitation scales as  $-c_m^2$  with no additional  $N$  dependence, thus dominating the entropic term for large  $N$  [14].

### 3.6. Semi-dilute polyelectrolyte solutions

In the semi-dilute concentration regime,  $c_m > c_m^*$ , different polymer coils are strongly overlapping, but the polymer solution is still far from being concentrated. This means that the volume fraction of the monomers in solution is much smaller than unity,  $a^3 c_m \ll 1$ . In this concentration range, the statistics of counterions and polymer fluctuations are intimately connected. One example where this feature is particularly prominent is furnished by neutron and X-ray scattering from semi-dilute PE solutions [76–82]. The structure factor  $S(q)$  shows a pronounced peak, which results from a competition between the connectivity of polymer chains and the electrostatic repulsion between charged monomers, as will be discussed below. An important length scale, schematically indicated in Fig. 9, is the mesh-size or correlation length  $\xi_b$ , which measures the length below which entanglement effects between different chains are unimportant. The mesh size can be viewed as the polymer (blob)

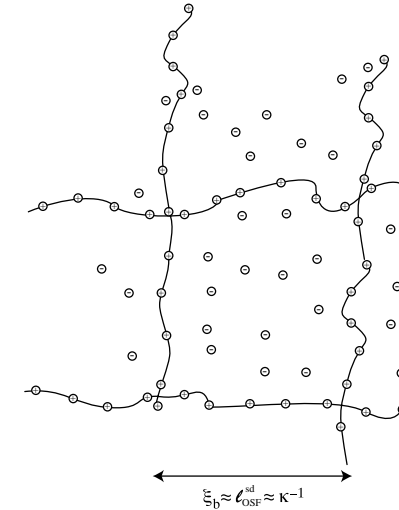


Fig. 9. Schematic view of the PE chain structure in the semi-dilute concentration range. The mesh size  $\xi_b$  is about equal to the persistence length  $\ell_{\text{OSF}}^{\text{sd}}$  and to the screening length  $\kappa^{-1}$  (if no salt is added to the system).

scale below which single-chain statistics are valid. A semi-dilute solution can be roughly thought of as being composed of a close-packed array of polymer blobs of size  $\xi_b$ .

The starting point for the present discussion is the screened interaction between two charges immersed in a semi-dilute PE solution containing charged polymers, their counterions and, possibly, additional salt ions. Screening in this case is produced not only by the ions, but also by the charged chain segments which can be easily polarized and shield any free charges.

Using the random-phase approximation (RPA), the effective Debye–Hückel (DH) interaction can be written in Fourier space as [83,84]

$$v_{\text{RPA}}(q) = \frac{1 + v_2 c_m S_0(q)}{c_m f^2 S_0(q) + v_{\text{DH}}^{-1}(q) + v_2 c_m v_{\text{DH}}^{-1}(q) S_0(q)}, \quad (3.21)$$

recalling that  $c_m$  is the average density of monomers in solution and  $f$  is the fraction of charged monomers on the PE chains. The second virial coefficient of non-electrostatic monomer–monomer interactions is  $v_2$  and the single-chain form factor (discussed below) is denoted by  $S_0(q)$ . In the case where no chains are present,  $c_m = 0$ , the RPA expression reduces to  $v_{\text{RPA}}(q) = v_{\text{DH}}(q)$ , the Fourier-transform of the Debye–Hückel potential of Eq. (3.3), given by

$$v_{\text{DH}}(q) = \frac{4\pi\ell_B}{q^2 + \kappa^2}. \quad (3.22)$$

As before,  $\kappa^{-1}$  is the DH screening length, which is due to all mobile ions. We can write  $\kappa^2 = \kappa_{\text{salt}}^2 + 4\pi\ell_B f c_m$ , where  $\kappa_{\text{salt}}^2 = 8\pi z^2 \ell_B c_{\text{salt}}$  describes the screening due to added  $z:z$  salt of concentration  $c_{\text{salt}}$ , and the second term describes the screening due to the counterions of the PE monomers. Within the same RPA approximation the monomer–monomer structure factor  $S(q)$  of a polymer solution with monomer density  $c_m$  is given by [83,84]

$$S^{-1}(q) = f^2 v_{\text{DH}}(q) + S_0^{-1}(q)/c_m + v_2. \quad (3.23)$$

The structure factor (or scattering function) depends only on the form factor of an isolated, non-interacting polymer chain,  $S_0(q)$ , the second virial coefficient  $v_2$ , the fraction  $f$  of charged monomers, and the interaction between monomers, which in the present case is taken to be the Debye–Hückel potential  $v_{\text{DH}}(q)$ . The structure factor of a non-interacting semi-flexible polymer is characterized, in addition to the monomer length  $b$ , by its persistence length  $\ell_{\text{eff}}$ . In general, this form factor is a complicated function which cannot be written down in closed form [15,85]. However, one can separate between three different ranges of wavenumbers  $q$ , and within each range the form factor shows a rather simple scaling behavior, namely

$$S_0^{-1}(q) \simeq \begin{cases} N^{-1} & \text{for } q^2 < 6/Nb\ell_{\text{eff}}, \\ q^2 b \ell_{\text{eff}}/6 & \text{for } 6/Nb\ell_{\text{eff}} < q^2 < 36/\pi^2 \ell_{\text{eff}}^2, \\ qb/\pi & \text{for } 36/\pi^2 \ell_{\text{eff}}^2 < q^2. \end{cases} \quad (3.24)$$

For small wavenumbers the polymer acts like a point scatterer, while in the intermediate wavenumber regime the polymer behaves like a flexible, Gaussian polymer, and for the largest wavenumbers the polymer can be viewed as a stiff rod.

One of the most interesting features of semi-dilute PE solutions is the fact that the structure factor  $S(q)$  shows a pronounced peak. For weakly charged PEs, the peak position scales as  $q \sim c_m^{1/4}$  with the monomer density [79], in agreement with the above random-phase approximation (RPA) [83,84] and other theoretical approaches [86,87]. We now discuss the scaling of the characteristic scattering peak within the present formalism. The position of the peak follows from the inverse structure factor, Eq. (3.23), via  $\partial S^{-1}(q)/\partial q = 0$ , which leads to the equation

$$q^2 + \kappa_{\text{salt}}^2 + 4\pi\ell_B f c_m = \left( \frac{8\pi q \ell_B f^2 c_m}{\partial S_0^{-1}(q)/\partial q} \right)^{1/2}. \quad (3.25)$$

In principle, there are two distinct scaling behaviors possible for the peak, depending on whether the chain form factor of Eq. (3.24) exhibits flexible-like or rigid-like scaling [88]. We concentrate now on the flexible case, i.e. the intermediate  $q$ -range in Eq. (3.24). A peak is only obtained if the left-hand side of Eq. (3.25) is dominated by the  $q$ -dependent part, i.e. if  $q^2 > \kappa_{\text{salt}}^2 + 4\pi\ell_B f c_m$ . In this case, the peak of  $S(q)$  scales as

$$q^* \simeq \left( \frac{24\pi\ell_B f^2 c_m}{b\ell_{\text{eff}}} \right)^{1/4}, \quad (3.26)$$

in agreement with experimental results.

In Fig. 10a we show density-normalized scattering curves for a PE solution characterized by the persistence length  $\ell_{\text{eff}} = 1$  nm (taken to be constant and thus independent of the monomer concentration), with monomer length  $b=0.38$  nm (as appropriate for Poly-DADMAC), polymerization

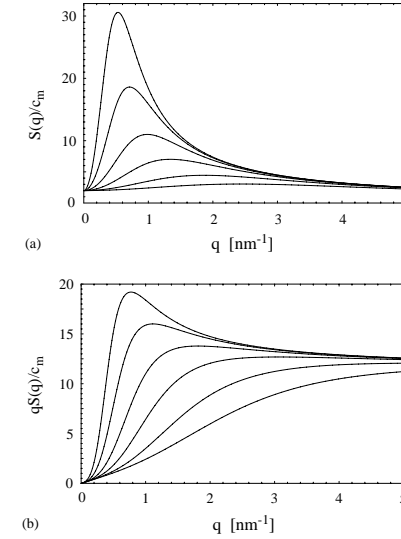


Fig. 10. (a) RPA prediction for the rescaled structure factor  $S(q)/c_m$  of a semi-dilute PE solution with persistence length  $\ell_{\text{eff}} = 1$  nm, monomer length  $b = 0.38$  nm, polymerization index  $N = 500$  and charge fraction  $f = 0.5$  in the salt-free case. The monomer densities are (from bottom to top)  $c_m = 1$  M, 0.3 M, 10 mM, 3 mM, 1 mM, 0.3 mM. (b) For the same series of  $c_m$  values as in (a) the structure factor is multiplied by the wavenumber  $q$ . The semi-flexibility becomes more apparent because for large  $q$  the curves tend towards a constant.

index  $N = 500$ , charge fraction  $f = 0.5$  and with no added salt. As the monomer density decreases (bottom to top in the figure), the peak moves to smaller wavenumbers and sharpens, in agreement with previous implementations of the RPA. In Fig. 10b we show the same data in a different representation. Here we clearly demonstrate that the large- $q$  region already is dominated by the  $1/q$  behavior of the single-chain structure factor,  $S_0(q)$ . Since neutron scattering data easily extend to wavenumbers as high as  $q \sim 5$  nm $^{-1}$ , the stiff-rod like behavior in the high  $q$ -limit, exhibited on such a plot, will be important in interpreting and fitting experimental data even at lower  $q$ -values.

In a semi-dilute solution there are three different, and in principle, independent length scales: The mesh size  $\xi_b$ , the screening length  $\kappa^{-1}$ , and the persistence length  $\ell_{\text{eff}}$ . In the absence of added salt, the screening length scales as

$$\kappa^{-1} \sim (\ell_B f c_m)^{-1/2}. \quad (3.27)$$

Assuming that the persistence length is larger or of the same order of magnitude as the mesh size, as is depicted in Fig. 9, the polymer chains can be thought of as straight segments between different cross-links. Denoting the number of monomers inside a correlation blob as  $g$ , this means

that  $\xi_b \sim bg$ . The average monomer concentration scales as  $c_m \sim g/\xi_b^3$ , from which we conclude that

$$\xi_b \sim (bc_m)^{-1/2}. \quad (3.28)$$

Finally, the persistence length within a semi-dilute PE solution can be calculated by considering the electrostatic energy cost for slightly bending a charged rod. In PE solutions, it is important to include in addition to the screening by salt ions also the screening due to charged chain segments. This can be calculated by using the RPA interaction, Eq. (3.21). Since the screening due to polymer chains is scale dependent and increases for large separations, a  $q$ -dependent instability is encountered and leads to a persistence length [88]

$$\ell_{\text{OSF}}^{\text{sd}} \sim (bc_m)^{-1/2}, \quad (3.29)$$

where the ‘sd’ superscript stands for ‘semi-dilute’. This result is a generalization of the OSF result for a single chain, Eq. (3.11), and applies to semi-dilute solutions. Comparing the three lengths, we see that

$$\xi_b \sim \ell_{\text{OSF}}^{\text{sd}} \sim \sqrt{\frac{\ell_B f}{b}} \kappa^{-1}. \quad (3.30)$$

Since the prefactor  $\sqrt{\ell_B f/b}$  for synthetic fully charged polymers is roughly of order unity, one finds that for salt-free semi-dilute PE solutions, all three length-scales scale in the same way with  $c_m$ , namely as  $\sim c_m^{-1/2}$ . This scaling relation has been found first in experiments [76–78] and was later confirmed by theoretical calculations [89,90]. The screening effects due to neighboring PE chains, which form the basis for the reduction of the electrostatic PE stiffness in a semi-dilute solution, have also been observed in computer simulations [91–94].

## 4. General considerations on adsorption

### 4.1. Adsorption and depletion

Polymers can adsorb spontaneously from solution onto surfaces if the interaction between the polymer and the surface is more favorable than that of the solvent with the surface. For example, a charged polymer like poly-styrene-sulfonate (PSS) is soluble in water but will adsorb on various hydrophobic surfaces and on the water/air interface [95]. This is the case of equilibrium adsorption where the concentration of the polymer monomers increases close to the surface with respect to their concentration in the bulk solution. We discuss this phenomenon at length both on the level of a single polymer chain (valid only for extremely dilute polymer solutions), Sections 5 and 6, and for polymers adsorbing from (semi-dilute) solutions, Sections 7 and 8. In Fig. 11a we show schematically the volume fraction profile  $\phi(x)$  of monomers as a function of the distance  $x$  from the adsorbing substrate. In the bulk, namely far away from the substrate surface, the volume fraction of the monomers is  $\phi_b$ , whereas at the surface, the corresponding value is  $\phi_s > \phi_b$ . The theoretical models address questions in relation to the polymer conformations at the interface, the local concentration of polymer in the vicinity of the surface and the total amount of adsorbing polymer chains. In turn, the knowledge of the polymer interfacial behavior is used to calculate thermodynamical properties like the surface tension in the presence of polymer adsorption.

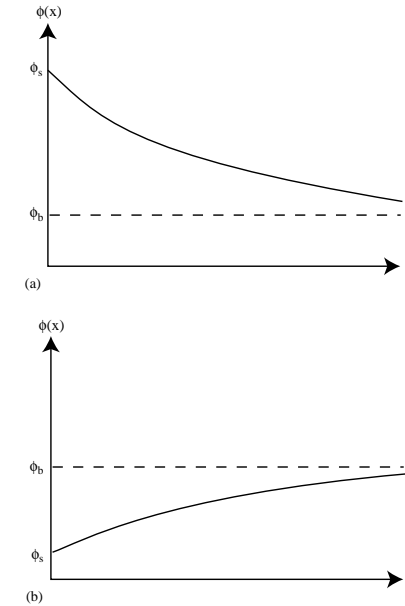


Fig. 11. Schematic profile of the monomer volume fraction  $\phi(x)$  as a function of the distance  $x$  from a flat substrate as appropriate (a) for the case of adsorption, where the substrate attracts monomers, leading to an increase of the polymer concentration close to the surface; and, (b) for the case of depletion, where the substrate repels the monomers leading to a depression of the polymer concentration close to the surface. The bulk volume fraction, i.e., the monomer volume fraction infinitely far away from the surface is denoted by  $\phi_b$ , and  $\phi_s$  denotes the surface volume fraction right at the substrate surface.

The opposite case of *depletion* can occur when the monomer–surface interaction is less favorable than the solvent–surface interaction, as entropy of mixing will always disfavor adsorption. This is, e.g., the case for polystyrene in toluene which is depleted from a mica substrate [96]. The depletion layer is defined as the layer adjacent to the surface from which the polymer is depleted. The concentration in the vicinity of the surface is lower than the bulk value, as shown schematically in Fig. 11b.

### 4.2. Surface characteristics

Clearly, any adsorption process will be sensitive to the type of surface and its internal structure. As a starting point for adsorption problems we assume that the solid surface is atomically smooth,

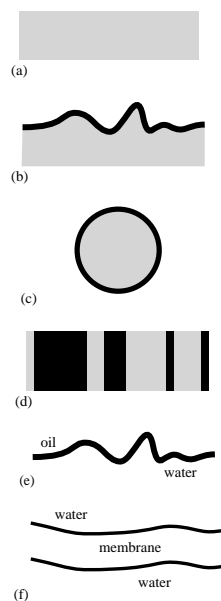


Fig. 12. Different possibilities of substrates: (a) the prototype, a flat, homogeneous substrate; (b) a corrugated, rough substrate. Note that experimentally, every substrate exhibits a certain degree of roughness on some length scale; (c) a spherical adsorption substrate, such as a colloidal particle. If the colloidal radius is much larger than the polymer size, curvature effects (which means the deviation from the planar geometry) can be neglected; (d) a flat but chemically heterogeneous substrate; (e) a liquid/liquid “soft” interface. For example between water and oil; (f) a lipid bilayer (membrane) which can have both shape undulations and lateral composition variations.

flat, and homogeneous, as shown in Fig. 12a. This ideal solid surface is impenetrable to the chains and imposes on them a surface interaction. The surface potential can be either short-ranged, affecting only monomers which are in direct contact with the substrate or in close vicinity of the surface. The surface can also have a longer range effect, like van der Waals, or electrostatic interactions if it is charged. Interesting extensions beyond ideal surface conditions are expected in several cases: (i) rough or corrugated surfaces, such as depicted in Fig. 12b; (ii) surfaces that are curved, e.g., adsorption on spherical colloidal particles, see Fig. 12c; (iii) substrates which are chemically inhomogeneous, i.e., which show some lateral organization, as shown schematically in Fig. 12d; (iv) polymer adsorbing on “soft” and “flexible” interfaces between two immiscible fluids or at the liquid/air surface, Fig. 12e; and, (v) surfaces that have internal degrees of freedom like surfactant monolayers or amphiphilic bilayer (membrane), Fig. 12f. We briefly mention those situations in Sections 11 and 12.

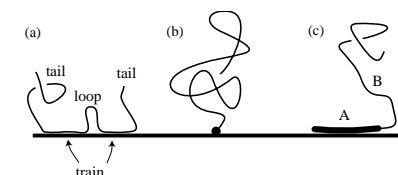


Fig. 13. The different adsorption mechanisms discussed in this chapter: (a) adsorption of a homopolymer, where each monomer has the same interaction with the substrate. The “tail”, “train” and “loop” sections of the adsorbing chain are shown; (b) grafting of an end-functionalized polymer via a chemical or a physical bond, and; (c) adsorption of a diblock copolymer where one of the two block is attached to the substrate surface, while the other is not.

#### 4.3. Surface–polymer interactions

Equilibrium adsorption of polymers is only one of the methods used to create a change in the polymer concentration close to a surface. For an adsorbed polymer, it is interesting to look at the detailed conformation of a single polymer chain at the substrate. One distinguishes polymer sections that are bound to the surface (trains), sections that form loops, and end sections that can form dangling tails. This is schematically depicted in Fig. 13a.

We mention two other methods to produce polymer layers at surfaces for polymers which do not adsorb spontaneously on a given surface.

(i) In the first method, the polymer is chemically attached (grafted) to the surface by one of the chain ends, as shown in Fig. 13b. In good solvent conditions the polymer chains look like “mushrooms” on the surface when the distance between grafting points is larger than the typical size of the chains. In some cases, it is possible to induce a much higher grafting density, resulting in a polymer “brush” extending in the perpendicular direction from the surface, as is discussed in detail in Section 13.

(ii) A variant on the grafting method is to use a diblock copolymer made out of two distinct blocks, as shown in Fig. 13c. The first block is insoluble and is attracted to the substrate. Thus, it acts as an “anchor” fixing the chain to the surface; it is drawn as a thick line in Fig. 13c. It should be long enough to cause irreversible fixation on the surface. The other block is a soluble one (the “buoy”), forming the brush layer (or “mushroom”). For example, fixation on hydrophobic surfaces from a water solution can be made using a polystyrene–polyethylene oxide (PS–PEO) diblock copolymer. The PS block is insoluble in water and attracted towards the substrate, whereas the PEO forms the brush layer. The process of diblock copolymer fixation has a complex dynamics during the formation stage but is very useful in applications [97]. A related application is to employ a polyethylene glycol (PEG) polymer connected to a lipid (PEG–lipid) chain and use the lipid to anchor the PEG chain onto a lipid membrane [98].

There are a variety of other adsorption phenomena not discussed in this review. For example the influence of different polymer topologies on the adsorption characteristics. In Ref. [99] the adsorption of star polymers, where a number of polymer chains are connected to one center, is discussed. The adsorption of ring polymers has also received considerable attention [100,101]. Another important

class of polymers is made up of random copolymers, which are used to manipulate the interfacial properties of a variety of systems. The adsorption of such random copolymers has been studied at solid substrates [102–104] and at penetrable interfaces [105–109].

### 5. Adsorption of a single neutral chain

Let us consider now the interaction of a single polymer chain with a solid substrate. The main effects particular to the adsorption of polymers (as opposed to the adsorption of simple molecules) are due to the reduction of conformational states of the polymer at the substrate, which is caused by the impenetrability of the substrate for monomers [110–115]. The second factor determining the adsorption behavior is the substrate–monomer interaction. Typically, for the case of an adsorbing substrate, the interaction potential  $V(x)$  (measured in units of  $k_B T$ ) between the substrate and a single monomer has a form similar to the one shown in Fig. 14, where  $x$  measures the distance of the monomer from the substrate surface,

$$V(x) \simeq \begin{cases} \infty & \text{for } x < 0, \\ -V_0 & \text{for } 0 < x < B, \\ -wx^{-\tau} & \text{for } x > B. \end{cases} \quad (5.1)$$

The separation of  $V(x)$  into three parts is done for convenience. It consists of a hard wall at  $x = 0$ , which embodies the impenetrability of the substrate, i.e.,  $V(x) = \infty$  for  $x < 0$ . For positive  $x$  we

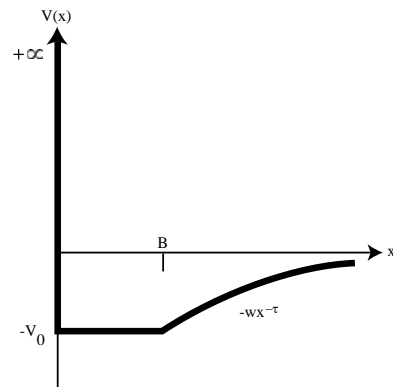


Fig. 14. A typical surface potential felt by a monomer as a function of the distance  $x$  from an adsorbing surface. First the surface is impenetrable. Then, the attraction is of strength  $V_0$  and range  $B$ . For separations larger than  $B$ , typically a long-ranged tail exists and is modelled by  $-wx^{-\tau}$ .

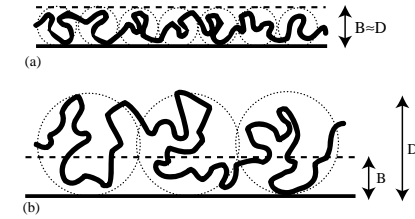


Fig. 15. Schematic drawing of single-chain adsorption. (a) In the limit of strong coupling, the polymer decorrelates into a number of blobs (shown as dotted circles) and the chain is confined to a layer thickness  $D$ , of the same order of magnitude as the potential range  $B$ ; (b) in the case of weak coupling, the width of the polymer layer  $D$  is much larger than the interaction range  $B$  and the polymer forms large blobs, within which the polymer is not perturbed by the surface.

assume the potential to be given by an attractive well of depth  $V_0$  and width  $B$ . At large distances,  $x > B$ , the potential can be modelled by a long-ranged attractive tail decaying as  $V(x) \sim -wx^{-\tau}$ .

For the important case of (non-retarded) van-der-Waals interactions between the substrate and the polymer monomers, the potential shows a decay governed by the exponent  $\tau = 3$  and can be attractive or repulsive, depending on the solvent, the chemical nature of the monomers and the substrate material. The decay power  $\tau = 3$  follows from the van-der-Waals pair interaction, which decays as the inverse sixth power with distance, by integrating over the three spatial dimensions of the substrate, which is supposed to be a semi-infinite half-space [116].

The strength of the potential well is measured by  $V_0$ , i.e., by comparing the potential depth with the thermal energy  $k_B T$ . For strongly attractive potentials, i.e., for  $V_0$  large or, equivalently, for low temperatures, the polymer is strongly adsorbed and the thickness of the adsorbed layer,  $D$ , approximately equals the potential range  $B$ . The resulting polymer structure is shown in Fig. 15a, where the width of the potential well,  $B$ , is denoted by a broken line.

For weakly attractive potentials, or for high temperatures, we anticipate a weakly adsorbed polymer layer, with a diffuse layer thickness  $D$  much larger than the potential range  $B$ . This structure is depicted in Fig. 15b. For both cases shown in Fig. 15, the polymer conformations are unperturbed on a spatial scale of the order of  $D$ ; on larger length scales, the polymer is broken up into decorrelated *polymer blobs* [14,15], which are denoted by dotted circles in Fig. 15. The idea of introducing polymer blobs is related to the fact that very long and flexible chains have different spatial arrangement at small and large length scales. Within each blob the short range interaction is irrelevant, and the polymer structure inside the blob is similar to the structure of an unperturbed polymer far from the surface. Since all monomers are connected, the blobs themselves are linearly connected and their spatial arrangement represents the behavior on large length scales. In the adsorbed state, the formation of each blob leads to an entropy loss of the order of one  $k_B T$  (with a numerical prefactor of order unity that is neglected in this scaling argument), so the total entropy loss of a chain of  $N$  monomers is  $\mathcal{F}_{\text{rep}} \sim N/g$  in units of  $k_B T$ , where  $g$  denotes the number of monomers inside each blob.

Using the scaling relation  $D \simeq ag^v$  for the blob size dependence on the number of monomers  $g$ , Eq. (2.8), the entropy penalty for the confinement of a polymer chain to a width  $D$  above the

surface can be written as [117]:

$$\mathcal{F}_{\text{rep}} \simeq N \left( \frac{a}{D} \right)^{1/\nu}. \quad (5.2)$$

The adsorption behavior of a polymer chain results from a competition between the attractive potential  $V(x)$ , which tries to bind the monomers to the substrate, and the entropic repulsion  $\mathcal{F}_{\text{rep}}$ , which tries to maximize entropy, and favors a delocalized state where a large fraction of monomers is located farther away from the surface.

It is of interest to compare the adsorption of long-chain polymers with the adsorption of small molecular solutes. Small molecules adsorb onto a surface only if there is a bulk reservoir with non-zero concentration in equilibrium with the surface. An infinite polymer chain  $N \rightarrow \infty$  behaves differently as it remains adsorbed also in the limit of zero bulk concentration. This corresponds to a true thermodynamic phase transition in the limit  $N \rightarrow \infty$  [118]. For finite polymer length, however, the equilibrium adsorption resembles that of small molecules. Only a non-zero bulk polymer concentration will lead to adsorption of finite-length polymer chains on the substrate. Indeed, as all real polymers are of finite length, the adsorption of single polymers is never observed in practice. However, for fairly long polymers, the desorption of a single polymer is almost a ‘true’ phase transition, and corrections due to finite (but long) polymer length are often below experimental resolution.

### 5.1. Mean-field regime

Fluctuations of the local monomer concentration are of importance for polymers at surfaces because of the large number of possible chain conformations. These fluctuations are treated theoretically using field-theoretic or transfer-matrix techniques. In a field-theoretic formalism, the problem of accounting for different polymer conformations is converted into a functional integral over different monomer-concentration profiles [15]. Within transfer-matrix techniques, the Markov-chain property of ideal polymers is exploited to re-express the conformational polymer fluctuations as a product of matrices [119].

However, there are cases where fluctuations in the local monomer concentration become unimportant. Then, the adsorption behavior of a single polymer chain is obtained using simple *mean-field theory* arguments. Mean-field theory is a very useful approximation applicable in many branches of physics, including polymer physics. In a nutshell, each monomer is placed in a ‘‘field’’, generated by the external potential plus the averaged interaction with all the other monomers.

The mean-field theory can be justified for two cases: (i) a *strongly adsorbed polymer chain*, i.e., a polymer chain which is entirely confined inside the potential well; and, (ii) the case of *long-ranged attractive surface potentials*. To proceed, we assume that the adsorbed polymer layer is confined with an average thickness  $D$ , as depicted in Fig. 15a or b. Within mean-field theory, the polymer chain feels an average of the surface potential,  $\langle V(x) \rangle$ , which is replaced by the potential evaluated at the average distance from the surface,  $\langle x \rangle \simeq D/2$ . Therefore,  $\langle V(x) \rangle \simeq V(D/2)$ . Further stringent conditions when such a mean-field theory is valid are detailed below. The full free energy of one chain,  $\mathcal{F}$ , of polymerization index  $N$ , can be expressed as the sum of the repulsive entropic term,

Eq. (5.2), and the average potential

$$\mathcal{F} \simeq N \left( \frac{a}{D} \right)^{1/\nu} + NV(D/2). \quad (5.3)$$

Let us consider first the case of a strongly adsorbed polymer, confined to a potential well of depth  $\sim V_0$ . In this case the potential energy per monomer becomes  $V(D/2) \simeq -V_0$ . Comparing the repulsive entropic term with the potential term, we find the two terms to be of equal strength for a well depth  $V_0^* \simeq (a/D)^{1/\nu}$ . Hence, the strongly adsorbed state, which is depicted in Fig. 15a, should be realized for a high attraction strength  $V_0 > V_0^*$ . For intermediate attraction strength,  $V_0 \approx V_0^*$ , the adsorbed chain will actually be adsorbed in a layer of width  $D$  larger than the potential width  $B$ , as shown in Fig. 15b, which will be discussed further below. Since the potential depth  $V_0$  is measured in units of  $k_B T$ , it follows that at high temperatures it becomes increasingly difficult to confine the chain. This can be seen from expressing the bare potential depth as  $\tilde{V}_0 = k_B T V_0$ , so that the critical potential depth becomes  $\tilde{V}_0^* \simeq k_B T (a/D)^{1/\nu}$  and thus increases linearly with temperature. In fact, for an ideal chain, with  $\nu = 1/2$ , the resulting scaling relation for the critical well depth,  $V_0^* \sim (a/D)^2$ , agrees with exact transfer-matrix predictions for the adsorption threshold in a square-well potential [120].

We turn now to the case of a weakly adsorbed polymer layer. The potential depth is smaller than the threshold, i.e.,  $V_0 < V_0^*$ , and the stability of the weakly adsorbed polymer chain, depicted in Fig. 15b, has to be examined. The thickness  $D$  of this polymer layer follows from the minimization of the free energy, Eq. (5.3), with respect to  $D$ , where we use the asymptotic form of the surface potential, Eq. (5.1), for large separations. The result is

$$D \simeq \left( \frac{a^{1/\nu}}{w} \right)^{\nu/(1-\nu\tau)}. \quad (5.4)$$

Under which circumstances is the prediction Eq. (5.4) correct, at least on a qualitative level? It turns out that the prediction for  $D$ , Eq. (5.4), obtained within the simple mean-field theory, is correct if the attractive tail of the substrate potential in Eq. (5.1) decays for large values of  $x$  slower than the entropic repulsion in Eq. (5.2) [121]. In other words, the mean-field theory is valid for weakly adsorbed polymers only for  $\tau < 1/\nu$ . This can already be guessed from the functional form of the layer thickness, Eq. (5.4), because for  $\tau > 1/\nu$  the layer thickness  $D$  goes to zero as  $w$  diminishes. Clearly an unphysical result. For ideal polymers (theta solvent,  $\nu = 1/2$ ), the validity condition is  $\tau < 2$ , whereas for swollen polymers (good solvent conditions,  $\nu = 3/5$ ), it is  $\tau < 5/3$ . For most interactions (including van der Waals interactions with  $\tau = 3$ ) this condition on  $\tau$  is not satisfied, and fluctuations are in fact important, as is discussed in the next section.

There are two notable exceptions. The first is for charged polymers close to an oppositely charged surface, in the *absence* of salt ions. Since the attraction of the polymer to an infinite, planar and charged surface is linear in  $x$ , the interaction is described by Eq. (5.1) with an exponent  $\tau = -1$ , and the inequality  $\tau < 1/\nu$  is satisfied. For charged surfaces, Eq. (5.4) predicts the thickness  $D$  to increase to infinity as the temperature increases or as the attraction strength  $w$  (proportional to the surface charge density) decreases. The resultant exponents for the scaling of  $D$  follow from Eq. (5.4) and are  $D \sim w^{-1/3}$  for ideal chains, and  $D \sim w^{-3/8}$  for swollen chains [122,123]. This case will be considered in more detail in Section 6.

A second example where the mean-field theory can be used is the adsorption of polyampholytes on charged surfaces [124,125]. Polyampholytes are polymers consisting of negatively and positively

charged monomers. In cases where the total charge on such a polymer adds up to zero, it might seem that the interaction with a charged surface should vanish. However, it turns out that local charge fluctuations (i.e., local spontaneous dipole moments) lead to a strong attraction of polyampholytes to charged substrates. In the absence of salt this attractive interaction has an algebraic decay with an exponent  $\tau = 2$  [124]. On the other hand, in the presence of salt, the effective interaction is exponentially screened, yielding a decay faster than the fluctuation repulsion, Eq. (5.2). Nevertheless, the mean-field theory, embodied in the free energy expression Eq. (5.3), can be used to predict the adsorption phase behavior within the strongly adsorbed case (i.e., far from any desorption transition) [126–129].

### 5.2. Fluctuation dominated regime

Here we consider the weakly adsorbed case for substrate potentials which decay (for large separations from the surface) faster than the entropic repulsion Eq. (5.2), i.e.,  $\tau > 1/\nu$ . This applies, e.g., to van-der-Waals attractive interaction between the substrate and monomers, screened electrostatic interactions, or any other short-ranged potential. In this case, fluctuations play a decisive role. In fact, for *ideal chains*, it can be rigorously proven (using transfer-matrix techniques) that all potentials decaying faster than  $x^{-2}$  for large  $x$  have a continuous adsorption transition at a finite critical temperature  $T^*$  [121]. This means that the thickness of the adsorbed polymer layer diverges as

$$D \sim (T^* - T)^{-1} \quad (5.5)$$

for  $T \rightarrow T^*$  [130]. The power law divergence of  $D$  is universal. Namely, it does not depend on the specific functional form and strength of the potential as long as they satisfy the above condition.

The case of *non-ideal chains* is much more complicated [131]. First progress has been made by de Gennes who recognized the analogy between the partition function of a self-avoiding chain and the correlation function of an  $n$ -component spin model in the zero-component ( $n \rightarrow 0$ ) limit [132]. The adsorption behavior of non-ideal chains has been treated by field-theoretic methods using the analogy to surface critical behavior of magnets (again in the  $n \rightarrow 0$  limit) [2,133]. The resulting behavior is similar to the ideal-chain case and shows an adsorption transition at a finite temperature, and a continuous increase towards infinite layer thickness characterized by a power law divergence as function of  $T - T^*$  [133].

The complete behavior for ideal and swollen chains can be described using scaling ideas in the following way. The entropic loss due to the confinement of the chain to a region of thickness  $D$  close to the surface is again given by Eq. (5.2). Assuming that the adsorption layer is much thicker than the range of the attractive potential  $V(x)$ , the attractive potential can be assumed to be localized at the substrate surface  $V(x) \simeq V(0)$ . The attractive free energy of the chain due to the substrate surface can then be written as [134]

$$\mathcal{F}_{\text{att}} \simeq -\tilde{\gamma} \frac{(T^* - T)}{T} N f_1 = -\gamma_1 a^2 N f_1, \quad (5.6)$$

where  $f_1$  is the probability to find a monomer at the substrate surface and  $\tilde{\gamma}$  is a dimensionless interaction parameter. Two surface excess energies are typically being used:  $\gamma_1 = \tilde{\gamma}(T^* - T)/Ta^2$  is the excess energy per unit area, while  $\gamma_1 a^2$  is the (dimensionless) excess energy per monomer at the surface. Both are positive for the attractive case (adsorption) and negative for the depletion case.

The dependence of  $\gamma_1$  on  $T$  in Eq. (5.6) causes the attraction to vanish at a critical temperature,  $T = T^*$ , in accord with our expectations.

The contact probability for a swollen chain with the surface,  $f_1$ , can be calculated as follows [135]. In order to force the chain of polymerization index  $N$  to be in contact with the surface, one of the chain ends is pinned to the substrate. The number of monomers which are in contact with the surface can be calculated using field-theoretic methods and is given by  $N^\varphi$ , where  $\varphi$  is called the *surface crossover exponent* [2,133]. The fraction of bound monomers follows to be  $f_1 \sim N^{\varphi-1}$ , and thus goes to zero as the polymer length increases, for  $\varphi < 1$ . Now instead of speaking of the entire chain, we refer to a ‘chain of blobs’ (see Fig. 15) adsorbing on the surface, each blob consisting of  $g$  monomers. We proceed by assuming that the size of an adsorbed blob  $D$  scales with the number of monomers per blob  $g$  similarly as in the bulk,  $D \sim ag^\nu$ , as is indeed confirmed by field theoretic calculations. The fraction of bound monomers can be expressed in terms of  $D$  and is given by

$$f_1 \sim \left(\frac{D}{a}\right)^{(\varphi-1)/\nu}. \quad (5.7)$$

Combining the entropic repulsion, Eq. (5.2), and the substrate attraction, Eqs. (5.6)–(5.7), the total free energy is given by

$$\mathcal{F} \simeq N \left(\frac{a}{D}\right)^{1/\nu} - N \frac{\tilde{\gamma}(T^* - T)}{T} \left(\frac{D}{a}\right)^{(\varphi-1)/\nu}. \quad (5.8)$$

Minimization with respect to  $D$  leads to the final result

$$D \simeq a \left[ \frac{\tilde{\gamma}(T^* - T)}{T} \right]^{-\nu/\varphi} \simeq a (a^2 \gamma_1)^{-\nu/\varphi}. \quad (5.9)$$

For ideal chains, one has  $\varphi = \nu = 1/2$ , and thus we recover the prediction from the transfer-matrix calculations, Eq. (5.5). For non-ideal chains, the crossover exponent  $\varphi$  is in general different from the swelling exponent  $\nu$ . However, extensive Monte Carlo computer simulations [133] and recent field-theoretic calculations [136] point to a value for  $\varphi$  close to  $\nu$ , such that the adsorption exponent  $\nu/\varphi$  appearing in Eq. (5.9) is close to unity, for polymers embedded in three-dimensional space.

A further point which has been calculated using field theory is the behavior of the monomer volume fraction  $\phi(x)$  close to the substrate. Rather general arguments borrowed from the theory of critical phenomena suggest a power-law behavior for  $\phi(x)$  at sufficiently small distances from the substrate [133,135,137]

$$\phi(x) \simeq (x/a)^{-m} \phi_s, \quad (5.10)$$

recalling that the monomer density is related to  $\phi(x)$  by  $c_m(x) = \phi(x)/a^3$ .

In the following, we relate the so-called *proximal exponent*  $m$  with the two other exponents introduced above,  $\nu$  and  $\varphi$ . First note that the surface value of the monomer volume fraction,  $\phi_s = \phi(x \approx a)$ , for one adsorbed blob follows from the number of monomers at the surface per blob, which is given by  $f_1 g$ , and the cross-section area of a blob, which is of the order of  $D^2$ . The

surface volume fraction is given by

$$\phi_s \sim \frac{f_1 g a^2}{D^2} \sim g^{\varphi-2\nu}. \quad (5.11)$$

Using the scaling prediction Eq. (5.10), we see that the monomer volume fraction at the blob center,  $x \simeq D/2$ , is given by  $\phi(D/2) \sim g^{\varphi-2\nu}(D/a)^{-m}$ , which (again using  $D \sim ag^\nu$ ) can be rewritten as  $\phi(D/2) \simeq g^{\varphi-2\nu-m\nu}$ .

On the other hand, at a distance  $D/2$  from the surface, the monomer volume fraction should have decayed to the average monomer volume fraction  $a^3 g/D^3 \sim g^{1-3\nu}$  inside the blob since the statistics of the chain inside the blob is like for a chain in the bulk. By direct comparison of the two volume fractions, we see that the exponents  $\varphi - 2\nu - m\nu$  and  $1 - 3\nu$  have to match in order to have a consistent result, yielding

$$m = \frac{\varphi + \nu - 1}{\nu}. \quad (5.12)$$

For ideal chain (theta solvents), one has  $\varphi = \nu = 1/2$ . Hence, the proximal exponent vanishes,  $m = 0$ . This means that the proximal exponent has no mean-field analog, explaining why it was discovered only within field-theoretic calculations [2,133]. In the presence of correlations (good solvent conditions) one has  $\varphi \simeq \nu \simeq 3/5$  and thus  $m \simeq 1/3$ .

Using  $D \simeq ag^\nu$  and Eq. (5.9), the surface volume fraction, Eq. (5.11), can be rewritten as

$$\phi_s \sim \left(\frac{D}{a}\right)^{(\varphi-2\nu)/\nu} \sim (a^2 \gamma_1)^{(2\nu-\varphi)/\varphi} \simeq a^2 \gamma_1, \quad (5.13)$$

where in the last approximation appearing in Eq. (5.13) we used the fact that  $\varphi \simeq \nu$ . The last result shows that the surface volume fraction within one blob can become large if the adsorption energy per monomer,  $a^2 \gamma_1$ , measured in units of  $k_B T$ , is of order unity. Experimentally, this is often the case, and additional interactions (such as multi-body interactions) between monomers at the surface have to be taken into account. Note that the polymer concentration in the adsorbed layer can become so high that a transition into a glassy state is induced. This glassy state depends on the details of the molecular interaction, which are not considered here. It should be kept in mind that such high-concentration effects can slow down considerably the adsorption dynamics while prolonging equilibration times [138].

After having discussed the adsorption behavior of a single chain, a word of caution is in order. Experimentally, one never looks at single chains adsorbed to a surface. First, this is due to the fact that one always works with polymer solutions, where there is a large number of polymer chains contained in the bulk reservoir, even when the bulk monomer (or polymer) concentration is quite low. Second, even if the bulk polymer concentration is very low, and in fact so low that polymers in solution barely interact with each other, the surface concentration of polymer is enhanced relative to that in the bulk. Hence, adsorbed polymers at the surface usually do interact with neighboring chains, due to the higher polymer concentration at the surface [137].

Nevertheless, the adsorption behavior of a single chain serves as a basis and guideline for the more complicated adsorption scenarios involving many-chain effects. It will turn out that the scaling of the adsorption layer thickness  $D$  and the proximal volume fraction profile, Eqs. (5.9) and (5.10), are not affected by the presence of other chains. This finding as well as other many-chain effects on polymer adsorption is the subject of Section 7.

## 6. Adsorption of a single polyelectrolyte chain

After reviewing bulk properties of PE solutions we address the complete adsorption diagram of a single semi-flexible PE on an oppositely charged substrate. In contrast to the adsorption of neutral polymers, the resulting phase diagram shows a large region where the adsorbed polymer is flattened out on the substrate and creates a dense adsorption layer.

The results on single PE adsorption summarized in this section are most relevant to the adsorption of highly charged synthetic PEs from dilute solutions [139–144] or the adsorption of rather stiff charged biopolymers such as DNA [145–147]. In all these experiments, the adsorbed phases can be quite dilute, and the description of a single adsorbing polymer is a good starting point. Repeated adsorption of anionic and cationic PEs can lead to well characterized multilayers on planar [148–151] and spherical substrates [152,153]. The adsorption of a single PE chain has been treated theoretically employing a variety of methods [122,154–156]. The adsorption process results from a subtle balance between electrostatic repulsion between charged monomers, leading to chain stiffening, and electrostatic attraction between the substrate and the polymer chain. It poses a much more complicated problem than the corresponding adsorption of neutral polymers.

The adsorption of a single semi-flexible and charged chain on an oppositely charged plane [157] can be treated as a generalization of the adsorption of flexible polymers [122]. A PE characterized by a linear charge density  $\tau$ , is subject to an electrostatic potential created by  $\sigma$ , the homogeneous surface charge density (per unit area). Because this potential is attractive for an oppositely charged substrate, we consider it as the driving force for the adsorption. Effects due to bad solvent [158] and more complex interactions are neglected. One example for the latter are interactions due to the dielectric discontinuity at the substrate surface and to the impenetrability of the substrate for salt ions.<sup>1</sup>

Within the linearized DH theory, the electrostatic potential of a homogeneously charged plane is in units of  $k_B T$

$$V_{\text{plane}}(x) = 4\pi\ell_B\sigma\kappa^{-1}e^{-\kappa x}. \quad (6.1)$$

Assuming that the polymer is adsorbed over a layer of width  $D$  smaller than the screening length  $\kappa^{-1}$ , the electrostatic attraction force per monomer unit length can be written as

$$\hat{f}_{\text{att}} = -4\pi\ell_B\sigma\tau. \quad (6.2)$$

For simplicity, we neglect non-linear effects due to counterion condensation on the PE (as obtained by the Manning theory, see Section 3.3) and on the surface (as obtained within the Gouy–Chapman theory). Although these effects are important for highly charged system [159], most of the important features of single PE adsorption already appear on the linearized Debye–Hückel level.

Because of the confinement in the adsorbed layer, the polymer feels an entropic repulsion. If the layer thickness  $D$  is much smaller than the effective persistence length of the polymer,  $\ell_{\text{eff}}$ , as depicted in Fig. 16a, a new length scale, the so-called deflection length  $\lambda$ , enters the description of the polymer statistics. The deflection length  $\lambda$  measures the average distance between two contact

<sup>1</sup> An ion in solution has a repulsive interaction from the surface when the solution dielectric constant is higher than that of the substrate. This effect can lead to desorption for highly charged PE chains. On the contrary, when the substrate is a metal there is a possibility to induce PE adsorption on non-charged substrates or on substrates bearing charges of the same sign as the PE. See Ref. [157] for more details.

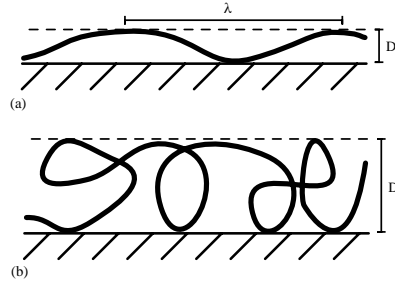


Fig. 16. (a) Schematic picture of the adsorbed polymer layer when the effective persistence length is larger than the layer thickness,  $\ell_{\text{eff}} > D$ . The distance between two contacts of the polymer with the substrate, the so-called deflection length, scales as  $\lambda \sim D^{2/3} \ell_{\text{eff}}^{1/3}$ . (b) Adsorbed layer for the case when the persistence length is smaller than the layer thickness,  $\ell_{\text{eff}} < D$ . In this case the polymer forms a random coil with many loops and a description in terms of a flexible polymer model becomes appropriate.

points of the polymer chain with the substrate. As shown by Odijk, the deflection length scales as  $\lambda \sim D^{2/3} \ell_{\text{eff}}^{1/3}$  and is larger than the layer thickness  $D$  but smaller than the persistence length  $\ell_{\text{eff}}$  [160]. The entropic repulsion follows in a simple manner from the deflection length by assuming that the polymer loses roughly a free energy of one  $k_B T$  per deflection length.

On the other hand, if  $D > \ell_{\text{eff}}$ , as shown in Fig. 16b, the polymer forms a random coil with many loops within the adsorbed layer. The chain can be viewed as an assembly of decorrelated blobs, each of a chain length of  $L \sim D^2 / \ell_{\text{eff}}$ , within which the polymer obeys Gaussian statistics. The decorrelation into blobs has an entropic cost of roughly one  $k_B T$  per blob. The entropic repulsion force per polymer unit length is thus [160]

$$\hat{f}_{\text{rep}} \sim \begin{cases} D^{-5/3} \ell_{\text{eff}}^{-1/3} & \text{for } D \ll \ell_{\text{eff}}, \\ \ell_{\text{eff}} D^{-3} & \text{for } D \gg \ell_{\text{eff}}, \end{cases} \quad (6.3)$$

where we neglected a logarithmic correction factor which is not important for our scaling arguments. As shown in the preceding section, the effective persistence length  $\ell_{\text{eff}}$  depends on the screening length and the line charge density; in essence, one has to keep in mind that  $\ell_{\text{eff}}$  is larger than  $\ell_0$  for a wide range of parameters because of electrostatic stiffening effects.<sup>2</sup>

The equilibrium layer thickness follows from equating the attractive and repulsive forces, Eqs. (6.2) and (6.3). For rather stiff polymers and small layer thickness,  $D < \kappa^{-1} < \ell_{\text{eff}}$ , we obtain

$$D \sim (\ell_B \sigma \tau \ell_{\text{eff}}^{1/3})^{-3/5}. \quad (6.4)$$

<sup>2</sup> The situation is complicated by the fact that the electrostatic contribution to the persistence length is scale dependent and decreases as the chain is bent at length scales smaller than the screening length. This leads to modifications of the entropic confinement force, Eq. (6.3), if the deflection length is smaller than the screening length. As can be checked explicitly, all results reported here are not changed by these modifications.

For a layer thickness corresponding to the screening length,  $D \approx \kappa^{-1}$ , scaling arguments predict a rather abrupt desorption transition [157]. This is in accord with previous calculations [161–165] and simulations [166] for a semi-flexible polymer bound by short-ranged (square-well) potentials. Setting  $D \sim \kappa^{-1}$  in Eq. (6.4), we obtain an expression for the adsorption threshold (for  $\kappa \ell_{\text{eff}} > 1$ )

$$\sigma^* \sim \frac{\kappa^{5/3}}{\tau \ell_B \ell_{\text{eff}}^{1/3}}. \quad (6.5)$$

For  $\sigma > \sigma^*$  the polymer is adsorbed and localized over a layer with a width smaller than the screening length (and with the condition  $\ell_{\text{eff}} > \kappa^{-1}$  also satisfying  $D < \ell_{\text{eff}}$ , indicative of a flat layer). As  $\sigma$  is decreased, the polymer abruptly desorbs at the threshold  $\sigma = \sigma^*$ . In the Gaussian regime, the effective persistence length  $\ell_{\text{eff}}$  is given by the bare persistence length  $\ell_0$  and the desorption threshold is obtained by replacing  $\ell_{\text{eff}}$  by  $\ell_0$  in Eq. (6.5), i.e.

$$\sigma^* \sim \frac{\kappa^{5/3}}{\tau \ell_B \ell_0^{1/3}}. \quad (6.6)$$

In the persistent regime, we have  $\ell_{\text{eff}} \sim \ell_{\text{OSF}}$  with  $\ell_{\text{OSF}}$  given by Eq. (3.11). The adsorption threshold follows from Eq. (6.5) as

$$\sigma^* \sim \frac{\kappa^{7/3}}{\tau^{5/3} \ell_B^{4/3}}. \quad (6.7)$$

Finally, in the Gaussian-persistent regime, we have an effective line charge density from Eq. (3.13) and a modified persistence length, Eq. (3.14). For the adsorption threshold we obtain from Eq. (6.5)

$$\sigma^* \sim \frac{\kappa^{7/3} \ell_0^{5/9}}{\tau^{5/9} \ell_B^{7/9}}. \quad (6.8)$$

Let us now consider the opposite limit,  $\ell_{\text{eff}} < \kappa^{-1}$ .<sup>3</sup> If the layer thickness is larger than the persistence length but smaller than the screening length,  $\ell_{\text{eff}} < D < \kappa^{-1}$ , the prediction for  $D$  obtained from balancing Eqs. (6.2) and (6.3) becomes

$$D \sim \left( \frac{\ell_{\text{eff}}}{\ell_B \sigma \tau} \right)^{1/3}, \quad (6.9)$$

which is in accord with our mean-field result in Eq. (5.4) for a linear potential characterized by  $\tau = -1$  and an ideal polymer chain with  $\nu = 1/2$ . From the expression Eq. (6.9) we see that  $D$  has the same size as the screening length  $\kappa^{-1}$  for

$$\sigma^* \sim \frac{\ell_{\text{eff}} \kappa^3}{\tau \ell_B}. \quad (6.10)$$

This in fact denotes the location of a continuous adsorption transition at which the layer grows to infinity [157]. The scaling results for the adsorption behavior of a flexible polymer, Eqs. (6.9) and (6.10), are in agreement with previous results [155].

<sup>3</sup> From Eq. (6.4) we see that the layer thickness  $D$  is of the same order as  $\ell_{\text{eff}}$  for  $\ell_B \sigma \tau \ell_{\text{eff}}^2 \sim 1$ , at which point the condition  $D \ll \ell_{\text{eff}}$  used in deriving Eq. (6.4) breaks down.

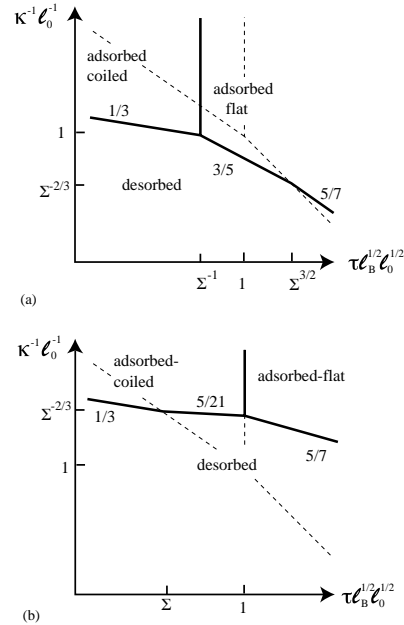


Fig. 17. Adsorption scaling diagram shown on a log–log plot for (a) strongly charged surfaces,  $\Sigma = \sigma \ell_0^{3/2} \ell_B^{1/2} > 1$  and for (b) weakly charged surfaces  $\Sigma < 1$ . We find a desorbed regime, an adsorbed phase where the polymer is flat and dense, and an adsorbed phase where the polymer shows loops. It is seen that a fully charged PE is expected to adsorb as a flat layer, whereas charge-diluted PEs can form coiled layers with loops and dangling ends. The broken lines denote the scaling boundaries of PE chains in the bulk as shown in Fig. 8. The numbers on the lines indicate the power law exponents of the crossover boundaries between the regimes.

In Fig. 17 we show the desorption transitions and the line at which the adsorbed layer crosses over from being flat,  $D < \ell_{\text{eff}}$ , to being crumpled or coiled,  $D > \ell_{\text{eff}}$ . The underlying PE behavior in the bulk, as shown in Fig. 8, is denoted by broken lines. We obtain two different phase diagrams, depending on the value of the parameter

$$\Sigma = \sigma \ell_0^{3/2} \ell_B^{1/2}. \quad (6.11)$$

For strongly charged surfaces,  $\Sigma > 1$ , we obtain the phase diagram as in Fig. 17a, and for weakly charged surfaces,  $\Sigma < 1$ , as in Fig. 17b. We see that strongly charged PEs, obeying  $\tau \sqrt{\ell_0} \ell_B > 1$ , always adsorb in flat layers. The scaling of the desorption transitions is in general agreement with recent computer simulations of charged PEs [167]. Assuming an image-charge repulsion between

the charged monomers and the substrate, as relevant for low-dielectric substrates, some of the phase boundaries in Fig. 17 are eliminated, as explained in Ref. [157]. However, note that not all substrates are low-dielectric materials, so that the full phase structure in Fig. 17 might be relevant to some experiments.

## 7. Neutral polymer adsorption from solution

### 7.1. The mean-field approach: ground state dominance

In this section we look at the equilibrium behavior of many chains adsorbing on (or equivalently depleting from) a surface in contact with a bulk reservoir of chains at equilibrium. The polymer chains in the reservoir are assumed to be in a semi-dilute concentration regime defined by  $c_m > c_m^*$ , where  $c_m$  denotes the monomer concentration (per unit volume) and  $c_m^*$  is the overlap-concentration Eq. (2.19).

As in the previous section, the adsorbing surface is taken as an ideal and smooth plane. Neglecting lateral concentration fluctuations (which will be considered in Section 9), one can reduce the problem to an effective one-dimensional problem, where the monomer concentration depends only on the distance  $x$  from the surface,  $c_m = c_m(x)$ . The two boundary values are:  $c_m^b = c_m(x \rightarrow \infty)$  in the bulk, while  $c_m^s = c_m(x = 0)$  on the surface.

In addition to the monomer concentration  $c_m$ , it is more convenient to work with the monomer volume fraction:  $\phi(x) = a^3 c_m(x)$  where  $a$  is the Kuhn length which characterizes the effective monomer size. While the bulk value (far away from the surface) is fixed by the concentration in the reservoir, the value on the surface at  $x = 0$  is self-adjusting in response to a given surface interaction. The simplest phenomenological surface interaction is linear in the surface polymer concentration. The resulting contribution to the surface free energy (per unit area) is

$$F_s = -\gamma_1 \phi_s, \quad (7.1)$$

where  $\phi_s = a^3 c_m^s$  and a positive (negative) value of  $\gamma_1 = \tilde{\gamma}(T - T^*)/Ta^2$ , defined in Eq. (5.6), enhances adsorption (depletion) of the chains on (from) the surface. However,  $F_s$  represents only the local reduction in the interfacial free energy due to the adsorption. In order to calculate the full interfacial free energy, it is important to note that monomers adsorbing on the surface are connected to other monomers belonging to the same polymer chain. The latter accumulate in the vicinity of the surface. Hence, the interfacial free energy does not only depend on the surface concentration of the monomers but also on their concentration in the *vicinity* of the surface. Due to the polymer flexibility and connectivity, the entire adsorbing layer can have a considerable width. The *total* interfacial free energy of the polymer chains will depend on this width and is quite different from the interfacial free energy for simple molecular liquids.

There are several theoretical frameworks to treat this polymer adsorption. One of the simplest methods which yet gives reasonable qualitative results is the Cahn–de Gennes approach [168,169]. In this approach, it is possible to write down a continuum functional which describes the contribution to the free energy of the polymer chains in the solution. This procedure was introduced by Edwards in the 1960s [112] and was applied to polymers at interfaces by de Gennes [169]. Below we present such a continuum version which can be studied analytically. Another approach is a discrete

one, where the monomers and solvent molecules are put on a lattice. The latter approach is quite useful in computer simulations and numerical self consistent field (SCF) studies and is reviewed elsewhere [1].

In the continuum approach and using a mean-field theory, the bulk contribution to the adsorption free energy is written in terms of the local monomer volume fraction  $\phi(x)$ , neglecting all kinds of monomer–monomer correlations. The total reduction in the surface tension  $\Delta F$  (interfacial free energy per unit area and in units of  $k_B T$ ) is then

$$\Delta F = -\gamma_1 \phi_s + \int_0^\infty dx \left[ G(\phi) \left( \frac{d\phi}{dx} \right)^2 + F_b(\phi) - F_b(\phi_b) + \mu_p(\phi - \phi_b) \right], \quad (7.2)$$

where  $\gamma_1$  was defined in Eq. (7.1). The stiffness function  $G(\phi)$  represents the energy cost of local concentration fluctuations and its form is specific to long polymer chains. For low polymer concentration it can be written as [14]:

$$G(\phi) = \frac{1}{a^3} \left( \frac{a^2}{24\phi} \right). \quad (7.3)$$

The other terms in Eq. (7.2) come from the Cahn–Hilliard free energy of mixing of the polymer solution,  $\mu_p$  being the polymer chemical potential, and [12]

$$F_b(\phi) = \frac{1}{a^3} \left( \frac{\phi}{N} \log \phi + \frac{1}{2} \tilde{v}_2 \phi^2 + \frac{1}{6} \tilde{v}_3 \phi^3 + \dots \right), \quad (7.4)$$

where  $N$  is the polymerization index. In the following, we neglect the first term in Eq. (7.4) (translational entropy), as can be justified in the long chain limit,  $N \gg 1$ . The second and third dimensionless virial coefficients are  $\tilde{v}_2 = v_2/a^3$  and  $\tilde{v}_3 = v_3/a^6$ , respectively. Good, bad and theta solvent conditions are achieved, respectively, for positive, negative or zero  $\tilde{v}_2$ . We concentrate hereafter only on good solvent conditions,  $\tilde{v}_2 > 0$ , in which case the higher order  $\tilde{v}_3$ -term can be safely neglected. In addition, the local monomer density is assumed to be small enough, in order to justify the omission of higher virial coefficients. Note that for small molecules the translational entropy always acts in favor of desorbing from the surface. As was discussed in the Section 1, the vanishing small translational entropy for polymers results in a stronger adsorption (as compared with small solutes) and makes the polymer adsorption much more of an irreversible process.

The key feature in obtaining Eq. (7.2) is the so-called *ground state dominance*, where for long enough chains  $N \gg 1$ , only the lowest energy eigenstate (ground state) of a diffusion-like equation is taken into account. This approximation gives us the leading behavior in the  $N \rightarrow \infty$  limit [118]. It is based on the fact that the weight of the first excited eigenstate is smaller than that of the ground state by an exponential factor:  $\exp(-N \Delta E)$  where  $\Delta E = E_1 - E_0 > 0$  is the difference in the eigenvalues between the two eigenstates. Clearly, close to the surface more details on the polymer conformations can be important. The adsorbing chains have tails (end-sections of the chains that are connected to the surface by only one end), loops (mid-sections of the chains that are connected to the surface by both ends), and trains (sections of the chains that are adsorbed on the surface), as depicted in Fig. 13a. To some extent it is possible to get profiles of the various chain segments even within mean-field theory, if the ground state dominance condition is relaxed as is discussed further below.

Taking into account all those simplifying assumptions and conditions, the mean-field theory for the interfacial free energy can be written as

$$\Delta F = -\gamma_1 \phi_s + \frac{1}{a^3} \int_0^\infty dx \left[ \frac{a^2}{24\phi} \left( \frac{d\phi}{dx} \right)^2 + \frac{1}{2} \tilde{v}_2 (\phi(x) - \phi_b)^2 \right], \quad (7.5)$$

where the monomer bulk chemical potential  $\mu_p$  is given by  $\mu_p = \partial f(\phi)/\partial \phi|_b = \tilde{v}_2 \phi_b$ .

It is also useful to define the total amount of monomers per unit area which take part in the adsorption layer. This is the so-called surface excess  $\Gamma$ ; it is measured experimentally using, e.g., ellipsometry, and is defined as

$$\Gamma = \frac{1}{a^3} \int_0^\infty dx [\phi(x) - \phi_b]. \quad (7.6)$$

(A different quantity, not used in our review, is the so-called adsorbed amount, which measures the total amount of polymers per unit area that have at least one monomer in contact with the substrate.) The next step is to minimize the free energy functional (7.5) with respect to both  $\phi(x)$  and  $\phi_s = \phi(0)$ . For the following algebraic manipulations, it is more convenient to re-express Eq. (7.5) in terms of the square root of the monomer volume fraction,  $\psi(x) = \phi^{1/2}(x)$  and  $\psi_s = \phi_s^{1/2}$

$$\Delta F = -\gamma_1 \psi_s^2 + \frac{1}{a^3} \int_0^\infty dx \left[ \frac{a^2}{6} \left( \frac{d\psi}{dx} \right)^2 + \frac{1}{2} \tilde{v}_2 (\psi^2(x) - \psi_s^2)^2 \right]. \quad (7.7)$$

Minimization of Eq. (7.7) with respect to  $\psi(x)$  and  $\psi_s$  leads to the following profile equation and boundary condition

$$\begin{aligned} \frac{a^2}{6} \frac{d^2 \psi}{dx^2} &= \tilde{v}_2 \psi (\psi^2 - \psi_s^2), \\ \frac{1}{\psi_s} \frac{d\psi}{dx} \Big|_s &= -6a\gamma_1 = -\frac{1}{2D}. \end{aligned} \quad (7.8)$$

The second equation sets a boundary condition on the logarithmic derivative of the monomer volume fraction,  $d \log \phi/dx|_s = 2\psi^{-1} d\psi/dx|_s = -1/D$ , where the strength of the surface interaction  $\gamma_1$  can be expressed in terms of a length  $D \equiv 1/(12a\gamma_1)$ . Note that exactly the same scaling of  $D$  on  $\gamma_1/T$  is obtained in Eq. (5.9) for the single chain behavior if one sets  $v = \phi = 1/2$  (ideal chain exponents). This is strictly valid at the upper critical dimension ( $d = 4$ ) and is a very good approximation in three dimensions.

The profile equation (7.8) can be integrated once, yielding

$$\frac{a^2}{6} \left( \frac{d\psi}{dx} \right)^2 = \frac{1}{2} \tilde{v}_2 (\psi^2 - \psi_s^2)^2. \quad (7.9)$$

The above differential equation can now be solved analytically for adsorption ( $\gamma_1 > 0$ ) and depletion ( $\gamma_1 < 0$ ).

We first present the results in more detail for polymer adsorption and then repeat the main findings for polymer depletion.

### 7.1.1. The adsorption case

Setting  $\gamma_1 > 0$  as is applicable for the adsorption case, the first-order differential equation (7.9) can be integrated and together with the boundary condition Eq. (7.8) yields

$$\phi(x) = \phi_b \coth^2 \left( \frac{x + x_0}{\xi_b} \right), \quad (7.10)$$

where the length  $\xi_b = a(3\bar{v}_2\phi_b)^{-1/2}$  is the Edwards correlation length characterizing the exponential decay of concentration fluctuations in the bulk [14,112]. (See also the discussion in Section 7.2). The length  $x_0$  is not an independent length since it depends on  $D$  and  $\xi_b$ , as can be seen from the boundary condition Eq. (7.8)

$$x_0 = \frac{\xi_b}{2} \operatorname{arcsinh} \left( \frac{4D}{\xi_b} \right) = \xi_b \operatorname{arccoth}(\sqrt{\phi_s/\phi_b}). \quad (7.11)$$

Furthermore,  $\phi_s$  can be directly related to the surface interaction  $\gamma_1$  and the bulk value  $\phi_b$

$$\frac{\xi_b}{2D} = \frac{6a^2\gamma_1}{\sqrt{3\bar{v}_2\phi_b}} = \sqrt{\frac{\phi_b}{\phi_s} \left( \frac{\phi_s}{\phi_b} - 1 \right)}. \quad (7.12)$$

In order to be consistent with the semi-dilute concentration regime, the correlation length  $\xi_b$  should be smaller than the size of a single chain,  $R = aN^\nu$ , where  $\nu = 3/5$  is the Flory exponent in good solvent conditions. This sets a lower bound on the polymer concentration in the bulk,  $c_m > c_m^*$ .

So far three length scales have been introduced: the Kuhn length or monomer size  $a$ , the adsorbed-layer width  $D$ , and the bulk correlation length  $\xi_b$ . It is more convenient for the discussion to consider the case where those three length scales are quite separated:  $a \ll D \ll \xi_b$ . Two conditions must be satisfied. On one hand, the adsorption parameter is not large,  $12a^2\gamma_1 \ll 1$  in order to have  $D \gg a$ . On the other hand, the adsorption energy is large enough to satisfy  $12a^2\gamma_1 \gg \sqrt{3\bar{v}_2\phi_b}$  in order to have  $D \ll \xi_b$ . The latter inequality can be regarded also as a condition for the polymer bulk concentration. The bulk correlation length is large enough if indeed the bulk concentration (assumed to be in the semi-dilute concentration range) is not too large. Roughly, let us assume in a typical case that the three length scales are well separated:  $a$  is of the order of a few Angstroms,  $D$  of the order of a few dozens of Angstroms, and  $\xi_b$  of the order of a few hundred Angstroms.

When the above two inequalities are satisfied, three spatial regions of adsorption can be differentiated: the proximal, central, and distal regions, as is outlined below. In addition, as soon as  $\xi_b \gg D$ ,  $x_0 \simeq 2D$ , as follows from Eq. (7.11).

(i) Close enough to the surface,  $x \sim a$ , the adsorption profile depends on the details of the short range interactions between the surface and monomers. Hence, this region is not universal. In the proximal region, for  $a \gg x \gg D$ , corrections to the mean-field theory analysis (which assumes the concentration to be constant) are presented below similarly to the treatment of the single chain section. These corrections reveal a new scaling exponent characterizing the concentration profile. They are of particular importance close to the adsorption/desorption transition.

(ii) In the distal region,  $x \gg \xi_b$ , the excess polymer concentration decays exponentially to its bulk value

$$\phi(x) - \phi_b \simeq 4\phi_b e^{-2x/\xi_b}, \quad (7.13)$$

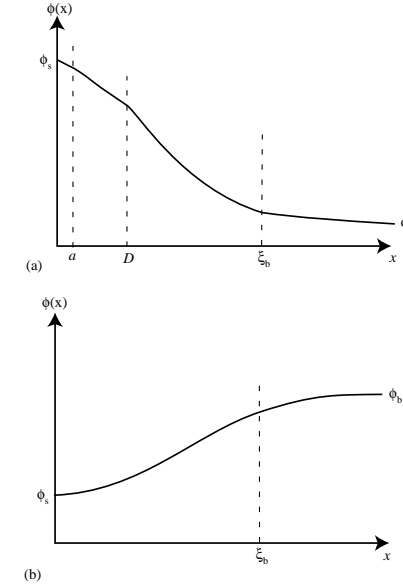


Fig. 18. (a) The schematic monomer volume fraction profile for the case of adsorption from a semi-dilute solution; we distinguish a layer of molecular thickness  $x \sim a$  where the polymer density depends on details of the interaction with the substrate and the monomer size, the proximal region  $a < x < D$  where the decay of the density is governed by a universal power law (which cannot be obtained within mean-field theory), the central region for  $D < x < \xi_b$  with a self-similar profile, and the distal region for  $\xi_b < x$ , where the monomer volume fraction relaxes exponentially towards its bulk value  $\phi_b$ . (b) The density profile for the case of depletion, where the concentration close to the surface is  $\phi_s$  and relaxes to its bulk value,  $\phi_b$ , at a distance of the order of the bulk correlation length  $\xi_b$ .

as follows from Eq. (7.10). This behavior is very similar to the decay of fluctuations in the bulk with  $\xi_b$  being the correlation length.

(iii) Finally, in the central region (and with the assumption that  $\xi_b$  is the largest length scale in the problem),  $D \ll x \ll \xi_b$ , the profile is universal and from Eq. (7.10) it can be shown to decay with a power law

$$\phi(x) = \frac{1}{3\bar{v}_2} \left( \frac{a}{x + 2D} \right)^2. \quad (7.14)$$

A sketch of the different scaling regions in the adsorption profile is given in Fig. 18a. Included in this figure are corrections in the proximal region, which is discussed further below.

A special consideration should be given to the formal limit of setting the bulk concentration to zero,  $\phi_b \rightarrow 0$  (and equivalently  $\xi_b \rightarrow \infty$ ), which denotes the limit of an adsorbing layer in contact

with a polymer reservoir of vanishing concentration. It should be emphasized that this limit is not consistent with the assumption of a semi-dilute polymer solution in the bulk. Still, some information on the polymer density profile close to the adsorbing surface, where the polymer solution is locally semi-dilute [137], can be obtained. Formally, we take the limit  $\xi_b \rightarrow \infty$  in Eq. (7.10), and the limiting expression, given by Eq. (7.14), does not depend on  $\xi_b$ . The profile in the central region decays algebraically. In the case of zero polymer concentration in the bulk, the natural cutoff is not  $\xi_b$  but rather  $R$ , the coil size of a single polymer in solution. Hence, the distal region loses its meaning and is replaced by a more complicated scaling regime [170]. The length  $D$  can be regarded as the layer thickness in the  $\xi_b \rightarrow \infty$  limit in the sense that a finite fraction of all the monomers are located in this layer of thickness  $D$  from the surface. Another observation is that  $\phi(x) \sim 1/x^2$  for  $x \gg D$ . This power law is a result of the mean-field theory and its modification is discussed below.

It is now possible to calculate within the mean-field theory the two physical quantities that are measured in many experiments: the surface tension reduction  $\Delta F$  and the surface excess  $\Gamma$ .

The surface excess, defined in Eq. (7.6), can be calculated in a close form by inserting Eq. (7.10) into Eq. (7.6),

$$\Gamma = \frac{1}{\sqrt{3\bar{v}_2}a^2} (\phi_s^{1/2} - \phi_b^{1/2}) = \frac{\xi_b \phi_b}{a^3} \left( \sqrt{\frac{\phi_s}{\phi_b}} - 1 \right). \quad (7.15)$$

For strong adsorption, we obtain from Eq. (7.12) that  $\phi_s \simeq (a/2D)^2/3\bar{v}_2 \gg \phi_b$ , and Eq. (7.15) reduces to

$$\Gamma = \frac{1}{3\bar{v}_2 a^2} \left( \frac{a}{D} \right) \sim \gamma_1, \quad (7.16)$$

while the surface volume fraction scales as  $\phi_s \sim \gamma_1^2$ . As can be seen from Eqs. (7.16) and (7.14), the surface excess as well as the entire profile does not depend (to leading order) on the bulk concentration  $\phi_b$ . We note again that the strong adsorption condition is always satisfied in the  $\phi_b \rightarrow 0$  limit. Hence, Eq. (7.16) can be obtained directly by integrating the profile in the central region, Eq. (7.14).

Finally, let us calculate the reduction in surface tension for the adsorbing case. Inserting the variational equations (7.8) in Eq. (7.5) yields

$$\Delta F = -\gamma_1 \phi_s + \frac{\sqrt{3\bar{v}_2}}{9a^2} \phi_s^{3/2} \left[ 1 - 3 \left( \frac{\phi_b}{\phi_s} \right) + 2 \left( \frac{\phi_b}{\phi_s} \right)^{3/2} \right]. \quad (7.17)$$

The surface term in Eq. (7.17) is negative while the second term is positive. For strong adsorption this reduction of  $\Delta F$  does not depend on  $\phi_b$  and reduces to

$$\Delta F \sim -(\alpha^2 \gamma_1)^3 \frac{1}{a^2} + \mathcal{O}(\gamma_1^{4/3}), \quad (7.18)$$

where the leading term is just the contribution of the surface monomers.

### 7.1.2. The depletion case

We highlight the main differences between the polymer adsorption and polymer depletion. Keeping in mind that  $\gamma_1 < 0$  for depletion, the solution of the same profile equation (7.9), with the appropriate

boundary condition results in

$$\phi(x) = \phi_b \tanh^2 \left( \frac{x + x_0}{\xi_b} \right), \quad (7.19)$$

which is schematically plotted in Fig. 18b. The limit  $\phi_b \rightarrow 0$  cannot be taken in the depletion case since depletion with respect to a null reservoir has no meaning. However, we can, alternatively, look at the strong depletion limit, defined by the condition  $\phi_s \ll \phi_b$ . Here we find

$$\phi(x) = 3\bar{v}_2 \phi_b^2 \left( \frac{x + 2D}{a} \right)^2. \quad (7.20)$$

In the same limit, we find for the surface volume fraction  $\phi_s \sim \phi_b^2 \gamma_1^{-2}$ , and the exact expression for the surface excess Eq. (7.15) reduces to

$$\Gamma = -\frac{1}{a^2} \sqrt{\frac{\phi_b}{3\bar{v}_2}} \simeq -\frac{\phi_b \xi_b}{a^3}. \quad (7.21)$$

The negative surface excess can be directly estimated from a profile varying from  $\phi_b$  to zero over a length scale of order  $\xi_b$ .

The dominating behavior for the surface tension can be calculated from Eq. (7.5) where both terms are now positive. For the strong depletion case we get

$$\Delta F \simeq \frac{1}{a^2} \left( \frac{a}{\xi_b} \right)^3 \sim \phi_b^{3/2}. \quad (7.22)$$

## 7.2. Beyond mean-field theory: scaling arguments for good solvents

One of the mean-field theory results that should be corrected is the scaling of the correlation length with  $\phi_b$ . In the semi-dilute regime, the correlation length can be regarded as the average mesh size created by the overlapping chains. It can be estimated using very simple scaling arguments [14] similar to our derivation of the overlap concentration in Eq. (2.19). The volume fraction of monomers inside a coil formed by a subchain consisting of  $g$  monomers embedded in  $d$  dimensional space is  $\phi_b \sim g^{1-d\nu}$  where  $\nu$  is the Flory exponent. The spatial scale of this subchain is given by  $\xi_b \sim ag^\nu$ . Combining these two relations we obtain the general scaling of the correlation length

$$\xi_b \simeq a \phi_b^{\nu/(1-d\nu)}, \quad (7.23)$$

and for good solvent condition and  $d = 3$

$$\xi_b \simeq a \phi_b^{-3/4}. \quad (7.24)$$

This relation corrects the mean-field theory result  $\xi_b \sim \phi_b^{-1/2}$  which can be obtained from, e.g., Eq. (7.5), and also directly from Eq. (7.23) by setting  $d=4$  and inserting the Gaussian exponent  $\nu=1/2$ .

### 7.2.1. Scaling for polymer adsorption

We repeat here an argument due to de Gennes [169]. The main idea is to assume that the relation Eq. (7.23) holds locally:  $\phi(x) = [\xi(x)/a]^{-4/3}$ , where  $\xi(x)$  is the local ‘‘mesh size’’ of the semi-dilute polymer solution. Since there is no other length scale in the problem beside the distance from the

surface,  $x$ , the correlation length  $\zeta(x)$  should scale as the distance  $x$  itself,  $\zeta(x) \simeq x$  leading to the profile

$$\phi(x) \simeq \left(\frac{a}{x}\right)^{4/3}. \quad (7.25)$$

We note that this argument holds only in the central region  $D \ll x \ll \zeta_b$ . It has been confirmed experimentally using neutron scattering [171] and neutron reflectivity [172]. Eq. (7.25) satisfies the distal boundary condition:  $x \rightarrow \zeta_b$ ,  $\phi(x) \rightarrow \phi_b$ , but for  $x > \zeta_b$  we expect the regular exponential decay behavior of the distal region, Eq. (7.13). De Gennes also proposed (without a rigorous proof) a convenient expression for  $\phi(x)$ , which has the correct crossover from the central to the mean-field proximal region [169]

$$\phi(x) = \phi_s \left( \frac{\frac{4}{3}D}{x + \frac{4}{3}D} \right)^{4/3} \simeq \left( \frac{a}{x + \frac{4}{3}D} \right)^{4/3}. \quad (7.26)$$

Note that the above equation reduces to Eq. (7.25) for  $x \gg D$ . The extrapolation of Eq. (7.26) also gives the correct definition of  $D$ :  $D^{-1} = -d \log \phi / dx|_s$ . In addition,  $\phi_s$  is obtained from the extrapolation to  $x = 0$  and scales as

$$\phi_s = \phi(x = 0) = \left(\frac{a}{D}\right)^{4/3}. \quad (7.27)$$

For strong adsorption ( $\phi_s \gg \phi_b$ ), we have

$$\begin{aligned} \phi_s &\simeq \left(\frac{a}{D}\right)^{4/3} \sim \gamma_1^2, \\ D &\simeq a \left(\frac{1}{a^2 \gamma_1}\right)^{3/2} \sim \gamma_1^{-3/2}, \\ \Gamma &\simeq a^{-2} (a^2 \gamma_1)^{1/2} \sim \gamma_1^{1/2}, \\ \Delta F &\simeq -\frac{1}{a^2} \phi_s^{3/2} \sim -\gamma_1^3. \end{aligned} \quad (7.28)$$

It is interesting to note that although  $D$  and  $\Gamma$  have different scaling with the surface interaction  $\gamma_1$  in the mean-field theory and scaling approaches,  $\phi_s$  and  $\Delta F$  have the same scaling using both approaches. This is a result of the same scaling  $\phi_s \sim \gamma_1^2$ , which, in turn, leads to  $\Delta F \simeq \gamma_1 \phi_s \sim \gamma_1^3$ .

### 7.2.2. Scaling for polymer depletion

For polymer depletion similar arguments led de Gennes [169] to propose the following scaling form for the central and mean-field proximal regions,  $a < x < \zeta_b$ ,

$$\phi(x) = \phi_b \left( \frac{x + \frac{5}{3}D}{\zeta_b} \right)^{5/3}, \quad (7.29)$$

where the depletion thickness is  $\zeta_b - D$  whereas in the strong depletion regime ( $\phi_s \ll \phi_b$ )

$$\begin{aligned} \phi_s &\simeq \phi_b \left( \frac{D}{\zeta_b} \right)^{5/3} \sim \phi_b^{9/4} \gamma_1^{-5/2}, \\ D &= a (a^2 \gamma_1)^{-3/2}, \\ \Gamma &\simeq -\phi_b a^{-3} (\zeta_b - D) \sim \phi_b^{1/4}, \\ \Delta F &\simeq \frac{1}{a^2} \phi_b^{3/2}. \end{aligned} \quad (7.30)$$

Note that the above scaling of the surface tension with the bulk concentration,  $\phi_b$  is the same as that obtained by the mean-field theory approach in Section 7.1.2, Eq. (7.22).

### 7.3. Proximal region corrections

So far we did not address any corrections in the proximal region:  $a < x < D$  for the many chain adsorption. In the mean-field theory picture the profile in the proximal region is featureless and saturates smoothly to its extrapolated surface value,  $\phi_s > 0$ . However, in relation to surface critical phenomena which is in particular relevant close to the adsorption–desorption phase transition (the so-called ‘special’ transition), the polymer profile in the proximal region has a scaling form with another exponent  $m$ .

$$\phi(x) \simeq \phi_s \left(\frac{a}{x}\right)^m, \quad (7.31)$$

where  $m = (\varphi + \nu - 1)/\nu$  is the proximal exponent, Eq. (5.12). This is similar to the single chain treatment in Section 5.

For good solvents, one has  $m \simeq 1/3$ , as was derived using analogies with surface critical phenomena, exact enumeration of polymer configurations, and Monte-Carlo simulations [133]. It is different from the exponent 4/3 of the central region.

With the proximal region correction, the polymer profile can be written as [135]

$$\phi(x) \simeq \begin{cases} \phi_s & \text{for } 0 < x < a, \\ \phi_s \left(\frac{a}{x}\right)^{1/3} & \text{for } a < x < D, \\ \phi_s \left(\frac{a}{x}\right)^{1/3} \left(\frac{D}{x+D}\right) & \text{for } D < x < \zeta_b, \end{cases} \quad (7.32)$$

where

$$\phi_s = \frac{a}{D}. \quad (7.33)$$

The complete adsorption profile is shown schematically in Fig. 18a. By minimization of the free energy with respect to the layer thickness  $D$  it is possible to show that  $D$  is proportional to  $1/\gamma_1$

$$D \sim \gamma_1^{-1}, \quad (7.34)$$

in accord with the exact field-theoretic results for a single chain as discussed in Section 5.

The surface concentration, surface excess and surface tension have the following scaling [135]:

$$\begin{aligned}\phi_s &\simeq \frac{a}{D} \sim \gamma_1, \\ \Gamma &\simeq a^{-3} D \left(\frac{a}{D}\right)^{4/3} \sim \gamma_1^{1/3}, \\ \Delta F &\simeq -\gamma_1^2 a^2 \sim \gamma_1^2.\end{aligned}\quad (7.35)$$

Note the differences in the scaling of the surface tension and surface excess in Eq. (7.35) as compared with the results obtained with no proximity exponent ( $m = 0$ ) in the previous section, Eq. (7.28).

At the end of our discussion of polymer adsorption from solutions, we would like to add that for the case of adsorption from dilute solutions, there is an intricate crossover from the single-chain adsorption behavior, as discussed in Section 5, to the adsorption from semi-dilute polymer solutions, as discussed in this section [137]. Since the two-dimensional adsorbed layer has a higher local polymer concentration than the bulk, it is possible that the adsorbed layer forms a two-dimensional semi-dilute state, while the bulk is a truly dilute polymer solution. Only for extremely low bulk concentration or for very weak adsorption energies the adsorbed layer has a single-chain structure with no chain crossings between different polymer chains.

#### 7.4. Loops and tails

It has been realized quite some time ago that the so-called central region of an adsorbed polymer layer is characterized by a rather broad distribution of loop and tail sizes [1,173,174]. A loop is defined as a chain region located between two points of contact with the adsorbing surface, and a tail is defined as the chain region between the free end and the closest contact point to the surface, while a train denotes a chain section which is tightly bound to the substrate (see Fig. 13a). The relative statistical weight of loops and tails in the adsorbed layer is clearly of importance to applications. For example, it is expected that polymer loops which are bound at both ends to the substrate are more prone to entanglements with free polymers than tails and, thus, lead to enhanced friction effects. It was found in detailed numerical mean-field theory calculations that the external part of the adsorbed layer is dominated by dangling tails, while the inner part is mostly built up by loops [1,173].

Recently, an analytical theory was formulated which correctly takes into account the separate contributions of loops and tails and which thus goes beyond the *ground state dominance* assumption made in ordinary mean-field theories. The theory predicts that a crossover between tail-dominated and loop-dominated regions occurs at some distance  $x^* \simeq aN^{1/(d-1)}$  [175] from the surface, where  $d$  is the dimension of the embedding space. It is well known that mean-field theory behavior can formally be obtained by setting the embedding dimensionality equal to the upper critical dimension, which is for self-avoiding polymers given by  $d = 4$  [15]. Hence, the above expression predicts a crossover in the adsorption behavior at a distance  $x^* \simeq aN^{1/3}$ . For good-solvent conditions in three dimensions ( $d = 3$ ),  $x^* \simeq aN^{1/2}$ . In both cases, the crossover occurs at a separation much smaller than the size of a free polymer  $R \sim aN^\nu$  where, according to the classical Flory argument [12],  $\nu = 3/(d + 2)$ .

A further rather subtle result of these improved mean-field theories is the occurrence of a depletion hole, i.e., a region at a certain separation from the adsorbing surface where the monomer

concentration is smaller than the bulk concentration [175]. This depletion hole results from an interplay between the depletion of free polymers from the adsorbed layer and the slowly decaying density profile due to dangling tails. It occurs at a distance from the surface comparable with the radius of gyration of a free polymer, but also shows some dependence on the bulk polymer concentration. In a different formulation, the interfacial free energy of an adsorbed layer consisting of finite-length polymers has been calculated for the full concentration range from dilute to dense solutions [176]. These and other effects, related to the occurrence of loops and tails in the adsorbed layer, have been recently reviewed [177].

## 8. Adsorption of polyelectrolytes—mean field

In Section 6 we have been reviewing the behavior of single PE chains close to a charged wall (or surface). This will be now extended to include adsorption of PE from bulk (semi-dilute) solutions having a bulk concentration  $c_m^b$ . As before the chains are assumed to have a fraction  $f$  of charged monomers, each carrying a charge  $e$  resulting in a linear charge density,  $\tau = f/b$ . The interesting case of *polyampholytes* having negative and positive charges is not considered in this section. The solution can also contain salt (small ions) of concentration  $c_{\text{salt}}$  which is directly related to the Debye–Hückel screening length,  $\kappa^{-1}$ . For simplicity, the salt is assumed throughout this section to be monovalent ( $z = 1$ ).

We will consider adsorption only onto a single flat and charged surface. Clearly the most important quantity is the profile of the polymer concentration,  $c_m(x) = \phi(x)/a^3$ , as function of  $x$ , the distance from the surface. Another useful quantity mentioned already in Section 7 is the polymer surface excess (per unit area)

$$\Gamma = \int_0^\infty [c_m(x) - c_m^b] dx = \frac{1}{a^3} \int_0^\infty [\phi(x) - \phi_b] dx. \quad (8.1)$$

Related to the surface excess  $\Gamma$  is the amount of charges (in units of  $e$ ) carried by the adsorbing PE chains,  $f\Gamma$ . In some cases the adsorbed polymer layer carries a higher charge (per unit area) than the charged surface itself,  $f\Gamma > \sigma$ , and the surface charge is overcompensated by the PE as we will see later. This does not violate global charge neutrality in the system because of the presence of counterions in solution.

In many experiments, the total amount of polymer surface excess  $\Gamma$  is measured as a function of the bulk polymer concentration, pH and/or ionic strength of the bulk solution [178–185]. (For reviews see, e.g. Refs. [1,186–188].) More recently, spectroscopy [180] and ellipsometry [184] have been used to measure the width of the adsorbed PE layer. Other techniques such as neutron scattering can be employed to measure the entire profile  $c_m(x)$  of the adsorbed layer [172,189].

Electrostatic interactions play a crucial role in the adsorption of PEs [1,186,187]. Besides the fraction  $f$  of charged monomers, the important parameters are the surface charge density (or surface potential in case of conducting surfaces), the amount of salt (ionic strength of low molecular weight electrolyte) in solution and, in some cases, the solution pH.

For PEs the electrostatic interactions between the monomers themselves (same charges) are always repulsive, leading to an effective stiffening of the chain [22,23]. Hence, this interaction will *favor* the adsorption of single polymer chains, because their configurations are already quite extended [157],

but it will *oppose* the formation of dense adsorption layers close to the surface [1]. If the PE chains and the surface are oppositely charged, the electrostatic interactions between them will *enhance* the adsorption. In addition, the presence of salt has a subtle effect. It simultaneously screens the monomer–monomer repulsive interactions as well as the attractive interactions between the oppositely charged surface and polymer. Presence of multivalent salt ions (not considered in this section) makes the PE adsorption even more complex.

Two limiting adsorbing cases can be discussed separately: (i) a non-charged surface on which the chains like to adsorb due to, e.g., van-der-Waals attraction. Here the interaction between the surface and the chain does not have an electrostatic component. However, as the salt screens the monomer–monomer electrostatic repulsion, it leads to enhancement of the adsorption. (ii) The surface is charged but does not interact with the polymer besides the electrostatic interaction. This is called the pure electro-sorption case. At low-salt concentration, the polymer charge completely compensates the surface charge. At high-salt concentration some of the compensation is done by the salt, leading to a decrease in the amount of adsorbed polymer. In some cases, over-compensation of the surface charges by the polymer charges can also occur (as is reviewed below in Section 8.5), where the PE chains form a condensed layer and reverse the sign of the total surface charge. This is used, e.g., to build a multi-layered structure of cationic and anionic PEs—a process that can be continued for few dozen or even few hundred times [150,153]. The phenomenon of over-compensation is discussed in Refs. [157,190–193] but is still not well understood.

In practice, electrostatic and other types of interactions with the surface can occur in parallel, making the analysis more complex. In spite of the difficulties to treat theoretically PE's in solution because of the delicate interplay between the chain connectivity and the long range nature of electrostatic interactions [8,14,194,195], several simple approaches treating adsorption exist. One approach is a discrete *multi-Stern layer* model [196–200], where the system is placed on a lattice whose sites can be occupied by a monomer, a solvent molecule or a small ion. The electrostatic potential is determined self-consistently (mean-field theory) together with the concentration profiles of the polymer and the small ions. In another approach, the electrostatic potential and the PE concentration are treated as continuous functions [155,191,201–206]. These quantities are obtained from two coupled differential equations derived from the total free energy of the system. In some cases the salt concentration is considered explicitly [202,203], while in other works, (e.g., in Refs. [155,157]) it induces a screened Coulombic interaction between the monomers and the substrate. We will review the main results of the continuum approach, presenting numerical solutions of the mean field equations and scaling arguments.

### 8.1. Mean-field theory and its profile equations

The charge density on the polymer chains is assumed to be continuous and uniformly distributed along the chains. Further treatments of the polymer charge distribution (annealed and quenched models) can be found in Refs. [203,205]. Within mean-field approximation, the free energy of the system can be expressed in terms of the local electrostatic potential  $U(\mathbf{r})$ , the local monomer concentration  $c_m(\mathbf{r})$  and the local concentration of positive and negative ions  $c^\pm(\mathbf{r})$ . The mean-field approximation means that the influence of the charged surface and the inter and intra-chain interactions can be expressed in term of an external potential which will determine the local concentration of the monomers,  $c_m(\mathbf{r})$ . This external potential depends both on the electrostatic potential and on

the excluded volume interactions between the monomers and the solvent molecules. The excess free energy with respect to the bulk can then be calculated using another important approximation, the ground state dominance. This approximation is used often for neutral polymers [14] (see Section 7) and is valid for very long polymer chains,  $N \gg 1$ . As before, we introduce the (dimensionless) polymer order parameter  $\psi(\mathbf{r})$ , where  $\psi(\mathbf{r}) = \sqrt{\phi(\mathbf{r})} = \sqrt{a^3 c_m(\mathbf{r})}$ , and express the adsorption free energy  $\mathcal{F}$  (in units of  $k_B T$ ) in terms of  $\psi$  and  $U$  [201–206]

$$\mathcal{F} = \int d\mathbf{r} \{ F_{\text{pol}}(\mathbf{r}) + F_{\text{ions}}(\mathbf{r}) + F_{\text{el}}(\mathbf{r}) \}. \quad (8.2)$$

The polymer contribution is

$$F_{\text{pol}}(\mathbf{r}) = \frac{a^2}{6} |\nabla \psi|^2 + \frac{1}{2} \tilde{v}_2 (\psi^4 - \psi_b^4) - \mu_p (\psi^2 - \psi_b^2), \quad (8.3)$$

where the first term is the polymer elastic energy. Throughout this section we restrict ourselves to flexible chains described by a Kuhn length  $a$ . The second term is the excluded volume contribution where the dimensionless second virial coefficient  $\tilde{v}_2$  is positive and of order unity. The case of negative virial coefficients (bad-solvent condition) has been treated in Ref. [207]. The last term couples the system to a polymer reservoir via a chemical potential  $\mu_p$ , and  $\psi_b = \sqrt{\phi_b}$  is related to the bulk monomer concentration,  $c_m^b = \phi_b/a^3$ .

The entropic contribution of the small (monovalent) ions is

$$F_{\text{ions}}(\mathbf{r}) = \sum_{i=\pm} [c^i \ln c^i - c^i - c_{\text{salt}} \ln c_{\text{salt}} + c_{\text{salt}}] - \mu^i (c^i - c_{\text{salt}}), \quad (8.4)$$

where  $c^i(\mathbf{r})$  and  $\mu^i$  are, respectively, the local concentration and the chemical potential of the  $i = \pm$  ions, while  $c_{\text{salt}}$  is the bulk concentration of salt.

Finally, the electrostatic contributions (per  $k_B T$ ) are

$$F_{\text{el}}(\mathbf{r}) = \left[ f e \psi^2 U + e c^+ U - e c^- U - \frac{\epsilon}{8\pi} |\nabla U|^2 \right] / k_B T. \quad (8.5)$$

The first three terms are the electrostatic energies of the monomers (carrying  $f$  fractional charge per monomer), the positive ions and the negative ions, respectively. The last term is the self-energy of the electric field, where  $\epsilon$  is the dielectric constant of the solution. Note that the electrostatic contribution, Eq. (8.5), is equivalent to the well known result:  $(\epsilon/8\pi k_B T) \int d\mathbf{r} |\nabla U|^2$  plus surface terms. This can be seen by substituting the Poisson–Boltzmann equation (as obtained below) into Eq. (8.5) and then integrating by parts.

Minimization of the free energy Eqs. (8.2)–(8.5) with respect to  $c^\pm$ ,  $\psi$  and  $U$  yields a Boltzmann distribution for the density of the small ions,  $c^\pm(\mathbf{r}) = c_{\text{salt}} \exp(\mp eU/k_B T)$ , and two coupled differential equations for  $\psi$  and  $U$ :

$$\nabla^2 U(\mathbf{r}) = \frac{8\pi e}{\epsilon} c_{\text{salt}} \sinh(eU/k_B T) - \frac{4\pi e}{\epsilon} (f\psi^2 - f\psi_b^2 e^{eU/k_B T}), \quad (8.6)$$

$$\frac{a^2}{6} \nabla^2 \psi(\mathbf{r}) = \tilde{v}_2 (\psi^3 - \psi_b^2 \psi) + f\psi eU/k_B T. \quad (8.7)$$

Eq. (8.6) is a generalized Poisson–Boltzmann equation including the free ions as well as the charged polymers. The first term represents the salt contribution and the second term is due to the charged monomers and their counterions. Eq. (8.7) is a generalization of the self-consistent field equation of neutral polymers Eq. (7.8) [14]. In the bulk, the above equations are satisfied by setting  $U \rightarrow 0$  and  $\psi \rightarrow \psi_b$ .

## 8.2. Constant $U_s$ : the low-salt limit

### 8.2.1. Numerical solutions of mean-field equations

When the surface is taken as ideal, i.e., flat and homogeneous, the solutions of the mean-field equations depend only on the distance  $x$  from the surface. The surface imposes boundary conditions on the polymer order parameter  $\psi(x)$  and the electrostatic potential  $U(x)$ . Due to global electroneutrality, all charge carriers in solution should exactly balance the surface charges. The Poisson–Boltzmann equation (8.6), the self-consistent field equation (8.7) and the boundary conditions uniquely determine the polymer concentration profile and the electrostatic potential. In all cases of interest, these two coupled non-linear equations can only be solved numerically.

We present now numerical profiles obtained for surfaces with a constant potential  $U_s$ :

$$U|_{x=0} = U_s. \quad (8.8)$$

The boundary conditions for  $\psi(x)$  depend on the nature of the short range non-electrostatic interaction of the monomers and the surface. For simplicity, we take a non-adsorbing surface and require that the monomer concentration will vanish there:

$$\psi|_{x=0} = 0. \quad (8.9)$$

We note that the boundary conditions chosen in Eqs. (8.8) and (8.9) model the particular situation of electrostatic attraction at constant surface potential in competition with a steric (short range) repulsion of non-electrostatic origin. Possible variations of these boundary conditions include surfaces with a constant surface charge (discussed below) and surfaces with a non-electrostatic short range attractive (or repulsive) interaction with the polymer [190,209]. Far from the surface ( $x \rightarrow \infty$ ) both  $U$  and  $\psi$  reach their bulk values and their derivatives vanish:  $U'|_{x \rightarrow \infty} = 0$  and  $\psi'|_{x \rightarrow \infty} = 0$ .

The numerical solutions of the mean-field equations (8.6), (8.7) together with the boundary conditions discussed above are presented in Fig. 19, for several different physical parameters in the low-salt limit. The polymer is positively charged and is attracted to the non-adsorbing surface held at a constant negative potential. The aqueous solution contains a small amount of monovalent salt ( $c_{\text{salt}} = 0.1$  mM). The reduced concentration profile  $\phi(x)/\phi_b$  is plotted as a function of the distance from the surface  $x$ . Different curves correspond to different values of the reduced surface potential  $u_s \equiv eU_s/k_B T$ , the charge fraction  $f$  and the Kuhn length  $a$ . Although the spatial variation of the profiles differs in detail, they all have a single peak which can be characterized by its height and width. This observation serves as a motivation to using scaling arguments.

### 8.2.2. Scaling arguments

The numerical profiles of the previous section indicate that it may be possible to obtain simple analytical results for the PE adsorption by assuming that the adsorption is characterized by one

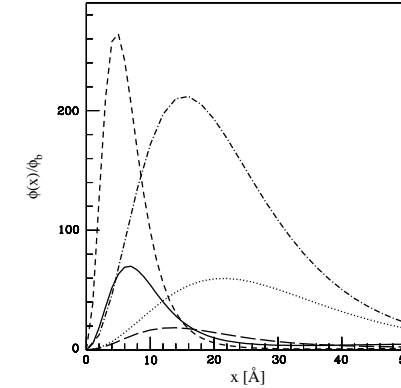


Fig. 19. Adsorption profiles obtained by numerical solutions of Eqs. (8.6), (8.7) for several sets of physical parameters in the low-salt limit. The monomer volume fraction  $\phi(x)$  scaled by its bulk value  $\phi_b = \psi_b^2$  is plotted as a function of the distance  $x$  from the surface. The different curves correspond to:  $f = 1$ ,  $a = 5$  Å and  $u_s = eU_s/k_B T = -0.5$  (solid curve);  $f = 0.1$ ,  $a = 5$  Å and  $u_s = -0.5$  (dots);  $f = 1$ ,  $a = 5$  Å and  $u_s = -1.0$  (short dashes);  $f = 1$ ,  $a = 10$  Å and  $u_s = -0.5$  (long dashes); and  $f = 0.1$ ,  $a = 5$  Å and  $u_s = -1.0$  (dot-dash line). For all cases  $c_m^0 = \phi_b a^3 = 10^{-6}$  Å<sup>-3</sup>,  $\bar{v}_2 = 50$  Å<sup>3</sup>/a<sup>3</sup>,  $\varepsilon = 80$ ,  $T = 300$  K and  $c_{\text{salt}} = 0.1$  mM. Adapted from Ref. [206].

dominant length scale  $D$ . Hence, we write the polymer order parameter profile in the form

$$\psi(x) = \sqrt{\phi_M} h(x/D), \quad (8.10)$$

where  $h(x/D)$  is a dimensionless function normalized to unity at its maximum and  $\phi_M$  sets the scale of polymer adsorption, such that  $\psi(D) = \sqrt{\phi_M}$ . The free energy can now be expressed in terms of  $D$  and  $\phi_M$ , while the exact form of  $h(x/D)$  affects only the numerical prefactors.

As discussed below, the scaling form Eq. (8.10), which describes the density profile as a function of a single scaling variable  $x/D$ , is only valid as long as  $\kappa^{-1}$  and  $D$  are not of the same order of magnitude. Otherwise, the scaling function  $h$  should be a function of both  $\kappa x$  and  $x/D$ . We concentrate now on the limiting low-salt regime,  $D \ll \kappa^{-1}$ , where Eq. (8.10) can be justified. In the other extreme of high-salt,  $D \gg \kappa^{-1}$ , the adsorption crosses over to a depletion, as is discussed below (Sections 8.3 and 8.4). Note that the latter limit is in agreement with the single-chain adsorption (Section 6), where in the high-salt limit and for weakly charged chains, the PE desorbs from the wall.

In the low-salt regime the effect of the small ions can be neglected and the free energy (per unit surface area), Eqs. (8.2)–(8.5), can be evaluated using the scaling form Eq. (8.10) and turns out to be given by (see also Refs. [202,206])

$$F \simeq \frac{1}{6aD} \phi_M - f|u_s| \phi_M \frac{D}{a^2} + 4\pi l_B f^2 \phi_M^2 \frac{D^3}{a^6} + \frac{1}{2} \bar{v}_2 \phi_M^2 \frac{D}{a^3}. \quad (8.11)$$

In what follows we drop prefactors of order unity from the various terms. The first term of Eq. (8.11) is the elastic energy characterizing the response of the polymer to concentration inhomogeneities. The second term accounts for the electrostatic attraction of the polymers to the charged surface. The third term represents the Coulomb repulsion between adsorbed monomers. The last term represents the excluded volume repulsion between adsorbed monomers, where we assume that the monomer concentration near the surface is much larger than the bulk concentration  $\phi_M \gg \phi_b$ . (The opposite limit,  $\phi_M \leq \phi_b$ , is consistent with depletion and will be discussed separately in the high-salt regime.)

In the low-salt regime and for strong enough PEs the electrostatic interactions are much stronger than the excluded volume ones. Neglecting the latter interactions and minimizing the free energy with respect to  $D$  and  $\phi_M$  gives

$$D^2 \simeq \frac{a^2}{f|u_s|} \sim \frac{1}{f|U_s|} \quad (8.12)$$

and

$$\phi_M \simeq \frac{a|u_s|^2}{4\pi l_B} \sim |U_s|^2, \quad (8.13)$$

recalling that  $u_s = eU_s/k_B T$ . These expressions are valid as long as (i)  $D \ll \kappa^{-1}$  and (ii) the excluded volume term in Eq. (8.11) is negligible. Condition (i) translates into  $c_{\text{salt}} \ll f|u_s|/(8\pi l_B a^2)$ . For  $|u_s| \simeq 1$ ,  $a = 5 \text{ \AA}$  and  $l_B = 7 \text{ \AA}$  this limits the salt concentration to  $c_{\text{salt}}/f \ll 0.4 \text{ M}$ . Condition (ii) on the magnitude of the excluded volume term can be shown to be equivalent to  $f \gg \tilde{v}_2 a |u_s|/l_B$ . These requirements are consistent with the numerical data presented in Fig. 19.

We recall that the profiles presented in Fig. 19 were obtained from the numerical solution of Eqs. (8.6) and (8.7), including the effect of small ions and excluded volume. The scaling relations are verified by plotting in Fig. 20 the same sets of data as in Fig. 19 using rescaled variables as defined in Eqs. (8.12), (8.13). Namely, the rescaled electrostatic potential  $U(x)/u_s$  and polymer concentration  $\phi(x)/\phi_M \sim \phi(x)/|u_s|^2$  are plotted as functions of the rescaled distance  $x/D \sim x f^{1/2} |u_s|^{1/2} / a$ . The different numerical data roughly collapse on the same curve, which demonstrates that the scaling results in Eqs. (8.12), (8.13) are valid for a whole range of parameters in the low-salt regime.

In many experiments the total amount of adsorbed polymer per unit area (surface excess)  $\Gamma$  is measured as function of the physical characteristics of the system such as the charge fraction  $f$ , the pH of the solution or the salt concentration  $c_{\text{salt}}$  (see, e.g. Refs. [178–185]). While in the next section we give general predictions for a wide range of salt concentration, we comment here on the low-salt limit, where the scaling expressions, Eqs. (8.10), (8.12) and (8.13), yield

$$\Gamma = \frac{1}{a^3} \int_0^\infty [\phi(x) - \phi_b] dx \simeq \frac{D}{a^2} \phi_M \simeq \frac{|u_s|^{3/2}}{l_B a f^{1/2}} \sim \frac{|U_s|^{3/2}}{f^{1/2}}. \quad (8.14)$$

This scaling prediction for the adsorbed amount  $\Gamma(f)$  compares favorably with the numerical results shown in Fig. 21a, adapted from Ref. [208], for the low-salt limit (solid line corresponds to  $c_{\text{salt}} = 1.0 \text{ mM}$ , and dashed line to  $10 \text{ mM}$ ). As a consequence of Eq. (8.14),  $\Gamma$  decreases with increasing charge fraction  $f$ . Similar behavior was also reported in experiments [181]. This effect is at first glance quite puzzling because as the polymer charge increases, the chains are subject to a stronger attraction to the surface. On the other hand, the monomer–monomer repulsion is stronger and indeed, in this regime, the monomer–monomer Coulomb repulsion scales as  $(f\phi_M)^2$ , and dominates over the adsorption energy that scales as  $f\phi_M$ .

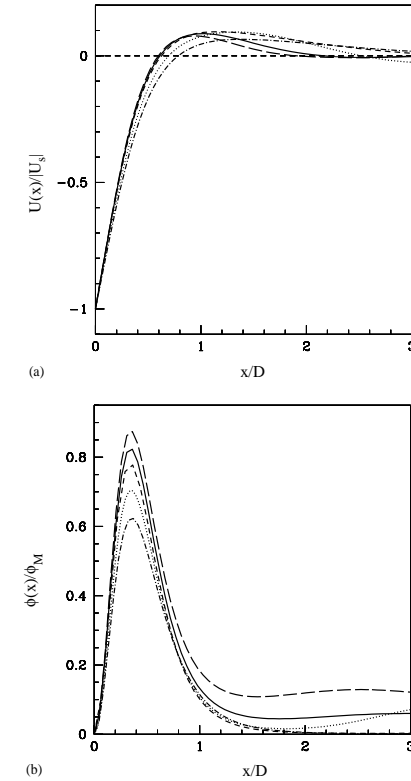


Fig. 20. Rescaled profiles of PE adsorption in the low-salt regime confirming the scaling relations, Eqs. (8.12), (8.13). (a) The rescaled electrostatic potential  $U(x)/|U_s|$  as a function of the rescaled distance  $x/D$ . (b) The rescaled monomer volume fraction  $\phi(x)/\phi_M$  as a function of the same rescaled distance. The profiles are taken from Fig. 19 (with the same notation). The numerical prefactors of a piecewise linear  $h(x/D)$  profile were used in the calculation of  $D$  and  $\phi_M$ . Adapted from Ref. [206].

### 8.3. Adsorption behavior in the presence of finite salt

The full dependence of  $\Gamma$  on  $c_{\text{salt}}$  and  $f$ , as obtained from the numerical solutions of the mean-field equations with fixed  $U_s$  boundary condition [208], is presented in Fig. 21. Our results are in agreement with numerical solutions of discrete lattice models (the multi-Stern layer theory)

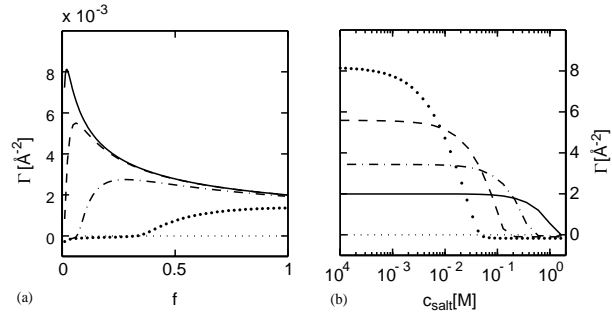


Fig. 21. (a) Surface excess of polyelectrolyte adsorption,  $\Gamma$ , as function of the chain charged fraction  $f$ , for constant surface potential and for several  $c_{\text{salt}}$  concentrations: 1.0 mM (solid line), 10 mM (dashed line), 0.1 M (dash-dot line), 0.5 M (dots). As the salt concentration increases, the peak in  $\Gamma$  shifts to higher  $f$  values and disappears for  $c_{\text{salt}} = 0.5$  M. The depletion–adsorption transition is defined to occur for  $\Gamma = 0$ . (b) Surface excess as function of salt concentration,  $c_{\text{salt}}$ , for constant surface potential and for several  $f$  values:  $f = 0.03$  (dots), 0.1 (dashes), 0.3 (dot-dash), 1.0 (solid line).  $\Gamma$  is almost independent of  $c_{\text{salt}}$  for low-salt concentrations in the adsorption region. It is then followed by a strong descent into a depletion region. The other parameters used here are:  $u_s = -1.0$ ,  $c_m^b = \phi_b a^3 = 10^{-6} \text{ Å}^{-3}$ ,  $v_2 = \bar{v}_2 a^3 = 50 \text{ Å}^3$ ,  $a = 5 \text{ Å}$ ,  $T = 300 \text{ K}$ ,  $\epsilon = 80$ . Adapted from Ref. [208].

[1,186,187,196–200]. In Fig. 21a the dependence of  $\Gamma$  on  $f$  is shown for several salt concentrations ranging from low-salt conditions,  $c_{\text{salt}} = 1.0$  mM, all the way to high salt,  $c_{\text{salt}} = 0.5$  M. For low enough  $f$ ,  $\Gamma < 0$  indicates depletion (as is discussed below). As  $f$  increases, a crossover to the adsorption region,  $\Gamma > 0$ , is seen. In the adsorption region, a peak in  $\Gamma(f)$  signals the maximum adsorption amount at constant  $c_{\text{salt}}$ . As  $f$  increases further, beyond the peak,  $\Gamma$  decreases as  $f^{-1/2}$  for low-salt concentrations, in agreement with Eq. (8.14). Looking at the variation of  $\Gamma$  with salt, as  $c_{\text{salt}}$  increases, the peak in  $\Gamma(f)$  decreases and shifts to higher values of  $f$ . For very large amount of salt, e.g.,  $c_{\text{salt}} = 0.5$  M, the peak occurs in the limit  $f \rightarrow 1$ , and only an increase in  $\Gamma(f)$  is seen from the negative depletion values (small  $f$ ) towards the peak at  $f \rightarrow 1$ .

In Fig. 21b, we plot  $\Gamma(c_{\text{salt}})$  for several  $f$  values: 0.03, 0.1, 0.3 and 1.0. For low enough salt condition, the surface excess is almost independent of  $c_{\text{salt}}$ . In this adsorption regime, the surface excess is well characterized by the scaling result of the previous section, Eq. (8.14),  $\Gamma \sim f^{-1/2}$ . As the amount of salt increases above some threshold, the adsorption regime crosses over to depletion quite sharply, signaling the adsorption–depletion transition. The salt concentration at the transition,  $c_{\text{salt}}^*$ , increases with the charge fraction  $f$ .

#### 8.4. Adsorption–depletion crossover in high-salt conditions

In the scaling discussion in Section 8.2.2, it was assumed implicitly that the PE chains are adsorbing to the surface. Namely, the electrostatic interaction with the surface is strong enough so that

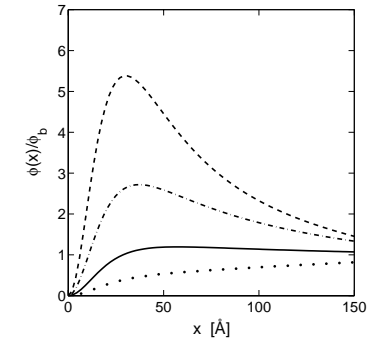


Fig. 22. Numerical monomer density profiles exhibiting the transition from adsorption to depletion. The dashed line corresponds to  $f = 0.12$ , the dot-dash line to  $f = 0.1$ , the solid line to  $f = 0.09$ , and the dotted line to  $f = 0.08$ . From the condition  $\Gamma = 0$  the adsorption–depletion transition is found to occur for  $f \simeq 0.09$ , corresponding to  $c_{\text{salt}}^* \simeq 0.16|u_s|f/l_B a^2$ . All profiles have  $u_s = -0.5$ ,  $c_{\text{salt}} = 70$  mM,  $c_m^b = \phi_b a^3 = 10^{-6} \text{ Å}^{-3}$ ,  $v_2 = \bar{v}_2 a^3 = 50 \text{ Å}^3$ ,  $a = 5 \text{ Å}$ ,  $T = 300 \text{ K}$ ,  $\epsilon = 80$ . Adapted from Ref. [208].

it overcomes any compression and entropy loss of the polymers in the adsorbing layer. This is not correct for highly screened systems (high salt) and weakly charged PEs.

The numerical PE profiles obtained from solving Eqs. (8.6)–(8.7) [208] demonstrating the adsorption–depletion transition (which is not a sharp transition but rather a crossover) are presented in Fig. 22. The profiles were obtained by solving numerically the differential equations for several values of  $f$  in a range including the adsorption–depletion transition. For salt concentration of about  $c_{\text{salt}}^* \simeq 0.16|u_s|f/(l_B a^2)$  (solid line in Fig. 22 with  $f = 0.09$ ), the figure demonstrates the disappearance of the peak in the concentration profile. Our way of identifying this crossover is by looking at the surface excess,  $\Gamma$ . The place where  $\Gamma = 0$  indicates an adsorption–depletion transition, separating positive  $\Gamma$  in the adsorption regime from negative ones in the depletion regime.

The numerical phase diagrams displaying the adsorption–depletion transition are presented in Fig. 23, where the line of vanishing surface excess,  $\Gamma = 0$ , is located in the  $(f, c_{\text{salt}})$  plane while fixing  $u_s$  (Fig. 23a), and in the  $(|u_s|, c_{\text{salt}})$  plane while fixing  $f$  (Fig. 23b). From the figure it is apparent that the adsorption–depletion transition line fits quite well a line of slope 1.0 in both Fig. 23a and b plotted on a log–log scale. Namely,  $c_{\text{salt}}^* \sim f$  for fixed  $u_s$ , and  $c_{\text{salt}}^* \sim |u_s|$  for fixed  $f$ .

These scaling forms of  $c_{\text{salt}}^*$  at the adsorption–depletion transition can be reproduced by using simplified scaling arguments, similar to the single-polyelectrolyte adsorption situation in Section 6. There we found that the exact scaling of the desorption transition is recovered by defining desorption to occur when the prediction for the adsorption layer thickness  $D$  reaches the screening length  $\kappa^{-1}$ . The condition for adsorption is thus  $\kappa D < 1$ . Using the scaling for  $D$ , Eq. (8.12), and the definition of  $\kappa$ , we find the adsorption–depletion transition to occur at the salt concentration

$$c_{\text{salt}}^* \simeq \frac{|u_s| f}{l_B a^2}. \quad (8.15)$$

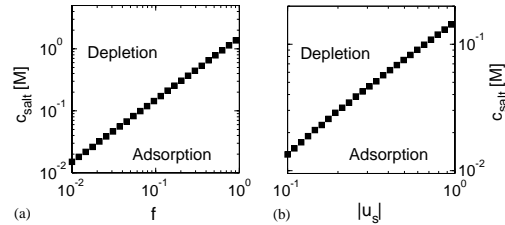


Fig. 23. Numerically calculated crossover diagram from adsorption to depletion on a log–log scale for constant surface potential conditions. In (a) the  $(f, c_{\text{salt}})$  parameter plane is presented for constant  $u_s = -1.0$ . The least-mean-square fit has a slope of  $1.00 \pm 0.02$ , in excellent agreement with the scaling arguments,  $c_{\text{salt}}^* \sim f$ . In (b) the  $(u_s, c_{\text{salt}})$  parameter plane is presented, for constant  $f = 0.1$ . The least-mean-square fit has a slope of  $1.04 \pm 0.02$ , in good agreement with scaling arguments,  $c_{\text{salt}}^* \sim u_s$ . All profiles have  $c_m^* = \phi_0 a^3 = 10^{-6} \text{ \AA}^{-3}$ ,  $v_2 = \bar{v}_2 a^3 = 50 \text{ \AA}^3$ ,  $a = 5 \text{ \AA}$ ,  $T = 300 \text{ K}$ ,  $\epsilon = 80$ . Adapted from Ref. [208].

in the case of a fixed surface potential. This explains the numerical results of Fig. 23a and b. We mention the analogous results for fixed surface charge as well as the phenomenon of overcompensation in the next subsection.

### 8.5. Adsorption of PEs for constant surface charge and its overcompensation

We turn now to a different electrostatic boundary condition of constant surface charge density and look at the interesting phenomenon of charge overcompensation by the PE chains in relation to experiments for PE adsorption on flat surfaces, as well as on charged colloidal particles [150,152,153]. What was observed in experiments is that PEs adsorbing on an oppositely charged surface can overcompensate the original surface charge. Because the PEs create a thin layer close to the surface, they can act as an effective absorbing surface to a second layer of PEs having an opposite charge compared to the first layer. Repeating the adsorption of alternating positively and negatively charged PEs, it is possible to create a multilayer structure of PEs at the surface. Although many experiments and potential applications for PE multilayers exist, the theory of PE overcompensation is only starting to be developed [157,190,191,193,205,206,209].

The scaling laws presented for constant  $U_s$  can be used also for the case of constant surface charge. A surface held at a constant potential  $U_s$  will induce a surface charge density  $\sigma$  (in units of  $e$ ). The two quantities are related by:  $dU/dx = -4\pi\sigma e/\epsilon$  at  $x = 0$ . We will now consider separately the two limits: low salt  $D \ll \kappa^{-1}$ , and high salt  $D \geq \kappa^{-1}$ .

As will be explained in Section 9, an alternative mechanism for overcharging is produced by lateral correlations between adsorbed PEs, which in conjunction with screening by salt ions leads to strongly overcharged surfaces [157,193].

#### 8.5.1. Low-salt limit: $D \ll \kappa^{-1}$

Assuming that there is only one length scale characterizing the potential behavior in the vicinity of the surface, as demonstrated in Fig. 20, the surface potential  $U_s$  and the surface charge  $\sigma$  are

related by  $U_s \sim \sigma e D/\epsilon$ . In the low-salt limit we find from Eq. (8.12)

$$D \sim (f\sigma l_B)^{-1/3} \quad (8.16)$$

in accord with the single-chain result Eq. (6.9). Let us define two related concepts via the effective surface charge density defined as  $\Delta\sigma \equiv f\Gamma - \sigma$ , which is sum of the adsorbed polymer charge density  $f\Gamma$  and the charge density  $\sigma$  of the bare substrate. For  $\Delta\sigma = 0$  the adsorbed polymer charge exactly compensates the substrate charge. If  $\Delta\sigma$  is positive the PE overcompensates the substrate charge, more polymer adsorbs than is needed to exactly cancel the substrate charge. If  $\Delta\sigma$  is negative and reaches the value  $\Delta\sigma = -\sigma$  it means that the PE charge is  $f\Gamma = 2\sigma$  and leads to an exact charge inversion of the substrate charge. In this case, the effective surface charge consisting of the substrate charge plus the PE layer has a charge density which is exactly opposite to the original substrate charge density  $\sigma$ .

Do we obtain overcompensation or even charge inversion in the low-salt limit within mean-field theory? Using scaling arguments this is not clear since one finds that  $\Delta\sigma \sim f\Gamma \sim \sigma$ . Namely each of the two terms in  $\Delta\sigma$  scales linearly with  $\sigma$ , and the occurrence of overcompensation or charge inversion will depend on numerical prefactors (which are difficult to obtain using scaling arguments) determining the relative sign of the two opposing terms. However, if we look on the numerical solution for the mean-field electrostatic potential, Fig. 20, we see indeed that all plotted profiles have a maximum of  $U(x)$  as function of  $x$ . An extremum in  $U$  means a zero local electric field. Or equivalently, using Gauss law, this means that the integrated charge density from the surface to this special extremum point (including surface charges) is exactly zero. At this point the charges in solution exactly compensate the surface charges. For larger distances from the surface, the adsorption layer overcompensates the substrate charge.

#### 8.5.2. High-salt limit: $D \geq \kappa^{-1}$ and depletion

When we include salt in the solution and look at the high-salt limit, the only length characterizing the exponential decay of  $U$  close to the surface is the Debye–Hückel screening length. Hence, using  $dU/dx|_s \sim -\sigma e/\epsilon$  yields  $U_s \sim \sigma e/\kappa\epsilon$  or  $u_s \sim \sigma l_B/\kappa$ . Inserting this relation into the adsorption threshold for constant surface potential, Eq. (8.15), we obtain for the crossover between adsorption and depletion

$$c_{\text{salt}}^* \simeq \sigma^{2/3} f^{2/3} l_B^{-1/3} a^{-4/3} \sim \sigma^{2/3} f^{2/3}, \quad (8.17)$$

in accord with Refs. [154,155,195] and as confirmed by the numerical studies of Eqs. (8.6) and (8.7) with constant  $\sigma$  boundary conditions. More details can be found in Ref. [208]. We note that the same threshold is obtained by equating the adsorption layer thickness in the constant-surface-charge ensemble, Eq. (8.16), with the screening length  $\kappa^{-1}$ .

We end this section with a short comment on the relation between the semi-dilute and single-chain adsorption behaviors. By construction of the scaling argument, the desorption threshold obtained here in the semi-dilute regime for fixed surface charge, Eq. (8.17), is the same as the single-chain desorption transition, Eq. (6.10). It is important to point out that this equivalence is perfectly confirmed by our numerical solutions of the full mean-field equations. Therefore, it follows that multi-chain effects (within mean-field level) do not modify the location of the single-polyelectrolyte chain adsorption transition.

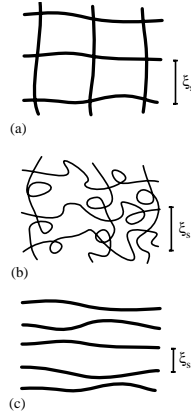


Fig. 24. Schematic top views of the different adsorbed surface phases considered. (a) Disordered uncrumpled phase, with an average mesh size  $\xi_s$  smaller than the persistence length, exhibiting an average density of chain crossings of  $\sim 1/\xi_s^2$ . (b) Disordered crumpled phase, with a mesh size  $\xi_s$  larger than the persistence length. (c) Lamellar phase, with a lamellar spacing  $\xi_s$  smaller than the persistence length.

## 9. Lateral correlation effects in polyelectrolyte adsorption

In this section we go beyond the mean-field approach by considering lateral correlation effects (for recent reviews on related subjects see [210,211]). The mean-field theories discussed before average the polymer profile in the lateral direction and only consider a spatially varying profile in the direction perpendicular to the substrate. Although mean-field equations can in principle be formulated which take also lateral order into account, this would be very involved and complicated. In this section we generalize the discussion of the single PE chain adsorption from Section 6 and consider the effect of interactions between different adsorbed polymers on a simple scaling level. In order to do so, we assume that the adsorption energy is strong enough such that the polymers essentially lie flat on the substrate. Lateral correlations are large enough to locally induce the polymers to form some type of ordered lattice. Due to the formation of two-dimensionally ordered adsorbed layers, the local chain structure becomes important and we therefore describe the PE chains as semi-flexible polymers in this section.

We follow here the original ideas of Ref. [157], which were subsequently elaborated by Nguyen et al. [193]. To understand the idea, consider Fig. 24, where schematic top views of different adsorbed phases are shown. A strongly adsorbed, flat polymer phase can form a *disordered* surface pattern with many chain crossings, characterized by a certain mesh size  $\xi_s$  which corresponds to the average distance between chain crossings. We distinguish two different cases: if the effective persistence length  $l_{\text{eff}}$  is larger than the mesh size, we obtain a disordered *uncrumpled* phase, as depicted

schematically in Fig. 24a; if the effective persistence length is smaller than the mesh size, we expect a phase which is *crumpled* between consecutive chain crossings, as depicted in Fig. 24b. We also anticipate a *lamellar* phase where different polymer strands are parallel locally, characterized by an average lamellar spacing  $\xi_s$ , as shown in Fig. 24c. The lamellar phase is stabilized either by steric or by electrostatic repulsions between neighboring polymers; we will in fact encounter both stabilization mechanisms for different values of the parameters.

We now calculate the free energy and other characteristics of these adsorbed phases. In all the following calculations, we assume that we are inside the adsorbed regime of a single polymer, as discussed in Section 6. We basically assume, later on, that the desorption transitions obtained for the single-chain case also apply to the case of many-chain adsorption. As was shown in Ref. [157], to obtain the complete phase diagram it is sufficient to consider the lamellar phase depicted in Fig. 24c, since the other phase morphologies are metastable or degenerate. We assume that the distance between neighboring polymer strands,  $\xi_s$ , is much smaller than the effective persistence length,  $\xi_s < l_{\text{eff}}$  (this assumption is checked self-consistently at the end). Since the possible conformations of the adsorbed polymers are severely restricted in the lateral directions, we have to include, in addition to the electrostatic interactions, a repulsive free energy contribution coming from steric interactions between stiff polymers [160]. This is the same type of entropic repulsion that was used in Section 6 to estimate the pressure inducing desorption from a substrate. The total free energy density is given by

$$F_{\text{lam}} \simeq -\frac{2\pi\ell_B\sigma\tau}{\xi_s\kappa} + \frac{1}{\ell_{\text{eff}}^{1/3}\xi_s^{2/3}} \ln\left(\frac{\ell_{\text{eff}}}{\xi_s}\right) + F_{\text{rep}}, \quad (9.1)$$

where the first term comes from the electrostatic attraction to the oppositely charged surface (which for consistency is taken to be penetrable to ions), the second term is the Odijk entropic repulsion [160] and  $F_{\text{rep}}$  is the electrostatic repulsion of a lamellar array.

To obtain the electrostatic repulsive energy, we first note that the reduced potential created by a charged line with line charge density  $\tau = f/b$  at a distance  $\xi_s$  is within the Debye–Hückel approximation given by

$$V_{\text{line}}(\xi_s) = \tau \int_{-\infty}^{\infty} ds v_{\text{DH}}(\sqrt{\xi_s^2 + s^2}) = 2\ell_B\tau K_0[\kappa\xi_s], \quad (9.2)$$

with the Debye–Hückel potential  $v_{\text{DH}}$  defined in Eq. (3.3).  $K_0$  denotes the modified Bessel function. The repulsive electrostatic free energy density of an array of parallel lines with a nearest-neighbor distance of  $\xi_s$  and line charge density  $\tau$  can thus be written as

$$F_{\text{rep}} = \frac{2\ell_B\tau^2}{\xi_s} \sum_{j=1}^{\infty} K_0[j\xi_s\kappa]. \quad (9.3)$$

This expression is also accurate for rods of finite radius  $d$  as long as  $d \ll \xi_s$  holds. In the limit  $\xi_s\kappa \ll 1$ , when the distance between strands is much smaller than the screening length, the sum can be transformed into an integral and we obtain

$$F_{\text{rep}} \simeq \frac{2\ell_B\tau^2}{\xi_s} \int_0^{\infty} ds K_0[s\xi_s\kappa] = \frac{\pi\ell_B\tau^2}{\xi_s^2\kappa}. \quad (9.4)$$

This expression neglects effects due to the presence of a solid substrate. For example, and as discussed in Ref. [157], for a low-dielectric substrate the electrostatic interactions are enhanced by a factor of two close to the substrate surface, a rather small effect which will be neglected in the following. Since the average adsorbed surface charge density is given by  $\sigma_{\text{ads}} = \tau/\xi_s$ , it follows that the self energy Eq. (9.4) in the limit  $\xi_s \kappa \ll 1$  is given by  $F_{\text{rep}} \simeq \pi \ell_B \sigma_{\text{ads}}^2 \kappa^{-1}$  and thus is identical to the self energy of a totally smeared-out charge distribution [157]. In this case, lateral correlations therefore do not matter.

In the opposite limit,  $\xi_s \kappa \gg 1$ , when the polymers are much farther apart than the screening length, the sum in Eq. (9.3) is dominated by the first term and (using the asymptotic expansion of the Bessel function) the free energy density (in units of  $k_B T$ ) becomes

$$F_{\text{rep}} \simeq \frac{\sqrt{2\pi} \ell_B \tau^2 e^{-\xi_s \kappa}}{\xi_s^{3/2} \kappa^{1/2}}. \quad (9.5)$$

In this limit, it is important to note that the smeared-out repulsive energy Eq. (9.4) is much larger and thus considerably overestimates the actual electrostatic repulsion between polymer strands. Conversely, this reduction of the electrostatic repulsion between polymers results in an enormous overcharging of the substrate, as we will see shortly.

In order to determine the equilibrium distance between the polymer strands, we balance the electrostatic attraction term, the first term in Eq. (9.1), with the appropriate repulsion term. There are three choices to do this. For  $d < \kappa^{-1} < \xi_s^* < \xi_s$  (with some crossover length  $\xi_s^*$  to be determined later on), the electrostatic repulsion between the polymers is irrelevant (i.e. the last term in Eq. (9.1) can be neglected), and the lamellar phase is *sterically* stabilized in this case. The equilibrium lamellar spacing is given by

$$\xi_s \sim \left[ \frac{\kappa}{\tau \sigma \ell_B \ell_{\text{eff}}^{1/3}} \ln \left( \frac{\tau \sigma \ell_B \ell_{\text{eff}}}{\kappa} \right) \right]^{3/2}. \quad (9.6)$$

In all what follows, we neglect the logarithmic cofactor.

For  $d < \kappa^{-1} < \xi_s < \xi_s^*$ , the steric repulsion between the polymers is irrelevant (i.e. the second term in Eq. (9.1) can be neglected). The free energy is minimized by balancing the electrostatic adsorption term, the first term in Eq. (9.1), with the electrostatic repulsion term appropriate for the case  $\xi_s \kappa > 1$ , Eq. (9.5), which leads to the *electrostatically* stabilized lamellar spacing

$$\xi_s \sim \kappa^{-1} \ln \left[ \frac{\tau \kappa}{\sigma} \right]. \quad (9.7)$$

The adsorbed charge density then follows from  $\sigma_{\text{ads}} \sim \tau/\xi_s$  as

$$\sigma_{\text{ads}} \sim \sigma \frac{\tau \kappa \sigma^{-1}}{\ln(\tau \kappa \sigma^{-1})} \quad (9.8)$$

(note that in the previous section the adsorbed charge density was obtained as the product of the surface amount  $\Gamma$  and the charged-monomer fraction  $f$ ,  $\sigma_{\text{ads}} = f\Gamma$ ). Therefore, the electrostatically stabilized lamellar phase shows charge reversal as long as the spacing  $\xi_s$  is larger than the screening length. As we will see, this is always the case. The crossover between the sterically stabilized lamellar phase, described by Eq. (9.6), and the lamellar phase which is stabilized by electrostatic

repulsion, Eq. (9.7), occurs when the predictions for  $\xi_s$  become simultaneously equal to the crossover spacing  $\xi_s^*$ , leading to a crossover for a surface charge density of (without logarithmic cofactors)

$$\sigma \sim \frac{\kappa^{5/3}}{\tau \ell_{\text{eff}}^{1/3} \ell_B}. \quad (9.9)$$

For  $\sigma$  larger than the crossover value in Eq. (9.9) the distance between neighboring polymer strands is smaller than  $\xi_s^*$  and the electrostatic stabilization mechanism is at work, for  $\sigma$  smaller than the crossover value in Eq. (9.9) the lamellar spacing  $\xi_s$  is larger than the characteristic crossover length  $\xi_s^*$  and the Odijk repulsion dominates. One notes that the transition Eq. (9.9) is, on the scaling level, the same as the adsorption threshold in Eq. (6.5) and it is therefore not clear a priori whether the sterically stabilized lamellar phase exists. However, we note that additional non-electrostatic adsorption forces will stabilize the sterically stabilized lamellar phase which should therefore occur in a finite range of parameters [157]. The electrostatically stabilized lamellar phase crosses over to the *charge-compensated* phase when  $\xi_s$  as given by Eq. (9.7) becomes of the order of the screening length  $\kappa^{-1}$ . In the charge-compensated phase, the lamellar spacing is obtained by balancing the electrostatic adsorption energy with the repulsion in the smeared-out limit Eq. (9.4) and is given by

$$\xi_s \simeq \frac{\tau}{\sigma}. \quad (9.10)$$

In this case the adsorbed surface charge density  $\sigma_{\text{ads}} = \tau/\xi_s$  exactly neutralizes the substrate charge density,

$$\sigma_{\text{ads}} \sim \sigma. \quad (9.11)$$

The crossover between the charged-reversed phase and charge-compensated phase is obtained by matching Eqs. (9.7) and (9.10), leading to a threshold surface charge density of

$$\sigma \sim \tau \kappa. \quad (9.12)$$

Finally, taking into account that the polymers have some width  $d$ , there is an upper limit for the amount of polymer that can be adsorbed in a single layer. Clearly, the lateral distance between polymers in the *full* phase is given by

$$\xi_s \simeq d \quad (9.13)$$

and thus the adsorbed surface charge density in the full phase reads

$$\sigma_{\text{ads}} = \frac{\tau}{d}. \quad (9.14)$$

The crossover between the full phase and the compensated phase is obtained by comparing Eqs. (9.10) and (9.13), leading to

$$\sigma \sim \tau/d. \quad (9.15)$$

In Fig. 25 we show the adsorption diagram, for strongly charged polymers, defined by  $\tau\sqrt{\ell_B \ell_0} > 1$ , as a function of the substrate charge density  $\sigma$  and the inverse screening length  $\kappa$ . The electrostatically stabilized lamellar phase shows strong charge reversal as described by Eq. (9.8). At slightly larger surface charge densities we predict a charge-compensated phase which is not full (i.e.  $\xi_s < d$ ) for a range of surface charge densities as determined by Eqs. (9.12) and (9.15). At even larger substrate charge density, the adsorbed polymer phase becomes close packed, i.e.  $\xi_s = d$ . We note

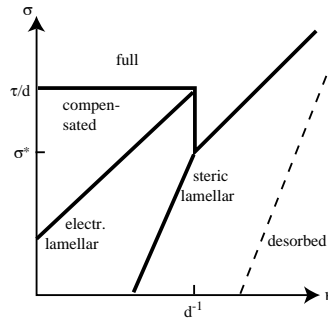


Fig. 25. Complete adsorption phase diagram as a function of the substrate charge density  $\sigma$  and the inverse screening length  $\kappa$ . Note that we use logarithmic scales on both axes. We find a desorbed regime, an adsorbed lamellar phase stabilized by electrostatic repulsions (which is strongly overcharged) and a lamellar phase which is stabilized by steric repulsion between polymer strands, an adsorbed charge-compensated phase, and a full phase, where the substrate charge cannot be compensated with a single adsorption layer because the layer is close-packed.

that since the full phase is not charge reversed, the full phase can consist of a second adsorbed layer (or even more layers). It should however be clear that close to charge compensation the effective substrate charge density an additional layer feels is so small that the condition for adsorption is not met. At low substrate charge densities the distance between adsorbed polymer strands becomes so large that the entropic repulsion between polymers dominates the electrostatic repulsion, and finally, at even lower charge densities, the polymers desorb. One notes that the transition between the electrostatically and sterically stabilized adsorbed phases, Eq. (9.9), has the same scaling form (disregarding logarithmic factors) as the desorption transition of semi-flexible polymers, Eq. (6.5). We have shifted the desorption transition to the right, though, because typically there are attractive non-electrostatic interactions as well, which tend to stabilize adsorbed phases. This is also motivated by the fact that the sterically stabilized phase has been seen in experiments on DNA adsorption, as will be discussed below. The critical charge density  $\sigma^*$  where the full phase, the electrostatically and the sterically stabilized phases meet at one point, is given by  $\sigma^* = 1/(d^{5/3} \ell_{\text{eff}}^{1/3} \tau \ell_B)$ . In the phase diagram we have assumed that the charge density threshold for the full phase,  $\sigma \sim \tau/d$ , satisfies the inequality  $\tau/d > \sigma^*$ , which for a fully charged PE at the Manning threshold,  $\tau = 1/\ell_B$ , amounts to the condition  $\ell_{\text{eff}} > \ell_B^3/d^2$ , which is true for a large class of PEs.

The most important result of our discussion is that in the electrostatically stabilized phase the substrate charge is strongly reversed by the adsorbed polymer layer. This can give rise to a charge-oscillating multilayer formation if the adsorption of oppositely charged polymer is done in a second step. The general trend that emerges is that charge reversal is more likely to occur for intermediate salt concentrations and rather low substrate charge density. For too high-salt concentration and too low substrate charge density, on the other hand, the polymer does not adsorb at all. In essence, the salt concentration and the substrate charge density have to be tuned to intermediate values in order to create charge multilayers.

In experiments on DNA adsorbed on oppositely charged substrates one typically observes a lamellar phase [145,146]. In one experiment, the spacing between DNA strands was found to increase with increasing salt concentration [145]. One theoretical explanation invokes an effective interaction between neighboring DNA strands mediated by elastic deformations of the membrane, which forms the substrate in these experiments [212]. In the sterically stabilized regime, the distance between adsorbed polymers increases as  $\xi_s \sim \kappa^{3/2}$  with the salt concentration, see Eq. (9.6), which offers an alternative explanation for the experimental findings. It would be interesting to redo DNA adsorption experiments on rigid substrates, where the elastic coupling to the membrane is absent. For high enough substrate charge densities and by varying the salt concentration one should be able to see the crossover from the electrostatically stabilized phase, Eq. (9.7), where the DNA spacing decreases with added salt, to the sterically stabilized phase, Eq. (9.6), where the DNA spacing increases with added salt.

Between the two limiting cases, diffusive mean-field adsorption profile with no lateral correlations (as treated in Section 8), and a flat, two-dimensional adsorption layer with short-ranged lateral correlations (as discussed in this section), there clearly exists a continuous crossover.

## 10. Interaction between two adsorbed layers

One of the many applications of polymers lies in their influence on the interaction between colloidal particles suspended in a solvent [97]. Depending on the details of substrate-polymer interactions and properties of polymers in solution, the effective interaction between colloids in a polymer solution can be attractive or repulsive, explaining why polymers are widely used as flocculants and stabilizers in industrial processes [97]. The various regimes and effects obtained for the interaction of polymer solutions between two surfaces have recently been reviewed [213]. It transpires that force-microscope experiments done on adsorbed polymer layers form an ideal tool for investigating the basic mechanisms of polymer adsorption, colloidal stabilization and flocculation.

### 10.1. Non-adsorbing polymers

Let us first discuss briefly the relatively simple case when the polymers do not adsorb on the surface of the colloidal particles but are repelled from it. For low concentration of polymer, i.e. below the overlap concentration  $c_m^*$ , the depletion of polymer around the colloidal particles induces a strong attraction between the colloidal particles. The range of this attraction is about the same as the radius of an isolated polymer and can lead to polymer-induced flocculation [214,215]. The effects of polymer excluded volume can be taken into account in analytical theories [216,217], while Monte-Carlo simulations in the grand-canonical ensemble confirm the existence and characteristics of these depletion-induced attractive forces [218]. At polymer concentration higher than the overlap concentration, the depletion zones around the particles become of the order of the mesh-size in the solution. The attraction in this case is predicted to set in at separations equal to or smaller than the mesh-size [219]. The force apparatus was used to measure the interaction between depletion layers [96], as realized with polystyrene in toluene, which is a good solvent for polystyrene but does not favor the adsorption of polystyrene on mica surfaces. Surprisingly, the resultant depletion force is too weak to be detected.

## 10.2. Adsorbing neutral polymers

(i) *Equilibrium adsorption in good solvents*: The case when polymers adsorb on the colloidal surface is much more complicated, and many cases have to be distinguished. If the polymer concentration is rather high and under good-solvent conditions, polymers show the experimentally well-known tendency to stabilize colloids against flocculation, i.e., to induce an effective repulsion between the colloidal particles and to hinder them from coming close enough to each other so that van-der-Waals attractions will induce flocculation [97]. We should also mention that in other applications, small polymer concentrations and high-molecular weight polymers are used in the opposite sense as flocculants, to induce binding between unwanted sub-micron particles and, thereby, removing them from solution. It follows that adsorbing polymers can have different effects on the stability of colloidal particles, depending on the detailed parameters.

Hereafter, we assume that the polymers form an adsorbed layer around the colloidal particles, with a typical thickness much smaller than the particle radius, and curvature effects can be neglected. In that case, the effective interaction between the colloidal particles with adsorbed polymer layers can be traced back to the interaction energy between two planar substrates covered with polymer adsorption layers. In the case when the approach of the two particles is slow and the adsorbed polymer chains are in *full equilibrium* with the chains in solution, the interaction between two opposing adsorbed layers is predominantly attractive [220,221], mainly because polymers form bridges between the two surfaces. Recently, it has been shown that there is a small repulsive component to the interaction at large separations [222,223]. For the case of diblock copolymers, the force between two surfaces depends in a subtle way on the relative affinities of the blocks to the surfaces [224].

The typical equilibration times of polymers are extremely long. This holds in particular for adsorption and desorption processes, and is due to the slow diffusion of polymers and their rather high adsorption energies. Note that the adsorption energy of a polymer can be much higher than  $k_B T$  even if the adsorption energy of a single monomer is small because many monomers of a single chain can be attached to the surface. Therefore, for the typical time scales of colloid contacts, the adsorbed polymers are not in equilibrium with the polymer solution.

(ii) *Constrained equilibrium*: This is also the case for most of the experiments done with a surface-force apparatus, where two polymer layers adsorbed on crossed mica cylinders are brought in contact. In all these cases one has a *constrained equilibrium* situation, where the polymer configurations and thus the density profile can adjust only with the constraint that the total adsorbed polymer excess stays constant. This case has been first considered by de Gennes [220] who found that two fully saturated adsorbed layers will strongly repel each other if the total adsorbed amount of polymer is not allowed to decrease. The repulsion is mostly due to osmotic pressure and originates from the steric interaction between the two opposing adsorption layers. It was experimentally verified in a series of force-microscope experiments on polyethylene-oxide layers in water (which is a good solvent for PEO) [225].

(iii) *Undersaturated layers*: In other experiments, the formation of the adsorption layer is stopped before the layer is fully saturated. The resulting adsorption layer is called *undersaturated*. If two of those undersaturated adsorption layers approach each other, a strong attraction develops, which only at smaller separation changes to an osmotic repulsion [226]. The theory developed for such non-equilibrium conditions predicts that any surface excess lower than the one corresponding to full equilibrium will lead to attraction at large separations [227,228]. Similar mechanisms are valid for

colloidal suspensions, if the total surface available for polymer adsorption is large compared to the total amount of polymer in solution. In this case, the adsorption layers are undersaturated, and the resulting attraction is utilized in applications of polymers as flocculation agents [97].

(iv) *Bad solvent conditions*: Another distinct mechanism leading to attractive forces between adsorption layers was investigated in experiments with dilute polymer solutions in bad solvents. As an example we mention polystyrene in cyclohexane below the theta temperature [229]. The subsequently developed theory [230] showed that the adsorption layers attract each other since the local concentration in the outer part of the adsorption layers is enhanced over the dilute solution and lies in the unstable two-phase region of the bulk phase diagram. Similar experiments have been repeated at the theta temperature [231].

(v) *Dynamic effects*: Additional effects that have been considered are the dynamical approach between two surfaces bearing adsorbed polymer layers, which is controlled by the flow of solvent through the polymer network affixed to the surfaces [232].

## 10.3. Adsorbing charged polymers

More complicated effects are obtained for the interaction between two charged surfaces in the presence of oppositely charged PEs. Experimentally, this situation is encountered when one tries to flocculate or stabilize charge-stabilized dispersions by the addition of oppositely charged PEs [97]. In the absence of added PEs, two similarly charged surfaces repel each other over a range of the order of the screening length in the case of added salt. This can be calculated on the mean-field level [191] and agrees quantitatively with Monte-Carlo simulations and experimental results for monovalent salt [233,234]. For divalent or trivalent salt mean-field theory becomes inaccurate and attractive forces are generated by ion-ion correlations [233,234]. Attractive forces between the surfaces can result, at some separation range, even on a mean field level [191] from a combination of electrostatic interactions between all charged species and the adsorption energies of PE chains on the surfaces.

In simulations [235,236] and mean-field theories [191,235,237,238] it has been found that the predominant effect of added PEs is an attraction between the surfaces, due to bridging between the surfaces and screening of the surface repulsion. Like in the case of neutral polymers between adsorbing surfaces, the force between the surfaces depends on the adsorbed amount. Salt can be used to control the amount of adsorbed polymers, and it also has an important effect on the net force. Since the adsorbed amount for highly charged PEs increases with added salt, the force becomes less attractive in this case and, for large salt concentration, is purely repulsive. For small salt concentrations, on the other hand, the attraction is strongest. Clearly, in the case of constrained equilibrium, i.e. when the amount of adsorbed polymer is fixed as the plate separation changes, the force acquires an additional repulsive component as the plates approach each other, due to the force needed to compress the polymer layer. For larger separations and for undersaturated polymer layers, on the other hand, the forces are attractive. The precise crossover between attraction due to undersaturation (at large separation) to repulsion due to oversaturation (at small separations) depends on the adsorbed amount. This can be experimentally controlled for example by the total amount of added PE.

Measurements of the disjoining pressure in thin liquid films of PE solutions as a function of film thickness demonstrated an oscillatory pressure [95,239–241] with a period of the oscillation of the order of the peak position in the bulk structure factor (which was discussed in Section 3.6).

Theoretically, those oscillations have been seen in mean-field calculations [204] as well as more elaborate integral-equation calculations [242].

An effect which is missed by mean-field theories is the so-called mosaic-binding of charged surfaces in the presence of a very low concentration of oppositely charged PE [97]. In this case the adsorbed layers of the separate surfaces are very undersaturated. Individual polymer coils form isolated patches on the substrate, where the local surface charge is reversed. The substrate shows a mosaic pattern of oscillating charge patches. If two of those patterned surfaces approach each other, the patterns will readjust in order to match oppositely charged patches, resulting in a very strong, irreversible binding [97].

### 11. Polymer adsorption on heterogeneous surfaces

Polymer adsorption can be coupled in a subtle way with lateral changes in the chemical composition or density of the surface. Such a surface undergoing lateral rearrangements at thermodynamical equilibrium is called an *annealed* surface [243,244]. A Langmuir monolayer of insoluble surfactant monolayers at the air/water interface is an example of such an annealed surface. As function of the temperature change, a Langmuir monolayer can undergo a phase transition from a high-temperature homogeneous state to a low-temperature demixed state, where domains of dilute and dense regions coexist. Alternatively, the transition from a dilute phase to a dense one may be induced by compressing the monolayer at constant temperature, in which case the adsorbed polymer layer contributes to the pressure [245]. The domain boundary between the dilute and dense phases can act as nucleation site for adsorption of bulky molecules [246].

The case where the insoluble surfactant monolayer interacts with a semi-dilute polymer solution solubilized in the water subphase was considered in some detail. The phase diagrams of the mixed surfactant/polymer system were investigated within the framework of mean-field theory [247]. The polymer enhances the fluctuations of the monolayer and induces an upward shift of the critical temperature. The critical concentration is increased if the monomers are more attracted (or at least less repelled) by the surfactant molecules than by the bare water/air interface. In the case where the monomers are repelled by the bare interface but attracted by the surfactant molecules (or vice versa), the phase diagram may have a triple point. The location of the polymer desorption transition line (i.e., where the substrate–polymer interaction changes from being repulsive to being attractive) appears to have a big effect on the phase diagram of the surfactant monolayer [247].

A similar effect is seen with DNA which adsorbs on a mixed lipid bilayer consisting of cationic and neutral lipid molecules [147]. Experimentally, it is seen that the negatively charged DNA attracts the positively charged lipid molecules and leads to a local demixing of the membrane [147]. Theoretically, this can be studied by formulating the Poisson–Boltzmann theory for a single charged cylinder (which models the rigid DNA molecule) at some distance from a surface with mobile charged lipids of a given density and size [248]. For low-salt concentrations, the charged DNA leads to a strong accumulation of cationic lipids in its vicinity. Depending on the size of the lipid heads, this lipid concentration profile can extend far away from the cylinder. For high-salt concentrations on the other hand, this accumulation effect is much weaker due to screening. Similar effects have been studied for periodic arrays of adsorbed DNA cylinders [249,250] which describe experimental results for bulk DNA–cationic lipid complexes [146].

The adsorption of DNA on laterally structured substrates was recently characterized by direct AFM visualization [251]. Patches of positively charged lipids were embedded in a matrix of negative surface potential, and the size of the cationic surface patches was varied from the micrometer down to the nanometer scale. DNA adsorption was found to depend both on the average surface charge density and on the size of positively charged patches. Similar phenomena were studied theoretically using off-lattice Monte-Carlo simulations [252,253].

## 12. Polymer adsorption on curved and fluctuating interfaces

### 12.1. Neutral polymers

The adsorption of polymers on rough substrates is of high interest to applications. One example is the reinforcement of rubbers by filler particles such as carbon black or silica particles [254]. Theoretical models considered sinusoidal surfaces [255], rough and corrugated substrates [256,257]. In all cases, enhanced adsorption was found and rationalized in terms of the excess surface available for adsorption.

The adsorption on macroscopically curved bodies, such as spheres and cylinders, leads to modified adsorption profiles [258]. Of considerable interest is the effective interaction between two colloidal particles covered by adsorption layers [259]. Another application is obtained for the adsorption of polymers on flexible interfaces or membranes [243,260,261]. Here one interesting aspect concerns the polymer-induced contribution to the elastic bending moduli of the flexible surface. The elastic energy of a liquid-like membrane can be expressed in terms of two bending moduli,  $\kappa$  and  $\kappa_G$ . The elastic energy (per unit area) is

$$\frac{\kappa}{2}(c_1 + c_2 - 2c_0)^2 + \kappa_G c_1 c_2, \quad (12.1)$$

where  $\kappa$  and  $\kappa_G$  are the elastic and Gaussian bending moduli, respectively. The principle curvatures of the surface are given by  $c_1$  and  $c_2$ , and  $c_0$  is the spontaneous curvature. Quite generally, in presence of adsorbing polymers  $\kappa_G$  turns out to be positive and thus favors the formation of surfaces with negative Gaussian curvature. An ‘egg-carton’ structure is an example to such a multi-saddle surface. On the other hand, the effective  $\kappa$  is reduced, leading to a more deformable and flexible surface due to the adsorbed polymer layer [243,262,263]. The spontaneous curvature  $c_0$  is only non-zero if the adsorption profile is different on both sides of the membrane [260]. This can be achieved, for example, by incubating vesicle solutions with polymers, so that the vesicle interior is devoid of polymers (neglecting polymer translocation through the membrane which is indeed a rather slow process). If the polymers do not adsorb on the membrane, the spontaneous curvature is such that the membrane bends towards the polymer solution [216,217]. If, on the other hand, the polymers do adsorb on the membrane, the membrane bends away from the polymer solution with a continuous crossover between the two cases as the adsorption strength is varied [264].

### 12.2. Charged polymers

Of particular interest is the adsorption of strongly charged polymers on oppositely charged cylinders [265–267] and spheres [268–273], because these are geometries encountered in many colloidal

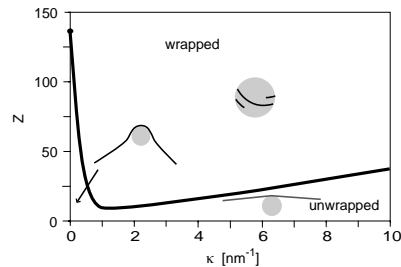


Fig. 26. Numerically determined adsorption diagram for a negatively charged semi-flexible polymer of length  $L = 50$  nm, linear charge density  $\tau = 6$  nm $^{-1}$ , persistence length  $\ell_0 = 30$  nm, interacting with an oppositely charged sphere of radius  $R_{sp} = 5$  nm. Shown is the main transition from the unwrapped configuration (at the bottom) to the wrapped configuration (at the top) as a function of sphere charge  $Z$  and inverse Debye-Hückel screening length  $\kappa$ . Wrapping is favored at intermediate salt concentrations. The parameters are chosen for the problem of DNA-histone complexation. Adapted from Ref. [275].

science applications and in bio-cellular processes. When the curvature of the small colloidal particles is large enough, it can lead to a much more pronounced effect for PE adsorption as compared with neutral polymer. This is mainly due to the fact that the electrostatic energy of the adsorbed PE layer depends sensitively on curvature [269,272–274]. Bending a charged polymer around a small sphere costs a large amount of electrostatic energy, which will disfavor adsorption of long, strongly charged PE at too low-salt concentration.

In Fig. 26 we show the adsorption phase diagram of a single stiff PE of finite length which interacts with an oppositely charged sphere of charge  $Z$  (in units of  $e$ ). The specific parameters were chosen as appropriate for the complexation of DNA (a negatively charged, relatively stiff biopolymer) with positively charged histone proteins, corresponding to a DNA length of  $L = 50$  nm, a chain persistence length of  $\ell_0 = 30$  nm, and a sphere radius of  $R_{sp} = 5$  nm. The phase diagram was obtained by minimization of the total energy including bending energy of the DNA, electrostatic attraction between the sphere and the DNA, and electrostatic repulsion between the DNA segments [275]. All interactions are represented by screened Debye-Hückel potentials of the form of Eq. (3.3). Fluctuations of the DNA shape are unimportant for such stiff polymers. Therefore, the ground-state analysis performed is an acceptable approximation.

We show in Fig. 26 the main transition between an unwrapped state, at low sphere charge  $Z$ , and the wrapped state, at large sphere charge  $Z$ . It is seen that at values of the sphere charge between  $Z = 10$  and 130 the wrapping only occurs at intermediate values of the inverse screening length  $\kappa \sim c_{\text{salt}}^{1/2}$ . At low-salt concentrations (lower left corner in the phase diagram), the self-repulsion between DNA segments prevents wrapping, while at large salt concentrations (lower right corner in the diagram), the electrostatic attraction is not strong enough to overcome the mechanical bending energy of the DNA molecule. These results are in good agreement with experiments on DNA/histone complexes [276]. Interestingly, the optimal salt concentration, where a minimal sphere charge is needed to wrap the DNA, occurs at physiological salt concentration, for  $\kappa^{-1} \approx 1$  nm. For colloidal

particles of larger size and for flexible synthetic polymers, configurational fluctuations become important. They have been treated using a mean-field description in terms of the average monomer density profile around the sphere [268,270].

### 13. Grafted polymer chains

The discussion so far assumed that all monomers of a polymer are alike, showing the same tendency to adsorb to the substrate surface. For industrial and technological applications, one is often interested in *end-functionalized polymers*. These are polymers which attach with one end only to the substrate, as is depicted in Fig. 13b, while the rest of the polymer is not particularly attracted to (or even repelled from) the grafting surface. Hence, it attains a random-coil structure in the vicinity of the surface. Another possibility of block copolymer grafting, as shown in Fig. 13c, will be briefly discussed below as well.

The motivation to study such terminally attached polymers lies in their enhanced power to stabilize particles and surfaces against flocculation. Attaching a polymer by its end to the surface opens up a much more effective route to stable surfaces. Bridging and creation of polymer loops on the same surface, as encountered in the case of homopolymer adsorption (and leading to attraction between two particle surfaces and destabilization, see Section 10), do not occur if the main-polymer section is chosen such that it does not adsorb to the surface.

Experimentally, the end-adsorbed polymer layer can be built in several different ways, depending on the application in mind. First, one of the polymer ends can be *chemically* bound to the grafting surface, leading to a tight and irreversible attachment [189] shown schematically in Fig. 13b. The second possibility consists of *physical* adsorption of a specialized end-group which favors interaction with the substrate. For example, polystyrene chains have been used which contain a zwitterionic end group that adsorbs strongly on mica sheets [277].

Physical grafting is also possible with a suitably chosen diblock copolymer (Fig. 13c), e.g., a polystyrene-polyvinylpyridine (PS-PVP) diblock in the solvent toluene at a quartz substrate [278]. Toluene is a *selective solvent* for this diblock. The PVP (polyvinylpyridine) block is strongly adsorbed to the quartz substrate and forms a collapsed anchor, while the PS (polystyrene) block is under good-solvent conditions. It does not adsorb to the substrate and remains solubilized in the solvent. General adsorption scenarios for diblock copolymers have been theoretically discussed, both for selective and non-selective solvents, with special consideration to the case when the asymmetry of the diblock copolymer, i.e., the length difference between the two blocks, is large [279].

Another experimental realization is possible with diblock copolymers which are anchored at the liquid-air [280] or at a liquid-liquid interface of two immiscible liquids [281]. This scenario offers the advantage that the surface pressure can be directly measured. A well studied example is that of a diblock copolymer of polystyrene-polyethylene oxide (PS-PEO). The PS block is shorter and functions as an anchor at the air/water interface because it is immiscible in water. The PEO block is miscible in water but because of attractive interaction with the air/water interface it forms a quasi-two dimensional layer at very low surface coverage. As the surface pressure increases and the area per polymer decreases, the PEO block is expelled from the surface and forms a quasi polymer ‘brush’.

In the following we simplify the discussion by assuming that the polymers are irreversibly grafted at one of their chain ends to the substrate. We limit the discussion to good solvent conditions and

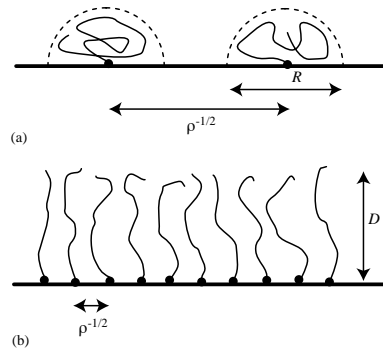


Fig. 27. For grafted chains, one distinguishes between: (a) the mushroom regime, where the distance between chains,  $\rho^{-1/2}$ , is larger than the size of a polymer coil; and, (b) the brush regime, where the distance between chains is smaller than the unperturbed coil size. Here, the chains are stretched away from the surface due to repulsive interactions between monomers. The brush height  $D$  scales linearly with the polymerization index,  $D \sim N$ , and thus is larger than the unperturbed coil radius  $R \sim aN^{\nu}$ .

absence of any attractive interactions between the polymer chains and the surface. The important new system parameter is the grafting density (or area per chain)  $\rho$ , which is the inverse of the average area available for each polymer at the surface. For small grafting densities,  $\rho < \rho^*$ , the polymer chains will be far apart from each other and hardly interact, as schematically shown in Fig. 27a. The overlap grafting density for chains in good solvent conditions (swollen chains) is  $\rho^* \sim a^{-2}N^{-6/5}$ , where  $N$  is the polymerization index [282].

For large grafting densities,  $\rho > \rho^*$ , the chains begin to overlap. Since we assume the solvent to be good, monomers repel each other. The lateral separation between the polymer coils is fixed by the grafting density, so that the polymers extend away from the grafting surface in order to avoid each other, as depicted in Fig. 27b. The resulting structure is called a polymer ‘brush’, with a vertical height  $D$  which greatly exceeds the unperturbed coil radius [282,283]. Similar stretched structures occur in many other situations, such as diblock copolymer melts in the strong segregation regime, or star polymers under good solvent conditions [284]. The universal occurrence of stretched polymer configurations in several seemingly unconnected situations warrants a detailed discussion. Below, this discussion is separated for neutral and charged grafted chains.

### 13.1. Neutral grafted polymers

The scaling behavior of the brush height  $D$  can be analyzed using a Flory-like mean-field theory, which is a simplified version of the original Alexander theory [283] for polymer brushes. The stretching of the chain leads to an entropic free energy loss of  $D^2/(a^2N)$  per chain, and the repulsive energy density due to unfavorable monomer–monomer contacts is proportional to the squared monomer density times the excluded-volume parameter  $v_2$  (introduced in Section 2.2). The free

energy per chain (and in units of  $k_B T$ ) is then

$$\mathcal{F} \simeq \frac{D^2}{a^2N} + v_2 \left( \frac{\rho N}{D} \right)^2 \frac{D}{\rho}. \quad (13.1)$$

The equilibrium height is obtained by minimizing Eq. (13.1) with respect to  $D$ , and the result is

$$D_{\text{eq}} = N(2v_2 a^2 \rho / 3)^{1/3}, \quad (13.2)$$

where the numerical constants have been added for numerical convenience in the following considerations. The vertical size of the brush scales linearly with the polymerization index  $N$ , a clear signature of the strong stretching of the polymer chains, as was originally obtained by Alexander [283]. At the overlap threshold,  $\rho^* \sim a^{-2}N^{-6/5}$ , the height scales as  $D_{\text{eq}} \sim N^{3/5}$ , and thus agrees with the scaling of an unperturbed chain radius in a good solvent, Eq. (2.8), as it should. The simple scaling calculation predicts the brush height  $D$  correctly in the asymptotic limit of long chains and strong overlap. It has been confirmed by experiments [189,277,278] and computer simulations [285,286].

The above scaling result assumes that all chains are stretched to exactly the same height, leading to a step-like shape of the density profile. Monte-Carlo and numerical mean-field calculations confirm the general scaling of the brush height, but exhibit a more rounded monomer density profile which goes continuously to zero at the outer perimeter [285]. A big step towards a better understanding of stretched polymer systems was made by Semenov [287], who recognized the importance of *classical paths* for such systems.

The classical polymer path is defined as the path which minimizes the free energy, for a given start and end positions, and thus corresponds to the most likely path a polymer can take. The name follows from the analogy with quantum mechanics, where the classical motion of a particle is given by the quantum path with maximal probability. Since for strongly stretched polymers the fluctuations around the classical path are weak, it is expected that a theory that takes into account only classical paths, is a good approximation in the strong-stretching limit. To quantify the stretching of the brush, let us introduce the (dimensionless) stretching parameter  $\beta$ , defined as

$$\beta \equiv N \left( \frac{3v_2^2 \rho^2}{2a^2} \right)^{1/3} = \frac{3}{2} \left( \frac{D_{\text{eq}}}{aN^{1/2}} \right)^2, \quad (13.3)$$

where  $D_{\text{eq}}$  is the brush height according to Alexander’s theory, compare Eq. (13.2). The parameter  $\beta$  is proportional to the square of the ratio of the Alexander prediction for the brush height,  $D_{\text{eq}}$ , and the unperturbed Gaussian chain radius  $R \sim aN^{1/2}$ , and, therefore, is a measure of the stretching of the brush. Constructing a classical theory in the infinite-stretching limit, defined as the limit  $\beta \rightarrow \infty$ , it was shown independently by Milner et al. [288] and Skvortsov et al. [289] that the resulting monomer volume-fraction profile depends only on the vertical distance from the grafting surface and has in fact a *parabolic* profile. Normalized to unity, the density profile is given by

$$\phi(x) = \left( \frac{3\pi}{4} \right)^{2/3} - \left( \frac{\pi x}{2D_{\text{eq}}} \right)^2. \quad (13.4)$$

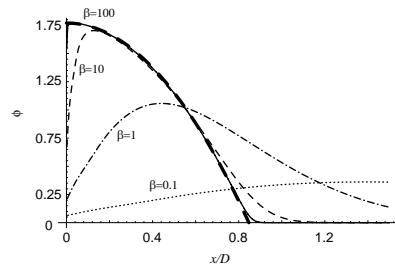


Fig. 28. Results for the density profile (normalized to unity) of a strongly compressed brush, as obtained within mean-field theory. As the compression increases, described by the stretching parameter  $\beta$ , which varies from 0.1 (dots) to 1 (dash-dots), 10 (dashes), and 100 (solid line), the density profile approaches the parabolic profile (shown as a thick, dashed line) obtained within a classical-path analysis (adapted from Ref. [290]).

The brush height, i.e., the value of  $x$  for which the monomer density becomes zero, is given by  $x^* = (6/\pi^2)^{1/3} D_{\text{eq}}$  and is thus proportional to the scaling prediction for the brush height, Eq. (13.2). The parabolic brush profile has subsequently been confirmed in computer simulations [285,286] and experiments [189] as the limiting density profile in the strong-stretching limit, and constitutes one of the cornerstones in this field. Intimately connected with the density profile is the distribution of *polymer end points*, which is non-zero everywhere inside the brush, in contrast with the original scaling description leading to Eq. (13.2).

However, deviations from the parabolic profile become progressively important as the length of the polymers  $N$  or the grafting density  $\rho$  decreases. In a systematic derivation of the mean-field theory for Gaussian brushes [290] it was shown that the mean-field theory is characterized by a single parameter, namely the stretching parameter  $\beta$ . In the limit  $\beta \rightarrow \infty$ , the difference between the classical approximation and the mean-field theory vanishes, and one obtains the parabolic density profile. For finite  $\beta$  the full mean-field theory and the classical approximation lead to different results and both show deviations from the parabolic profile.

In Fig. 28 we show the density profiles (normalized to unity) for four different values of  $\beta$ , obtained with the full mean-field theory [290]. The parameter values used are  $\beta = 100$  (solid line),  $\beta = 10$  (thin dashed line),  $\beta = 1$  (dotted-dashed line), and  $\beta = 0.1$  (dotted line). For comparison, we also show the asymptotic result according to Eq. (13.4) as a thick dashed line. In contrast to earlier numerical implementations [1], the self-consistent mean-field equations were solved in the continuum limit, where the results depend only on the single parameter  $\beta$  and direct comparison with other continuum theories becomes possible. Already for  $\beta = 100$  the density profile obtained within mean-field theory is almost indistinguishable from the parabolic profile denoted by a thick dashed line.

Experimentally, the highest achievable  $\beta$  values are in the range of  $\beta \simeq 20$ . Namely, deviations from the asymptotic parabolic profile are important. For moderately large values of  $\beta > 10$ , the classical approximation (not shown here), derived from the mean-field theory by taking into account only one polymer path per end-point position, is still a good approximation, as judged by comparing

density profiles obtained from both theories [290], except very close to the surface. Unlike mean-field theory, the classical theory misses completely the depletion effects at the substrate. Depletion effects at the substrate lead to a pronounced density depression close to the grafting surface, as is clearly visible in Fig. 28.

A further interesting question concerns the behavior of individual polymer paths. As was already discussed for the infinite-stretching theories ( $\beta \rightarrow \infty$ ), polymers paths can end at any distance from the surface. Analyzing the polymer paths which end at a common distance from the surface, two rather unexpected features are obtained: (i) free polymer ends, in general, are stretched; and, (ii) the end-points lying close to the substrate are pointing towards the surface (such that the polymer path first turns away from the grafting surface before moving back towards it). In contrast, end-points lying *beyond* a certain distance from the substrate, point away from the surface (such that the paths move monotonously towards the surface). We should point out that these two features have been recently confirmed in molecular-dynamics simulations [291]. They are not an artifact of the continuous self-consistent theory used in Ref. [290] nor are they due to the neglect of fluctuations. These are interesting results, especially since it has been long assumed that free polymer ends are unstretched, based on the assumption that no forces act on free polymer ends.

Let us now turn to the thermodynamic behavior of a polymer brush. Using the Alexander description, we can calculate the free energy per chain by putting the result for the optimal brush height, Eq. (13.2), into the free-energy expression, Eq. (13.1):

$$\mathcal{F} \sim N(v_2\rho/a)^{2/3}. \quad (13.5)$$

In the presence of excluded-volume correlations, i.e., when the chain overlap is rather moderate, the brush height  $D$  is still correctly predicted by the Alexander calculation, but the prediction for the free energy is in error. Including correlations [283], the free energy is predicted to scale as  $\mathcal{F} \sim N\rho^{5/6}$ . The osmotic surface pressure  $\Pi$  is related to the free energy per chain by

$$\Pi = \rho^2 \frac{\partial \mathcal{F}}{\partial \rho}, \quad (13.6)$$

and should thus scale as  $\Pi \sim \rho^{5/3}$  in the absence of correlations, and as  $\Pi \sim \rho^{11/6}$  in the presence of correlations. However, these theoretical predictions do not compare well with all experimental results for the surface pressure of a compressed brush [280]. Currently there is still some debate about the cause for this discrepancy. An alternative theoretical method to study tethered chains is the so-called single-chain mean-field method [292], where the statistical mechanics of a single chain is treated exactly, and the interactions with the other chains are taken into account on a mean-field level. This method is especially useful for short chains, where fluctuation effects are important, and for dense systems, where excluded volume interactions play a role. The calculated profiles and brush heights agree very well with experiments and computer simulations. Moreover, these calculations explain the pressure isotherms measured experimentally [280] and in molecular-dynamics simulations [293].

As we described earlier, the main interest in end-adsorbed or grafted polymer layers stems from their ability to stabilize surfaces against van-der-Waals attraction. The force between colloids with grafted polymers is repulsive if the polymers do not adsorb on the grafting substrates [294]. This is in accord with our discussion of the interaction between adsorption layers, where attraction was found to be caused mainly by bridging and creation of polymer loops, which of course are absent for non-adsorbing brushes. A stringent test of brush theories was possible with accurate experimental

measurements of the repulsive interaction between two opposing grafted polymer layers using a surface force apparatus [277]. The resultant force could be fitted very nicely by the infinite-stretching theory of Milner et al. [295]. It was also shown that polydispersity effects, as appear in experiments, have to be taken into account theoretically in order to obtain a good fit of the data [296].

### 13.2. Solvent and substrate effects on polymer grafting

So far we assumed that the polymer grafted layer is in contact with a good solvent. In this case, the grafted polymers try to minimize their mutual contacts by stretching out into the solvent. If the solvent is bad, the monomers try to avoid the solvent by forming a collapsed brush, the height of which is considerably reduced with respect to the good-solvent case. It turns out that the collapse transition, which leads to phase separation in the bulk, is smeared out for the grafted layer and does not correspond to a true phase transition [297]. The height of the collapsed layer scales linearly in  $\rho N$ , which reflects the constant density within the brush, in agreement with experiments [298]. Some interesting effects have been described theoretically [299] and experimentally [298] for brushes in mixtures of good and bad solvent, which can be rationalized in terms of a partial solvent demixing.

For a theta solvent ( $v_2=0$ ) the relevant interaction is described by the third-virial coefficient; using a simple Alexander approach similar to the one leading to Eq. (13.2), the brush height is predicted to vary with the grafting density as  $D \sim \rho^{1/2}$ , in agreement with computer simulations [300].

Up to now we discussed planar grafting layers. It is of much interest to consider the case where polymers are grafted to curved surfaces. The first study taking into account curvature effects of stretched and tethered polymers was done in the context of star polymers [301]. It was found that chain tethering in the spherical geometry leads to a universal density profile, showing a densely packed core, an intermediate region where correlation effects are negligible and the density decays as  $\phi(r) \sim 1/r$ , and an outside region where correlations are important and the density decays as  $\phi \sim r^{-4/3}$ . These considerations were extended using the infinite-stretching theory of Milner et al. [302], self-consistent mean-field theories [303], and molecular-dynamics simulations [304]. Of particular interest is the behavior of the bending rigidity of a polymer brush, which can be calculated from the free energy of a cylindrical and a spherical brush and forms a conceptually simple model for the bending rigidity of a lipid bilayer [305].

A different scenario is obtained with special functionalized lipids linked to the polymer chain. If such lipids are incorporated into lipid vesicles, the water-soluble polymers (typically one uses PEG (poly-ethylene glycol) for its non-toxic properties) form well-separated mushrooms, or, at higher concentration of PEG lipid, a dense brush. These modified vesicles are very interesting in the context of drug delivery, because they show prolonged circulation times in vivo [306]. This is probably due to a steric serum-protein-binding inhibition by the hydrophilic brush coat consisting of the PEG lipids. Since the lipid bilayer is rather flexible and undergoes thermal bending fluctuations, there is an interesting coupling between the polymer density distribution and the membrane shape [98,307,308]. For non-adsorbing, anchored polymers, the membrane will bend away from the polymer due to steric repulsion [309–311], but for adsorbing anchored polymer the membrane will bend towards the anchored polymer [312,313].

The behavior of a polymer brush in contact with a solvent, which is by itself also a polymer, consisting of chemically identical but somewhat shorter chains than the brush, had been first considered by de Gennes [282]. A complete scaling description has been given only recently [314]. One

distinguishes different regimes where the polymer solvent is expelled to various degrees from the brush. A somewhat related question concerns the behavior of two opposing brushes brought closely together, and separated by a solvent consisting of a polymer solution [315]. Here one distinguishes a regime where the polymer solution leads to a strong attraction between the surfaces via the ordinary depletion interaction (compare to Ref. [219]), but also a high polymer concentration regime where the attraction is not strong enough to induce colloidal flocculation. This phenomenon is called colloidal restabilization [315].

Considering a mixed brush made of mutually incompatible grafted chains, a novel transition to a brush characterized by a lateral composition modulation was found [316]. Even more complicated spatial structures are obtained with grafted diblock copolymers [317]. Finally, we would like to mention in passing that these static brush phenomena have interesting consequences on dynamic properties of polymer brushes [318].

### 13.3. Charged grafted polymers

Brushes can also be formed by charged polymers which are densely end-grafted to a surface; they are called polyelectrolyte or charged brushes. They have been the focus of numerous theoretical [319–327] and experimental [328–330] studies. In addition to the basic interest, charged brushes are considered for their applications because they serve as an efficient mean for preventing colloids in polar media (such as aqueous solutions) from flocculating and precipitating out of solution [97]. This stabilization arises from steric (entropic) as well as electrostatic repulsion. A strongly charged brush is able to trap its own counterions and generates a layer of locally enhanced salt concentration [321]. It is thus less sensitive to the salinity of the surrounding aqueous medium than a stabilization mechanism based on pure electrostatics (i.e. without polymers). Little is known from experiments on the scaling behavior of PE brushes, as compared to neutral brushes. The thickness of the brush layer has been calculated from neutron-scattering experiments on end-grafted polymers [328] and charged diblock-copolymers at the air–water interface [330].

Theoretical work on PE brushes was initiated by the works of Miklavic and Marcelja [319] and Misra et al. [320]. In 1991, Pincus [321] and Borisov et al. [322] presented scaling theories for charged brushes in the so-called osmotic regime, where the brush height results from the balance between the chain elasticity (which tends to decrease the brush height) and the repulsive osmotic counterion pressure (which tends to increase the brush height). In later studies, these works have been generalized to poor solvents [323] and to the regime where excluded volume effects become important, the so-called quasi-neutral or Alexander regime [326].

In what follows we assume that the charged brush is characterized by two length scales: the average vertical extension of polymer chains from the surface  $D$ , and the typical extent of the counterion cloud, denoted by  $H$ . We neglect the presence of additional salt, which has been discussed extensively in the original literature, and only consider screening effects due to the counterions of the charged brush. Two different scenarios emerge, as is schematically presented in Fig. 29. The counterions can either extend outside the brush,  $H \gg D$ , as shown in (a), or be confined inside the brush,  $H \approx D$  as shown in (b). As we show now, case (b) is indicative of strongly charged brushes, while case (a) is typical for weakly charged brushes.

The free energy density per unit area and in units of  $k_B T$  contains several contributions, which we now calculate one by one. We recall that the grafting density of PEs is denoted by  $\rho$ ,  $z$  is the

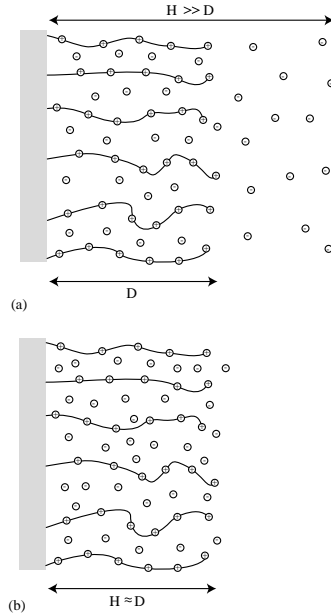


Fig. 29. Schematic PE brush structure. In (a) we show the weak-charge limit where the counterion cloud has a thickness  $H$  larger than the thickness of the brush layer,  $D$ . In (b) we show the opposite case of the strong-charge limit, where all counterions are contained inside the brush and a single length scale  $D \approx H$  exists.

counterion valency,  $N$  the polymerization index of grafted chains, and  $f$  the charge fraction. The osmotic free energy,  $F_{os}$ , associated with the ideal entropy cost of confining the counterions to a layer of thickness  $H$  is given by

$$F_{os} \simeq \frac{Nf\rho}{z} \ln \left( \frac{Nf\rho}{zH} \right). \quad (13.7)$$

$F_{v_2}$  is the second virial contribution to the free energy, arising from steric repulsion between the monomers (contributions due to counter ions are neglected). Throughout this section, the polymers are assumed to be in a good solvent (positive second virial coefficient  $v_2 > 0$ ). The contribution thus reads

$$F_{v_2} \simeq \frac{1}{2} D v_2 \left( \frac{N\rho}{D} \right)^2. \quad (13.8)$$

Finally, a direct electrostatic contribution  $F_{el}$  occurs if the PE brush is not locally electro-neutral throughout the system, as for example is depicted in Fig. 29a. This energy is given by

$$F_{el} = \frac{2\pi\ell_B(Nf\rho)^2(H-D)^2}{3H}. \quad (13.9)$$

This situation arises in the limit of low charge, when the counterion density profile extends beyond the brush layer, i.e.  $H > D$ .

The last contribution is the stretching energy of the chains which is

$$F_{st} = \frac{3D^2}{2Na^2} \rho. \quad (13.10)$$

Here,  $a$  is the Kuhn length of the polymer, implying that we neglect any chain stiffness for the brush problem. The different free energy contributions lead, upon minimization with respect to the two length scales  $H$  and  $D$ , to different behaviors. Let us first consider the weak charging limit, i.e. the situation where the counterions leave the brush,  $H > D$ . In this case, minimization of  $F_{os} + F_{el}$  with respect to the counterion height  $H$  leads to

$$H \sim \frac{1}{z\ell_B N f \rho} \quad (13.11)$$

which has the same scaling as the Gouy–Chapman length for  $z$ -valent counterions at a surface of surface charge density  $\sigma = Nf\rho$ . Balancing now the polymer stretching energy  $F_{st}$  and the electrostatic energy  $F_{el}$  one obtains the so-called Pincus brush height

$$D \simeq N^3 \rho a^2 \ell_B f^2, \quad (13.12)$$

which results from the electrostatic attraction between the counterions and the charged monomers. One notes the peculiar dependence on the polymerization index  $N$ . In the limit of  $H \approx D$  where  $D$  given by Eq. (13.12), the PE brush can be considered as neutral and the electrostatic energy vanishes. There are two ways of balancing the remaining free energy contributions. The first is obtained by comparing the osmotic energy of counterion confinement,  $F_{os}$ , with the polymer stretching term,  $F_{st}$ , leading to the height

$$D \sim \frac{Na f^{1/2}}{z^{1/2}}, \quad (13.13)$$

constituting the so-called osmotic brush regime. Finally comparing the second-virial free energy,  $F_{v_2}$ , with the polymer stretching energy,  $F_{st}$ , one obtains

$$D \sim Na(v_2\rho/a)^{1/3}, \quad (13.14)$$

and the PE brush is found to have the same scaling behavior as the neutral brush [283,282], compare Eq. (13.2). Comparing the brush heights in all three regimes we arrive at the phase diagram shown in Fig. 30. The three scaling regimes coexist at the characteristic charge fraction

$$f_{co} \sim \left( \frac{z v_2}{N^2 a^2 \ell_B} \right)^{1/3}, \quad (13.15)$$

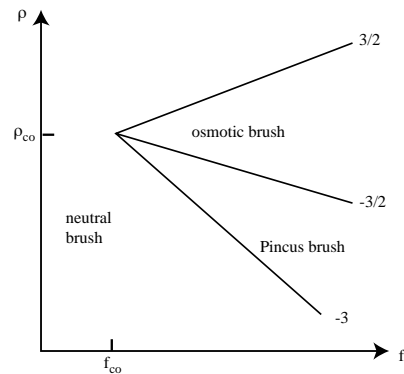


Fig. 30. Scaling diagram for PE brushes on a log–log plot as a function of the grafting density  $\rho$  and the fraction of charged monomers  $f$ . Featured are the Pincus-brush regime, where the counterion layer thickness is much larger than the brush thickness, the osmotic-brush regime, where all counterions are inside the brush and the brush height is determined by an equilibrium between the counterion osmotic pressure and the PE stretching energy, and the neutral-brush regime, where charge effects are not important and the brush height results from a balance of PE stretching energy and second-virial repulsion. The power law exponents of the various lines are denoted by numbers.

and the characteristic grafting density

$$\rho_{co} \sim \frac{1}{N \ell_B^{1/2} v_2^{1/2}} \quad (13.16)$$

For large values of the charge fraction  $f$  and the grafting density  $\rho$  it has been found numerically that the brush height does not follow any of the scaling laws discussed here [331]. This has been recently rationalized in terms of another scaling regime, the collapsed regime. In this regime one finds that correlation and fluctuation effects, which are neglected in the discussion in this section, lead to a net attraction between charged monomers and counterions [332]. Similarly, two charged surfaces, one decorated with a charged brush, the other one neutralized by counter ions, attract each other at large enough grafting densities [333].

Another way of creating a charged brush is to dissolve a diblock copolymer consisting of a hydrophobic and a charged block in water. The diblocks associate to form a hydrophobic core, thereby minimizing the unfavorable interaction with water, while the charged blocks form a highly charged corona or brush [334]. The micelle morphology depends on different parameters. Most importantly, it can be shown that salt acts as a morphology switch, giving rise to the sequence spherical, cylindrical, to planar micellar morphology as the salt concentration is increased [334]. Theoretically, this can be explained by the entropy cost of counterion confinement in the charged corona [335]. The charged corona can be studied by neutron scattering [336] or atomic-force microscopy [337] and gives information on the behavior of highly curved charged brushes.

#### 14. Concluding remarks

We reviewed simple physical concepts underlying the main theories which deal with equilibrium and static properties of neutral and charged polymers adsorbed or grafted to substrates. Most of the review dealt with somewhat ideal situations: smooth and flat surfaces which are chemically homogeneous; long and linear homopolymer chains where chemical properties can be averaged on; simple phenomenological type of interactions between the monomers and the substrate as well as between the monomers and the solvent.

Even with all the simplifying assumptions, the emerging physical picture is quite rich and robust. Adsorption of polymers from dilute solutions can be understood in terms of single-chain adsorption on the substrate. Mean-field theory is quite successful but in some cases fluctuations in the local monomer concentration play an important role. Adsorption from more concentrated solutions results in even more complex density profiles, with several regimes (proximal, central, distal). Each regime is characterized by a different physical behavior. We reviewed the principle theories used to model the polymer behavior. We also mentioned briefly more recent ideas about the statistics of polymer loops and tails. For charged polymers, the structure of the adsorbed layer is in part controlled by the counterion distribution which is coupled to the polymer layer.

The second part of this review is about neutral and charged polymers which are terminally grafted on one end to the surface and are called polymer brushes. The theories here are quite different since the statistics of the grafted layer depends crucially on the fact that the chain is not attracted to the surface but is forced to be in contact to the surface since one of its ends is chemically or physically bonded to the surface. Here as well we review the classical mean-field theory and more advanced theories giving the concentration profiles of the entire polymer layer as well as that of the polymer free ends.

In general, the theory for neutral polymers is more advanced than the one for charged polymers, partly because charged polymers became the target for theoretical modelling fairly recently. In addition, due to the long-range interactions between charged monomers, and due to a number of additional relevant parameters (such as salt concentration, pH), the resultant behavior for charged polymers is more complex. We have introduced some of the basic concepts of charged polymers, such as the Manning condensation of counterions and the electrostatic chain stiffening. Due to this increased stiffness of polyelectrolytes, their chain statistics is described by semi-flexible models. We have, therefore, introduced such models in some detail and also demonstrated some effects specific to semi-flexible charged polymers.

At present, studies of polyelectrolytes in solutions and at surfaces is shifting more towards biological systems. We mentioned in this review the complexation of DNA and histones. This is only one of many examples of interest where charged biopolymers, receptors, proteins and DNA molecules interact with each other or with other cellular components. The challenge for future fundamental research will be to try to understand the role of electrostatic interactions combined with specific biological (lock–key) mechanisms and to infer on biological functionality of such interactions.

In this review, we also discussed additional factors that have an effect on the polymer adsorption and grafted layers: the quality of the solvent, undulating and flexible substrates such as fluid/fluid interfaces or lipid membranes; adsorption and grafting on curved surfaces such as spherical colloidal particles.

Although our main aim was to review the theoretical progress in this field, we mentioned many relevant experiments. In this active field several advanced experimental techniques are used to probe adsorbed or grafted polymer layers: neutron scattering and high-resolution X-ray reflectivity, light scattering using fluorescent probes, ellipsometry, surface isotherms as well as the surface force apparatus for the force measurement between two surfaces.

This paper should be viewed as a general introduction to adsorption phenomena involving charged and neutral chains and can serve as a starting point to understand more complex systems as encountered in applications and current experiments.

### Acknowledgements

It is a pleasure to thank our collaborators G. Ariel, I. Borukhov, M. Breidenich, Y. Burak, H. Diamant, H. Gaub, J.-F. Joanny, K. Kunze, L. Leibler, R. Lipowsky, A. Moreira, H. Orland, M. Schick, C. Seidel, A. Shafir and Y. Tsori with whom we have been working on polymers and polyelectrolytes. One of us (DA) would like to acknowledge partial support from the Israel Science Foundation, Centers of Excellence Program and under grant no. 210/02, the Israel–US Binational Science Foundation (BSF) under grant no. 98-00429, and the Alexander von Humboldt Foundation for a research award. RRN acknowledges financial support by Deutsche Forschungsgemeinschaft (DFG, SFB 486 and German–French Network) and the Fonds der Chemischen Industrie.

### References

- [1] G.J. Fleer, M.A. Cohen Stuart, J.M.H.M. Scheutjens, T. Cosgrove, B. Vincent, *Polymers at Interfaces*, Chapman & Hall, London, 1993.
- [2] E. Eisenriegler, *Polymers Near Surfaces*, World Scientific, Singapore, 1993.
- [3] M.A. Cohen Stuart, T. Cosgrove, B. Vincent, *Adv. Colloid Interface Sci.* 24 (1986) 143.
- [4] P.G. de Gennes, *Adv. Colloid Interface Sci.* 27 (1987) 189.
- [5] I. Szleifer, *Curr. Opin. Colloid Interface Sci.* 1 (1996) 416.
- [6] G.J. Fleer, F.A.M. Leermakers, *Curr. Opin. Colloid Interface Sci.* 2 (1997) 308.
- [7] A.Yu. Grosberg, A.R. Khokhlov, *Statistical Physics of Macromolecules*, AIP Press, New York, 1994.
- [8] F. Oosawa, *Polyelectrolytes*, Dekker, New York, 1971.
- [9] H. Dautzenberg, W. Jaeger, B.P.J. Kötze, C. Seidel, D. Stscherbina, *Polyelectrolytes: Formation, Characterization and Application*, Hanser Press, Munich, 1994.
- [10] S. Förster, M. Schmidt, *Adv. Polym. Sci.* 120 (1995) 50.
- [11] J.-L. Barrat, J.-F. Joanny, *Adv. Chem. Phys.* 94 (1996) 1.
- [12] P.J. Flory, *Principles of Polymer Chemistry*, Cornell University, Ithaca, 1953.
- [13] H. Yamakawa, *Modern Theory of Polymer Solutions*, Harper & Row, New York, 1971.
- [14] P.G. de Gennes, *Scaling Concepts in Polymer Physics*, Cornell University, Ithaca, 1979.
- [15] J. des Cloizeaux, J. Jannink, *Polymers in Solution*, Oxford University, Oxford, 1990.
- [16] F. Gittes, B. Mickey, J. Nettleton, J. Howard, *J. Cell Biol.* 120 (1993) 923.
- [17] J. Käs, H. Strey, M. Bärmann, E. Sackmann, *Europhys. Lett.* 21 (1993) 865.
- [18] A. Ott, M. Magnasco, A. Simon, A. Libchaber, *Phys. Rev. E* 48 (1993) R1642.
- [19] C. Frontale, E. Dore, A. Ferrauto, E. Gratton, *Biopolymers* 18 (1979) 1353.
- [20] P.G. de Gennes, P.A. Pincus, R.M. Velasco, F. Brochard, *J. Phys. (France)* 37 (1976) 1461.
- [21] A.R. Khokhlov, K.A. Khachatryan, *Polymer* 23 (1982) 1742.
- [22] J.-L. Barrat, J.-F. Joanny, *Europhys. Lett.* 24 (1993) 333.
- [23] R.R. Netz, H. Orland, *Eur. Phys. J. B* 8 (1999) 81.
- [24] T. Odijk, *J. Polym. Sci. Part B: Polym. Phys.* 15 (1977) 477; T. Odijk, *Polymer* 19 (1978) 989.
- [25] J. Skolnick, M. Fixman, *Macromolecules* 10 (1977) 944.
- [26] G.A. Christos, S.L. Carnie, *J. Chem. Phys.* 92 (1990) 7661.
- [27] C. Seidel, H. Schlacken, I. Müller, *Macromol. Theory Simul.* 3 (1994) 333.
- [28] M. Ullner, B. Jönsson, C. Peterson, O. Sommelius, B. Söderberg, *J. Chem. Phys.* 107 (1997) 1279; M. Ullner, C.E. Woodward, *Macromolecules* 35 (2002) 1437.
- [29] U. Micka, K. Kremer, *Phys. Rev. E* 54 (1996) 2653; U. Micka, K. Kremer, *Europhys. Lett.* 38 (1997) 279.
- [30] R. Everaers, A. Milchev, V. Yamakov, *Eur. Phys. J. E* 8 (2002) 3.
- [31] T.T. Nguyen, B.I. Shklovskii, *Phys. Rev. E* 66 (2002) 021801.
- [32] H. Li, T. Witten, *Macromolecules* 28 (1995) 5921.
- [33] B.-Y. Ha, D. Thirumalai, *J. Chem. Phys.* 110 (1999) 7533.
- [34] B.-Y. Ha, D. Thirumalai, *Macromolecules* 28 (1995) 577.
- [35] T.B. Liverpool, M. Stapper, *Europhys. Lett.* 40 (1997) 485.
- [36] M. Olvera de la Cruz, L. Belloni, M. Delsanti, J.P. Dalbiez, O. Spalla, M. Drifford, *J. Chem. Phys.* 103 (1995) 5781.
- [37] J. Wittmer, A. Johner, J.F. Joanny, *J. Phys. II (France)* 5 (1995) 635.
- [38] R.G. Winkler, M. Gold, P. Reineker, *Phys. Rev. Lett.* 80 (1998) 3731.
- [39] N.V. Brilliantov, D.V. Kuznetsov, R. Klein, *Phys. Rev. Lett.* 81 (1998) 1433.
- [40] M.O. Khan, B. Jönsson, *Biopolymers* 49 (1999) 121.
- [41] F.J. Solis, M. Olvera de la Cruz, *Eur. Phys. J. E* 4 (2001) 143.
- [42] R. Golestanian, M. Kardar, T.B. Liverpool, *Phys. Rev. Lett.* 82 (1999) 4456.
- [43] P.L. Hansen, D. Svensek, V.A. Parsegian, R. Podgornik, *Phys. Rev. E* 60 (1999) 1956.
- [44] T.T. Nguyen, I. Rouzina, B.I. Shklovskii, *Phys. Rev. E* 60 (1999) 7032.
- [45] G. Ariel, D. Andelman, *Europhys. Lett.* 61 (2003) 67.
- [46] G. Ariel, D. Andelman, *Phys. Rev. E* 67 (2003) 011805.
- [47] N. Grønbech-Jensen, R.J. Mashl, R.F. Bruinsma, W.M. Gelbart, *Phys. Rev. Lett.* 78 (1997) 2477.
- [48] B.-Y. Ha, A.J. Liu, *Phys. Rev. Lett.* 79 (1997) 1289.
- [49] R. Podgornik, V.A. Parsegian, *Phys. Rev. Lett.* 80 (1998) 1560.
- [50] J.J. Arenzon, J.F. Stilck, Y. Levin, *Eur. Phys. J. B* 12 (1999) 79.
- [51] F.J. Solis, M. Olvera de la Cruz, *Phys. Rev. E* 60 (1999) 4496.
- [52] G.S. Manning, *J. Chem. Phys.* 51 (1969) 924.
- [53] G.S. Manning, *J. Chem. Phys.* 51 (1969) 934.
- [54] C.A. Tracy, H. Widom, *Physica A* 244 (1997) 402.
- [55] G.S. Manning, J. Ray, *J. Biomol. Struct. Dyn.* 16 (1998) 461.
- [56] M. Fixman, *J. Chem. Phys.* 76 (1982) 6346.
- [57] M. Le Bret, *J. Chem. Phys.* 76 (1982) 6243.
- [58] G.S. Manning, U. Mohanty, *Physica A* 247 (1997) 196.
- [59] M. Deserno, C. Holm, S. May, *Macromolecules* 33 (2000) 199.
- [60] H.J. Limbach, C. Holm, *J. Chem. Phys.* 114 (2001) 9674.
- [61] G.S. Manning, *J. Chem. Phys.* 89 (1988) 3772.
- [62] P.S. Kuhn, Y. Levin, M.C. Barbosa, *Macromolecules* 31 (1998) 8347.
- [63] A. Deshkovski, S. Obukhov, M. Rubinstein, *Phys. Rev. Lett.* 86 (2001) 2341.
- [64] C. Wandrey, D. Hunkeler, U. Wendler, W. Jaeger, *Macromolecules* 33 (2000) 7136.
- [65] J. Blaul, M. Wittmann, M. Ballauff, M. Rehahn, *J. Phys. Chem. B* 104 (2000) 7077.
- [66] H. Schiessel, P.A. Pincus, *Macromolecules* 31 (1998) 7953; H. Schiessel, *Macromolecules* 32 (1999) 5673.
- [67] T.O. Odijk, A.C. Houwaart, *J. Polym. Sci.* 16 (1978) 627.
- [68] M. Fixman, J. Skolnick, *Macromolecules* 11 (1978) 863.
- [69] A.R. Khokhlov, *J. Phys. A* 13 (1980) 979.

- [70] Y. Kantor, M. Kardar, *Phys. Rev. E* 51 (1995) 1299.
- [71] A.V. Dobrynin, M. Rubinstein, S.P. Obukhov, *Macromolecules* 29 (1996) 2974.
- [72] F.J. Solis, M. Olvera de la Cruz, *Macromolecules* 31 (1998) 5502.
- [73] A.L. Lyulin, B. Dünweg, O.V. Borisov, A.A. Darinskii, *Macromolecules* 32 (1999) 3264.
- [74] U. Micka, C. Holm, K. Kremer, *Langmuir* 15 (1999) 4033.
- [75] T.A. Waigh, R. Ober, C.E. Williams, J.-C. Galin, *Macromolecules* 34 (2001) 1973.
- [76] M. Nierlich, F. Boue, A. Lapp, R. Oberthür, *Colloid Polym. Sci.* 263 (1985) 955.
- [77] M. Nierlich, F. Boue, A. Lapp, R. Oberthür, *J. Phys. (France)* 46 (1985) 649.
- [78] M.N. Spiteri, F. Boue, A. Lapp, J.P. Cotton, *Phys. Rev. Lett.* 77 (1996) 5218.
- [79] A. Moussaïd, F. Schosseler, J.P. Munch, S.J. Candau, *J. Phys. II (France)* 3 (1993) 573.
- [80] W. Essafi, F. Lafuma, C.E. Williams, *J. Phys. II (France)* 5 (1995) 1269.
- [81] K. Nishida, K. Kaji, T. Kanaya, *Macromolecules* 28 (1995) 2472.
- [82] W. Essafi, F. Lafuma, C.E. Williams, *Eur. Phys. J. B* 9 (1999) 261.
- [83] V.Y. Borue, I.Y. Erukhimovich, *Macromolecules* 21 (1988) 3240.
- [84] J.F. Joanny, L. Leibler, *J. Phys. (France)* 51 (1990) 545.
- [85] T. Yoshizaki, H. Yamakawa, *Macromolecules* 13 (1980) 1518.
- [86] M. Dymitrowska, L. Belloni, *J. Chem. Phys.* 109 (1998) 4659.
- [87] A. Yethiraj, *J. Chem. Phys.* 108 (1998) 1184.
- [88] R.R. Netz, to be published.
- [89] T.A. Witten, P.A. Pincus, *Europhys. Lett.* 3 (1987) 315.
- [90] J.-L. Barrat, J.-F. Joanny, *J. Phys. II (France)* 4 (1994) 1089.
- [91] M.J. Stevens, K. Kremer, *J. Chem. Phys.* 103 (1995) 1669.
- [92] M.J. Stevens, K. Kremer, *J. Phys. II (France)* 6 (1996) 1607.
- [93] H. Schäfer, C. Seidel, *Macromolecules* 30 (1997) 6658.
- [94] M.J. Stevens, S.J. Plimpton, *Eur. Phys. J. B* 2 (1998) 341.
- [95] R. von Klitzing, A. Espert, A. Asnacios, T. Hellweg, A. Colin, D. Langevin, *Colloids Surfaces A* 149 (1999) 131.
- [96] P.F. Luckham, J. Klein, *Macromolecules* 18 (1985) 721.
- [97] D.H. Napper, *Polymeric Stabilization of Colloidal Dispersions*, Academic Press, London, 1983.
- [98] R. Lipowsky, *Europhys. Lett.* 30 (1995) 197.
- [99] A. Halperin, J.F. Joanny, *J. Phys. II (France)* 1 (1991) 623.
- [100] B. van Lent, J. Scheutjens, T. Cosgrove, *Macromolecules* 20 (1987) 366.
- [101] G. Stratouras, M. Kosmas, *Macromolecules* 25 (1992) 3307.
- [102] C.M. Marques, J.F. Joanny, *Macromolecules* 23 (1990) 268.
- [103] B. van Lent, J.M.H.M. Scheutjens, *J. Phys. Chem.* 94 (1990) 5033.
- [104] J.P. Donley, G.H. Fredrickson, *Macromolecules* 27 (1994) 458.
- [105] T. Garel, D.A. Huse, S. Leibler, H. Orland, *Europhys. Lett.* 8 (1989) 9.
- [106] S.T. Milner, G.H. Fredrickson, *Macromolecules* 28 (1995) 7953.
- [107] S. Stepanow, J.-U. Sommer, I.Y. Erukhimovich, *Phys. Rev. Lett.* 81 (1998) 4412.
- [108] A. Maritan, M.P. Riva, A. Trovato, *J. Phys. A: Math. Gen.* 32 (1999) L275.
- [109] X. Chatellier, J.-F. Joanny, *Eur. Phys. J. E* 1 (2000) 9.
- [110] H.L. Frish, R. Simha, F.R. Eirish, *J. Chem. Phys.* 21 (1953) 365;  
R. Simha, H.L. Frish, F.R. Eirish, *J. Phys. Chem.* 57 (1953) 584.
- [111] A. Silberberg, *J. Phys. Chem.* 66 (1962) 1872;  
A. Silberberg, *J. Phys. Chem.* 66 (1962) 1884.
- [112] S.F. Edwards, *Proc. Phys. Soc. (London)* 85 (1965) 613;  
S.F. Edwards, *Proc. Phys. Soc. (London)* 88 (1966) 255.
- [113] E.A. DiMarzio, *J. Chem. Phys.* 42 (1965) 2101;  
E.A. DiMarzio, F.L. McCrackin, *J. Chem. Phys.* 43 (1965) 539;  
C. Hoeve, E.A. DiMarzio, P. Peysers, *J. Chem. Phys.* 42 (1965) 2558.
- [114] R.J. Rubin, *J. Chem. Phys.* 43 (1965) 2392.
- [115] I.S. Jones, P. Richmond, *J. Chem. Soc. Faraday Trans. 2* (1977) 73.
- [116] J.N. Israelachvili, *Intermolecular and Surface Forces*, Academic Press, London, 1992.

- [117] M. Daoud, P.G. de Gennes, *J. Phys. (France)* 38 (1977) 85.
- [118] P.G. de Gennes, *Rep. Prog. Phys.* 32 (1969) 187.
- [119] P.J. Flory, *Statistical Mechanics of Chain Molecules*, Hanser Press, Munich, 1988.
- [120] J.M.J. van Leeuwen, H.J. Hilhorst, *Physica A* 107 (1981) 319;  
T.W. Burkhardt, *J. Phys. A* 14 (1981) L63;  
D.M. Kroll, *Z. Phys. B* 41 (1981) 345.
- [121] R. Lipowsky, A. Baumgärtner, *Phys. Rev. A* 40 (1989) 2078;  
R. Lipowsky, *Phys. Scr. T* 29 (1989) 259.
- [122] O.V. Borisov, E.B. Zhulina, T.M. Birshtein, *J. Phys. II (France)* 4 (1994) 913.
- [123] R.R. Netz, *Phys. Rev. E* 51 (1995) 2286.
- [124] J.F. Joanny, *J. Phys. II (France)* 4 (1994) 1281.
- [125] A.V. Dobrynin, M. Rubinstein, J.F. Joanny, *Macromolecules* 30 (1997) 4332.
- [126] R.R. Netz, J.F. Joanny, *Macromolecules* 31 (1998) 5123.
- [127] A.V. Dobrynin, S.P. Obukhov, M. Rubinstein, *Macromolecules* 32 (1999) 5689.
- [128] E. Zhulina, A.V. Dobrynin, M. Rubinstein, *Eur. Phys. J. E* 5 (2001) 41.
- [129] M.O. Khan, T. Akesson, B. Jönsson, *Macromolecules* 34 (2001) 4216.
- [130] D. Poland, H.A. Scheraga, *J. Chem. Phys.* 45 (1966) 1456;  
D. Poland, H.A. Scheraga, *J. Chem. Phys.* 45 (1966) 1464.
- [131] M.E. Fisher, *J. Chem. Phys.* 45 (1966) 1469.
- [132] P.G. de Gennes, *Phys. Lett. A* 38 (1972) 339.
- [133] E. Eisenriegler, K. Kremer, K. Binder, *J. Chem. Phys.* 77 (1982) 6296;  
E. Eisenriegler, *J. Chem. Phys.* 79 (1983) 1052.
- [134] P.G. de Gennes, *J. Phys. (Paris)* 37 (1976) 1445.
- [135] P.G. de Gennes, P.A. Pincus, *J. Phys. Lett. (Paris)* 44 (1983) L241.
- [136] H.W. Diehl, M. Sphot, *Phys. Rev. Lett.* 73 (1994) 3431.
- [137] E. Bouchaud, M. Daoud, *J. Phys. (Paris)* 48 (1987) 1991.
- [138] J. Baschnagel, in: M.T. Tant, A.J. Hill (Eds.), *Structure, Properties of Glassy Polymers*, ACS Symposium Series 710 ACS, Washington, DC, 1998.
- [139] K. de Meijere, G. Brezesinski, H. Möhwald, *Macromolecules* 30 (1997) 2337.
- [140] K. de Meijere, G. Brezesinski, K. Kjaer, H. Möhwald, *Langmuir* 14 (1998) 4204.
- [141] H. von Berlepsch, C. Burger, H. Dautzenberg, *Phys. Rev. E* 58 (1998) 7549.
- [142] C. Stubenrauch, P.-A. Albouy, R. von Klitzing, D. Langevin, *Langmuir* 16 (2000) 3206.
- [143] A. Asnacios, R. von Klitzing, D. Langevin, *Colloids Surfaces A* 167 (2000) 189.
- [144] H. Ahrens, H. Balmes, J. Schmitt, H. Möhwald, C.A. Helm, *Macromolecules* 34 (2001) 4504.
- [145] Y. Fang, J. Yang, *J. Phys. Chem. B* 101 (1997) 441.
- [146] J.O. Rädler, I. Koltover, T. Salditt, C.R. Safinya, *Science* 275 (1997) 810;  
T. Salditt, I. Koltover, J.O. Rädler, C.R. Safinya, *Phys. Rev. Lett.* 79 (1997) 2582.
- [147] B. Maier, J.O. Rädler, *Phys. Rev. Lett.* 82 (1999) 1911.
- [148] G. Decher, J.D. Hong, J. Schmitt, *Thin Solid Films* 210/211 (1992) 831.
- [149] R. von Klitzing, H. Möhwald, *Langmuir* 11 (1995) 3554;  
R. von Klitzing, H. Möhwald, *Macromolecules* 29 (1996) 6901.
- [150] G. Decher, *Science* 277 (1997) 1232;  
M. Lösche, J. Schmitt, G. Decher, W.G. Bouwman, K. Kjaer, *Macromolecules* 31 (1998) 8893.
- [151] F. Caruso, K. Niikura, D.N. Furlong, Y. Okahata, *Langmuir* 13 (1997) 3422.
- [152] E. Donath, G.B. Sukhorukov, F. Caruso, S.A. Davis, H. Möhwald, *Angew. Chem. Int. Ed.* 16 (1998) 37;  
G.B. Sukhorukov, E. Donath, S.A. Davis, H. Lichtenfeld, F. Caruso, V.I. Popov, H. Möhwald, *Polym. Adv. Technol.* 9 (1998) 759.
- [153] F. Caruso, R.A. Caruso, H. Möhwald, *Science* 282 (1998) 1111;  
F. Caruso, *Adv. Mater.* 13 (2001) 11.
- [154] F.W. Wiegand, *J. Phys. A* 10 (1977) 299.
- [155] M. Muthukumar, *J. Chem. Phys.* 86 (1987) 7230.
- [156] X. Chatellier, T.J. Senden, J.F. Joanny, J.M. di Meglio, *Europhys. Lett.* 41 (1998) 303.

- [157] R.R. Netz, J.F. Joanny, *Macromolecules* 32 (1999) 9013.
- [158] O.V. Borisov, F. Hakem, T.A. Vilgis, J.F. Joanny, A. Johner, *Eur. Phys. J. E* 6 (2001) 37.
- [159] A.V. Dobrynin, A. Deshkovski, M. Rubinstein, *Macromolecules* 34 (2001) 3421.
- [160] T. Odijk, *Macromolecules* 16 (1983) 1340;  
T. Odijk, *Macromolecules* 17 (1984) 502.
- [161] A.C. Maggs, D.A. Huse, S. Leibler, *Europhys. Lett.* 8 (1989) 615.
- [162] G. Gompper, T.W. Burkhardt, *Phys. Rev. A* 40 (1989) 6124;  
G. Gompper, U. Seifert, *J. Phys. A* 23 (1990) L1161.
- [163] R. Bundschuh, M. Lässig, R. Lipowsky, *Eur. Phys. J. E* 3 (2000) 295.
- [164] D.V. Kuznetsov, W. Sung, *Macromolecules* 31 (1998) 2679;  
D.V. Kuznetsov, W. Sung, *J. Chem. Phys.* 107 (1997) 4729.
- [165] S. Stepanow, *J. Chem. Phys.* 115 (2001) 1565.
- [166] T. Sintres, K. Sumithra, E. Straube, *Macromolecules* 34 (2001) 1352.
- [167] V. Yamakov, A. Milchev, O. Borisov, B. Dünweg, *J. Phys.: Condens. Matter* 11 (1999) 9907.
- [168] J.W. Cahn, J.E. Hilliard, *J. Chem. Phys.* 28 (1958) 258.
- [169] P.G. de Gennes, *Macromolecules* 14 (1981) 1637.
- [170] O. Guiselin, *Europhys. Lett.* 17 (1992) 225.
- [171] L. Auvray, J.P. Cotton, *Macromolecules* 20 (1987) 202.
- [172] L.T. Lee, O. Guiselin, B. Farnoux, A. Lapp, *Macromolecules* 24 (1991) 2518;  
O. Guiselin, L.T. Lee, B. Farnoux, A. Lapp, *J. Chem. Phys.* 95 (1991) 4632;  
O. Guiselin, *Europhys. Lett.* 17 (1992) 57.
- [173] J.M.H.M. Scheutjens, G.J. Fleer, M.A. Cohen Stuart, *Colloids Surf.* 21 (1986) 285;  
G.J. Fleer, J.M.H.M. Scheutjens, M.A. Cohen Stuart, *Colloids Surf.* 31 (1988) 1.
- [174] A. Johner, J.F. Joanny, M. Rubinstein, *Europhys. Lett.* 22 (1993) 591.
- [175] A.N. Semenov, J.F. Joanny, *Europhys. Lett.* 29 (1995) 279;  
A.N. Semenov, J. Bonet-Avalos, A. Johner, J.F. Joanny, *Macromolecules* 29 (1996) 2179;  
A. Johner, J. Bonet-Avalos, C.C. van der Linden, A.N. Semenov, J.F. Joanny, *Macromolecules* 29 (1996) 3629.
- [176] M. Manghi, M. Aubouy, *Macromolecules* 33 (2000) 5721.
- [177] A.N. Semenov, J.F. Joanny, A. Johner, in: A. Grosberg (Ed.), *Theoretical and Mathematical Models in Polymer Research*, Academic Press, Boston, 1998.
- [178] P. Peyser, R. Ullman, *J. Polym. Sci. A* 3 (1965) 3165.
- [179] M. Kawaguchi, H. Kawaguchi, A. Takahashi, *J. Colloid Interface Sci.* 124 (1988) 57.
- [180] J. Meadows, P.A. Williams, M.J. Garvey, R. Harrop, G.O. Phillips, *J. Colloid Interface Sci.* 132 (1989) 319.
- [181] R. Denoyel, G. Durand, F. Lafuma, R. Audbert, *J. Colloid Interface Sci.* 139 (1990) 281.
- [182] J. Blaakmeer, M.R. Böhmer, M.A. Cohen Stuart, G.J. Fleer, *Macromolecules* 23 (1990) 2301.
- [183] H.G.A. van de Steeg, A. de Keizer, M.A. Cohen Stuart, B.H. Bijsterbosch, *Colloids Surf. A* 70 (1993) 91.
- [184] V. Shubin, P. Linse, *J. Phys. Chem.* 99 (1995) 1285.
- [185] N.G. Hoogeveen, Ph.D. Thesis, Wageningen Agricultural University, The Netherlands, 1996.
- [186] M.A. Cohen Stuart, *J. Phys. (France)* 49 (1988) 1001.
- [187] M.A. Cohen Stuart, G.J. Fleer, J. Lyklema, W. Norde, J.M.H.M. Scheutjens, *Adv. Colloid Interface Sci.* 34 (1991) 477.
- [188] C.A. Haynes, W. Norde, *Colloids Surf. B* 2 (1994) 517.
- [189] P. Auroy, L. Auvray, L. Leger, *Phys. Rev. Lett.* 66 (1991) 719;  
P. Auroy, L. Auvray, L. Leger, *Macromolecules* 24 (1991) 2523;  
P. Auroy, L. Auvray, L. Leger, *Macromolecules* 24 (1991) 5158.
- [190] J.F. Joanny, *Eur. Phys. J. B* 9 (1999) 117.
- [191] I. Borukhov, D. Andelman, H. Orland, *J. Phys. Chem. B* 24 (1999) 5057.
- [192] F.J. Solis, M. Olvera de la Cruz, *J. Chem. Phys.* 110 (1999) 11517.
- [193] T.T. Nguyen, A.Y. Grosberg, B.I. Shklovskii, *J. Chem. Phys.* 113 (2000) 1110.
- [194] T. Odijk, *Macromolecules* 12 (1979) 688.
- [195] A.V. Dobrynin, R.H. Colby, M. Rubinstein, *Macromolecules* 28 (1995) 1859.
- [196] H.A. van der Schee, J. Lyklema, *J. Phys. Chem.* 88 (1984) 6661.

- [197] J. Papenhuijzen, H.A. van der Schee, G.J. Fleer, *J. Colloid Interface Sci.* 104 (1985) 540.
- [198] O.A. Evers, G.J. Fleer, J.M.H.M. Scheutjens, J.M.H.M.J. Lyklema, *J. Colloid Interface Sci.* 111 (1985) 446.
- [199] H.G.M. van de Steeg, M.A. Cohen Stuart, A. de Keizer, B.H. Bijsterbosch, *Langmuir* 8 (1992) 8.
- [200] P. Linse, *Macromolecules* 29 (1996) 326.
- [201] R. Varoqui, A. Johner, A. Elaissari, *J. Chem. Phys.* 94 (1991) 6873.
- [202] R. Varoqui, *J. Phys. (France)* II 3 (1993) 1097.
- [203] I. Borukhov, D. Andelman, H. Orland, *Europhys. Lett.* 32 (1995) 499;  
I. Borukhov, D. Andelman, H. Orland, in: J. Daillant, P. Guenou, C. Marques, P. Muller, J. Trần Thanh Vân (Eds.), *Short and Long Chains at Interfaces*, Edition Frontieres, GiF-sur-Yvette, 1995, pp. 13–20.
- [204] X. Chatellier, J.-F. Joanny, *J. Phys. II (France)* 6 (1996) 1669.
- [205] I. Borukhov, D. Andelman, H. Orland, *Eur. Phys. J. B* 5 (1998) 869.
- [206] I. Borukhov, D. Andelman, H. Orland, *Macromolecules* 31 (1998) 1665.
- [207] A.V. Dobrynin, *J. Chem. Phys.* 114 (2001) 8145.
- [208] A. Shafir, D. Andelman, R.R. Netz, *J. Chem. Phys.*, 2003, submitted; cond-mat/0302126.
- [209] D. Andelman, J.F. Joanny, *C. R. Acad. Sci. (Paris)*, Ser. IV 1 (2000) 1153.
- [210] A.Y. Grosberg, T.T. Nguyen, B.I. Shklovskii, *Rev. Mod. Phys.* 74 (2002) 329.
- [211] Y. Levin, *Rep. Prog. Phys.* 65 (2002) 1577.
- [212] N. Dan, *Biophys. J.* 71 (1996) 1267;  
N. Dan, *Biophys. J.* 73 (1997) 1842.
- [213] J. Klein, G. Rossi, *Macromolecules* 31 (1998) 1979.
- [214] S. Asakura, F. Oosawa, *J. Chem. Phys.* 22 (1954) 1255.
- [215] D. Rudhardt, C. Bechinger, P. Leiderer, *Phys. Rev. Lett.* 81 (1998) 1330.
- [216] A. Hanke, E. Eisenriegler, S. Dietrich, *Phys. Rev. E* 59 (1999) 6853.
- [217] E. Eisenriegler, *J. Phys.: Condens. Matter* 12 (2000) A227.
- [218] A. Broukhno, B. Jönsson, T. Akesson, P.N. Vorontsov-Velyaminov, *J. Chem. Phys.* 113 (2000) 5493.
- [219] J.F. Joanny, L. Leibler, P.G. de Gennes, *J. Polym. Sci.: Polym. Phys. Ed.* 17 (1979) 1073.
- [220] P.G. de Gennes, *Macromolecules* 15 (1982) 492.
- [221] J.M.H.M. Scheutjens, G.J. Fleer, *Macromolecules* 18 (1985) 1882;  
G.J. Fleer, J.M.H.M. Scheutjens, *J. Colloid Interface Sci.* 111 (1986) 504.
- [222] J. Bonet-Avalos, J.F. Joanny, A. Johner, A.N. Semenov, *Europhys. Lett.* 35 (1996) 97;  
J. Bonet-Avalos, A. Johner, J.F. Joanny, *J. Chem. Phys.* 101 (1994) 9181.
- [223] A.N. Semenov, *J. Phys. II (France)* 6 (1996) 1759.
- [224] J. Ennis, B. Jönsson, *J. Phys. Chem. B* 103 (1999) 2248.
- [225] J. Klein, P.F. Luckham, *Nature* 300 (1982) 429;  
J. Klein, P.F. Luckham, *Macromolecules* 17 (1984) 1041.
- [226] J. Klein, P.F. Luckham, *Nature* 308 (1984) 836;  
Y. Almog, J. Klein, *J. Colloid Interface Sci.* 106 (1985) 33.
- [227] G. Rossi, P.A. Pincus, *Europhys. Lett.* 5 (1988) 641;  
G. Rossi, P.A. Pincus, *Macromolecules* 22 (1989) 276.
- [228] J.M. Mendez-Alcaraz, A. Johner, J.F. Joanny, *Macromolecules* 31 (1998) 8297.
- [229] J. Klein, *Nature* 288 (1980) 248;  
J. Klein, P.F. Luckham, *Macromolecules* 19 (1986) 2007.
- [230] J. Klein, P.A. Pincus, *Macromolecules* 15 (1982) 1129;  
K. Ingersent, J. Klein, P.A. Pincus, *Macromolecules* 19 (1986) 1374.
- [231] K. Ingersent, J. Klein, P.A. Pincus, *Macromolecules* 23 (1990) 548.
- [232] G.H. Fredrickson, P.A. Pincus, *Langmuir* 7 (1991) 786.
- [233] L. Guldbrand, B. Jönsson, H. Wennerström, P. Linse, *J. Chem. Phys.* 80 (1984) 2221.
- [234] A.G. Moreira, R.R. Netz, *Phys. Rev. Lett.* 87 (2001) 8301.
- [235] T. Akesson, C. Woodward, B. Jönsson, *J. Chem. Phys.* 91 (1989) 2461.
- [236] M.K. Granfeldt, B. Jönsson, C.E. Woodward, *J. Phys. Chem.* 95 (1991) 4819.
- [237] M.R. Böhmer, O.A. Evers, J.M.H.M. Scheutjens, *Macromolecules* 23 (1990) 2223.
- [238] R. Podgornik, *J. Phys. Chem.* 96 (1992) 884.

- [239] A. Asnacios, A. Espert, A. Colin, D. Langevin, *Phys. Rev. Lett.* 78 (1997) 4974.
- [240] B. Kolaric, W. Jaeger, R. von Klitzing, *J. Phys. Chem. B* 104 (2000) 5096.
- [241] R. von Klitzing, A. Espert, A. Colin, D. Langevin, *Colloids Surfaces A* 176 (2001) 109.
- [242] A. Yethiraj, *J. Chem. Phys.* 111 (1999) 1797.
- [243] P.G. de Gennes, *J. Phys. Chem.* 94 (1990) 8407.
- [244] D. Andelman, J.F. Joanny, *Macromolecules* 24 (1991) 6040;  
J.F. Joanny, D. Andelman, *Makromol. Chem. Macromol. Symp.* 62 (1992) 35;  
D. Andelman, J.F. Joanny, *J. Phys. II (France)* 3 (1993) 121.
- [245] V. Aharonson, D. Andelman, A. Zilman, P.A. Pincus, E. Raphaël, *Physica A* 204 (1994) 1;  
V. Aharonson, D. Andelman, A. Zilman, P.A. Pincus, E. Raphaël, *Physica A* 227 (1996) 158.
- [246] R.R. Netz, D. Andelman, H. Orland, *J. Phys. II (France)* 6 (1996) 1023.
- [247] X. Châtellier, D. Andelman, *Europhys. Lett.* 32 (1995) 567;  
X. Châtellier, D. Andelman, *J. Phys. Chem.* 22 (1996) 9444.
- [248] C. Fleck, R.R. Netz, H. von Grünberg, *Biophys. J.* 82 (2002) 76.
- [249] R. Bruinsma, J. Mashl, *Europhys. Lett.* 41 (1998) 165.
- [250] D. Harries, S. May, W.M. Gelbart, A. Ben-Shaul, *Biophys. J.* 75 (1998) 159.
- [251] H. Clausen-Schaumann, H.E. Gaub, *Langmuir* 15 (1999) 8246.
- [252] M. Ellis, C.Y. Kong, M. Muthukumar, *J. Chem. Phys.* 112 (2000) 8723.
- [253] J. McNamara, C.Y. Kong, M. Muthukumar, *J. Chem. Phys.* 117 (2002) 5354.
- [254] T.A. Vilgis, G. Heinrich, *Macromolecules* 27 (1994) 7846;  
G. Huber, T.A. Vilgis, *Eur. Phys. J. B* 3 (1998) 217.
- [255] D. Hone, H. Ji, P.A. Pincus, *Macromolecules* 20 (1987) 2543;  
H. Ji, D. Hone, *Macromolecules* 21 (1988) 2600.
- [256] M. Blunt, W. Barford, R. Ball, *Macromolecules* 22 (1989) 1458.
- [257] C.M. Marques, J.F. Joanny, *J. Phys. (France)* 49 (1988) 1103.
- [258] S. Alexander, *J. Phys. (Paris)* 38 (1977) 977.
- [259] P.A. Pincus, C.J. Sandroff, T.A. Witten, *J. Phys. (France)* 45 (1984) 725.
- [260] R. Podgornik, *Europhys. Lett.* 21 (1993) 245;  
R. Podgornik, *Phys. Rev. E* 51 (1995) 3368.
- [261] T. Garel, M. Kardar, H. Orland, *Europhys. Lett.* 29 (1995) 303.
- [262] J.T. Brooks, C.M. Marques, M.E. Cates, *Europhys. Lett.* 14 (1991) 713;  
J.T. Brooks, C.M. Marques, M.E. Cates, *J. Phys. II (France)* 1 (1991) 673.
- [263] F. Clement, J.F. Joanny, *J. Phys. II (France)* 7 (1997) 973.
- [264] M. Breidenich, R.R. Netz, R. Lipowsky, to be published.
- [265] T. Odijk, *Macromolecules* 13 (1980) 1542.
- [266] S.Y. Park, R.F. Bruinsma, W.M. Gelbart, *Europhys. Lett.* 46 (1999) 454.
- [267] K.K. Kunze, R.R. Netz, *Europhys. Lett.* 58 (2002) 299.
- [268] F. von Goeler, M. Muthukumar, *J. Chem. Phys.* 100 (1994) 7796.
- [269] T. Wallin, P. Linse, *Langmuir* 12 (1996) 305;  
T. Wallin, P. Linse, *J. Phys. Chem.* 100 (1996) 17873;  
T. Wallin, P. Linse, *J. Phys. Chem. B* 101 (1997) 5506.
- [270] E. Gurovitch, P. Sens, *Phys. Rev. Lett.* 82 (1999) 339.
- [271] R. Golestanian, *Phys. Rev. Lett.* 83 (1999) 2473.
- [272] E.M. Mateescu, C. Jeppesen, P.A. Pincus, *Europhys. Lett.* 46 (1999) 493.
- [273] R.R. Netz, J.F. Joanny, *Macromolecules* 32 (1999) 9026.
- [274] T.T. Nguyen, B.I. Shklovskii, *Physica A* 293 (2001) 324;  
T.T. Nguyen, B.I. Shklovskii, *J. Chem. Phys.* 114 (2001) 5905.
- [275] K.K. Kunze, R.R. Netz, *Phys. Rev. Lett.* 85 (2000) 4389.
- [276] T.D. Yager, C.T. McMurray, K.E. van Holde, *Biochemistry* 28 (1989) 2271.
- [277] H.J. Taunton, C. Toprakcioglu, L.J. Fetters, *J. Klein, Nature* 332 (1988) 712;  
H.J. Taunton, C. Toprakcioglu, L.J. Fetters, *J. Klein, Macromolecules* 23 (1990) 571.
- [278] J.B. Field, C. Toprakcioglu, L. Dai, G. Hadziioannou, G. Smith, W. Hamilton, *J. Phys. II (France)* 2 (1992) 2221.

- [279] C.M. Marques, J.F. Joanny, L. Leibler, *Macromolecules* 21 (1988) 1051;  
C.M. Marques, J.F. Joanny, *Macromolecules* 22 (1989) 1454.
- [280] M.S. Kent, L.T. Lee, B. Farnoux, F. Rondelez, *Macromolecules* 25 (1992) 6240;  
M.S. Kent, L.T. Lee, B.J. Factor, F. Rondelez, G.S. Smith, *J. Chem. Phys.* 103 (1995) 2320;  
H.D. Bijsterbosch, V.O. de Haan, A.W. de Graaf, M. Mellema, F.A.M. Leermakers, M.A. Cohen Stuart, A.A. van Well, *Langmuir* 11 (1995) 4467;  
M.C. Fauré, P. Bassereau, M.A. Carignano, I. Szleifer, Y. Gallot, D. Andelman, *Eur. Phys. J. B* 3 (1998) 365;  
E.P.K. Currie, F.A.M. Leermakers, M.A. Cohen Stuart, G.J. Fleer, *Macromolecules* 32 (1999) 487.
- [281] R. Teppner, M. Härke, H. Motschmann, *Rev. Sci. Inst.* 68 (1997) 4177;  
R. Teppner, H. Motschmann, *Macromolecules* 31 (1998) 7467.
- [282] P.G. de Gennes, *Macromolecules* 13 (1980) 1069.
- [283] S. Alexander, *J. Phys. (France)* 38 (1977) 983.
- [284] A. Halperin, M. Tirell, T.P. Lodge, *Adv. Polym. Sci.* 100 (1992) 31.
- [285] T. Cosgrove, T. Heath, B. van Lent, F.A.M. Leermakers, J. Scheutjens, *Macromolecules* 20 (1987) 1692.
- [286] M. Murat, G.S. Grest, *Macromolecules* 22 (1989) 4054;  
A. Chakrabarti, R. Toral, *Macromolecules* 23 (1990) 2016;  
P.Y. Lai, K. Binder, *J. Chem. Phys.* 95 (1991) 9288.
- [287] A.N. Semenov, *Sov. Phys. JETP* 61 (1985) 733.
- [288] S.T. Milner, T.A. Witten, M.E. Cates, *Europhys. Lett.* 5 (1988) 413;  
S.T. Milner, T.A. Witten, M.E. Cates, *Macromolecules* 21 (1988) 610;  
S.T. Milner, *Science* 251 (1991) 905.
- [289] A.M. Skvortsov, I.V. Pavlushkov, A.A. Gorbunov, Y.B. Zhulina, O.V. Borisov, V.A. Pryamitsyn, *Polym. Sci.* 30 (1988) 1706.
- [290] R.R. Netz, M. Schick, *Europhys. Lett.* 38 (1997) 37;  
R.R. Netz, M. Schick, *Macromolecules* 31 (1998) 5105.
- [291] C. Seidel, R.R. Netz, *Macromolecules* 33 (2000) 634.
- [292] M.A. Carignano, I. Szleifer, *J. Chem. Phys.* 98 (1993) 5006;  
M.A. Carignano, I. Szleifer, *J. Chem. Phys.* 100 (1994) 3210;  
M.A. Carignano, I. Szleifer, *Macromolecules* 28 (1995) 3197;  
M.A. Carignano, I. Szleifer, *J. Chem. Phys.* 102 (1995) 8662. A detailed summary of tethered layers is given in:  
I. Szleifer, M.A. Carignano, *Adv. Chem. Phys. XCIV* (1996) 165.
- [293] G.S. Grest, *Macromolecules* 27 (1994) 418.
- [294] T.A. Witten, P.A. Pincus, *Macromolecules* 19 (1986) 2509;  
E.B. Zhulina, O.V. Borisov, V.A. Priamitsyn, *J. Colloid Surf. Sci.* 137 (1990) 495.
- [295] S.T. Milner, *Europhys. Lett.* 7 (1988) 695.
- [296] S.T. Milner, T.A. Witten, M.E. Cates, *Macromolecules* 22 (1989) 853.
- [297] A. Halperin, *J. Phys. (France)* 49 (1988) 547;  
Y.B. Zhulina, V.A. Pryamitsyn, O.V. Borisov, *Polym. Sci.* 31 (1989) 205;  
E.B. Zhulina, O.V. Borisov, V.A. Pryamitsyn, T.M. Birshtein, *Macromolecules* 24 (1991) 140;  
D.R.M. Williams, *J. Phys. II (France)* 3 (1993) 1313.
- [298] P. Auroy, L. Auvray, *Macromolecules* 25 (1992) 4134.
- [299] J.F. Marko, *Macromolecules* 26 (1993) 313.
- [300] P.Y. Lai, K. Binder, *J. Chem. Phys.* 97 (1992) 586;  
G.S. Grest, M. Murat, *Macromolecules* 26 (1993) 3108.
- [301] M. Daoud, J.P. Cotton, *J. Phys. (France)* 43 (1982) 531.
- [302] R.C. Ball, J.F. Marko, S.T. Milner, A.T. Witten, *Macromolecules* 24 (1991) 693;  
H. Li, T.A. Witten, *Macromolecules* 27 (1994) 449.
- [303] N. Dan, M. Tirrell, *Macromolecules* 25 (1992) 2890.
- [304] M. Murat, G.S. Grest, *Macromolecules* 24 (1991) 704.
- [305] S.T. Milner, T.A. Witten, *J. Phys. (France)* 49 (1988) 1951.
- [306] T.M. Allen, C. Hansen, F. Martin, C. Redemann, A. Yau-Young, *Biochim. Biophys. Acta* 1006 (1991) 29;  
M.J. Parr, S.M. Ansell, L.S. Choi, P.R. Cullis, *Biochim. Biophys. Acta* 1195 (1994) 21.

- [307] K. Hristova, D. Needham, *Macromolecules* 28 (1995) 991.
- [308] K. Hristova, A. Kenworthy, T.J. McIntosh, *Macromolecules* 28 (1995) 7693.
- [309] C. Hiergeist, R. Lipowsky, *J. Phys. II (France)* 6 (1996) 1465.
- [310] M. Breidenich, R.R. Netz, R. Lipowsky, *Europhys. Lett.* 49 (2000) 431.
- [311] T. Bickel, C. Marques, C. Jeppesen, *Phys. Rev. E* 62 (2000) 1124.
- [312] C. Hiergeist, V.A. Indrani, R. Lipowsky, *Europhys. Lett.* 36 (1996) 491.
- [313] M. Breidenich, R.R. Netz, R. Lipowsky, *Eur. Phys. J. E* 5 (2001) 189.
- [314] M. Aubouy, G.H. Fredrickson, P.A. Pincus, E. Raphael, *Macromolecules* 28 (1995) 2979.
- [315] A.P. Gast, L. Leibler, *Macromolecules* 19 (1986) 686.
- [316] J.F. Marko, T.A. Witten, *Phys. Rev. Lett.* 66 (1991) 1541.
- [317] G. Brown, A. Chakrabarti, J.F. Marko, *Macromolecules* 28 (1995) 7817;  
E.B. Zhulina, C. Singhm, A.C. Balazs, *Macromolecules* 29 (1996) 8254.
- [318] A. Halperin, S. Alexander, *Europhys. Lett.* 6 (1988) 329;  
A. Johner, J.F. Joanny, *Macromolecules* 23 (1990) 5299;  
C. Ligoure, L. Leibler, *J. Phys. (France)* 51 (1990) 1313;  
S.T. Milner, *Macromolecules* 25 (1992) 5487;  
A. Johner, J.F. Joanny, *J. Chem. Phys.* 98 (1993) 1647.
- [319] S.J. Miklavic, S. Marcelja, *J. Phys. Chem.* 92 (1988) 6718.
- [320] S. Misra, S. Varanasi, P.P. Varanasi, *Macromolecules* 22 (1989) 5173.
- [321] P.A. Pincus, *Macromolecules* 24 (1991) 2912.
- [322] O.V. Borisov, T.M. Birstein, E.B. Zhulina, *J. Phys. II (France)* 1 (1991) 521.
- [323] R.S. Ross, P.A. Pincus, *Macromolecules* 25 (1992) 2177;  
E.B. Zhulina, T.M. Birstein, O.V. Borisov, *J. Phys. II (France)* 2 (1992) 63.
- [324] J. Wittmer, J.-F. Joanny, *Macromolecules* 26 (1993) 2691.
- [325] R. Israels, F.A.M. Leermakers, G.J. Fleer, E.B. Zhulina, *Macromolecules* 27 (1994) 3249.
- [326] O.V. Borisov, E.B. Zhulina, T.M. Birstein, *Macromolecules* 27 (1994) 4795.
- [327] E.B. Zhulina, O.V. Borisov, *J. Chem. Phys.* 107 (1997) 5952.
- [328] Y. Mir, P. Auvroy, L. Auvray, *Phys. Rev. Lett.* 75 (1995) 2863.
- [329] P. Guenoun, A. Schlachli, D. Sentenac, J.M. Mays, J.J. Benattar, *Phys. Rev. Lett.* 74 (1995) 3628.
- [330] H. Ahrens, S. Förster, C.A. Helm, *Macromolecules* 30 (1997) 8447;  
H. Ahrens, S. Förster, C.A. Helm, *Phys. Rev. Lett.* 81 (1998) 4172.
- [331] F. Csajka, C. Seidel, *Macromolecules* 33 (2000) 2728.
- [332] F.S. Csajka, R.R. Netz, C. Seidel, J.F. Joanny, *Eur. Phys. J. E* 4 (2001) 505.
- [333] J. Ennis, L. Sjöström, T. Akesson, B. Jönsson, *J. Phys. Chem. B* 102 (1998) 2149.
- [334] L. Zhang, A. Eisenberg, *Science* 268 (1995) 1728;  
L. Zhang, K. Yu, A. Eisenberg, *Science* 272 (1996) 1777;  
H. Shen, L. Zhang, A. Eisenberg, *J. Am. Chem. Soc.* 121 (1999) 2728.
- [335] R.R. Netz, *Europhys. Lett.* 47 (1999) 391.
- [336] P. Guenoun, F. Muller, M. Delsanti, L. Auvray, Y.J. Chen, J.W. Mays, M. Tirrell, *Phys. Rev. Lett.* 81 (1998) 3872;  
P. Guenoun, M. Delsanti, D. Gazeau, J.W. Mays, D.C. Cook, M. Tirrell, L. Auvray, *Eur. Phys. J. B* 1 (1998) 77.
- [337] S. Förster, N. Hermsdorf, W. Leube, H. Schnablegger, M. Regenbrecht, S. Akarai, P. Lindner, C. Böttcher, *J. Phys. Chem. B* 103 (1999) 6657;  
M. Regenbrecht, S. Akarai, S. Förster, H. Möhwal, J. Phys. Chem. B 103 (1999) 6669.

 David  
Andelman  
Signature  
Not Verified

Digitally signed by  
David Andelman  
DN: cn=David  
Andelman, o=IL  
Date: 2003.05.27  
06:57:53 +02'00'